

Peripheral contribution to pain hypersensitivity in a T-cell mediated model of multiple sclerosis:
The female perspective

by

Muhammad Saad Yousuf

A thesis submitted in partial fulfillment of the requirements for the degree of

Doctor of Philosophy

Neuroscience
University of Alberta

© Muhammad Saad Yousuf, 2019

Abstract

Multiple sclerosis (MS) is a neuroinflammatory disease characterised by immune activation, demyelination, and degeneration in the central nervous system (CNS). Chronic pain is a common symptom of MS and current treatment options for pain in MS are ineffective. Pain arises from aberrant excitability of the somatosensory nervous system, typically initiated in the peripheral sensory neurons. To study the underlying immune-mediated pathophysiology of pain in MS, I employed the myelin oligodendrocyte glycoprotein (MOG)-induced experimental autoimmune encephalitis (EAE) model in mice. Since sensory neurons are crucial for nociceptive transduction, we investigated the effect of this disease on sensory neurons of the dorsal root ganglia (DRG).

In Chapter 1, I report that EAE was associated with activation of the complement system and the NLRP3 inflammasome in the DRG. I further observed a transient increase in the number of complement component 5a receptor 1-positive (C5aR1+) immune cells, CD4+ T-cells, and Iba1+ macrophages in the DRG. Moreover, I noted an induction of activating transcription factor 3 (ATF3) at disease onset and chronic disruption of cytoskeletal proteins in the DRG demonstrating neuronal injury in the PNS in response to the disease. Electrophysiological analysis revealed neuronal hyperexcitability at the onset of MOG-EAE signs.

In Chapter 2, I investigated the role of NKCC1 and KCC2 in neuropathic pain observed in EAE. Although I observed no change in the levels of NKCC1 transcripts in the DRG throughout the disease course, NKCC1 and KCC2 mRNA levels in the dorsal spinal cord were significantly reduced at disease onset and peak only to recover by the chronic time point. Similarly, Western blot data revealed a significant downregulation of NKCC1 and KCC2 in the dorsal spinal cord at disease onset but an upregulation of NKCC1 protein in the dorsal root

ganglia at this time point. Treatment with bumetanide, an NKCC1 inhibitor, had no effect on mechanical hypersensitivity seen in mice with EAE even though it reversed the changes in the levels of NKCC1 and KCC2.

In Chapter 3, I investigated whether endoplasmic reticulum (ER) stress in the dorsal root ganglia (DRG) contributes to pain hypersensitivity in EAE and by extension in MS. I observed inflammation and ER stress in post-mortem DRGs from MS patients. My results show that a class of sensory neurons undergo ER stress early in the EAE disease course and relieving ER stress with administration of a chemical chaperone, 4-phenylbutyric acid (4-PBA), can significantly reduce pain hypersensitivity in affected animals. Further *in vitro* investigations revealed that 4-PBA and AMG44, a selective PERK inhibitor, reduce Ca^{2+} transients in putative nociceptors. I also identified changes in the functional properties of BK channels in IB4⁺ neurons. These changes were reversed with 4-PBA and AMG44 application *in vitro*.

Collectively, my results suggest that DRGs in EAE mice and MS patients experience immune activation, inflammation, injury, and ER stress. Using EAE as a proxy to understanding MS pathophysiology, my work also shows that ER stress contributes to pain hypersensitivity by altering Ca^{2+} dynamics and the functional properties of BK channels, ultimately impacting the electrophysiology of sensory neurons. Hence, novel approaches to treating pain in MS must take into consideration the effect of the disease on the peripheral nervous system.

Preface

This thesis is an original work by Muhammad Saad Yousuf. The research project, of which this thesis is a part, received research ethics approval from the University of Alberta Research Ethics Board, Project Name “Assessing sensory function in EAE”, AUP00000274, Approved Fall 2007.

Parts of the introduction chapter have been published as:

- Yousuf, M.S., Kerr, B.J. (2018) The challenges of animal models of pain. *Landmark Papers in Pain: Seminal Papers in Pain with Expert Commentaries*. 10(4): 36.
- Yousuf, M.S., Kerr, B.J. (2016) The role of regulatory transporters in neuropathic pain. *Advances in Pharmacology*. 75: 245-271.

For each of these reviews, I was responsible for concept formation, analysis, and manuscript composition. B.J.K. was the supervisory author, involved with concept formation and manuscript edits.

Chapter 1 of this thesis has been published as:

- Yousuf, M.S., Noh, M., Friedman, T., Zubkow, K., Johnson, J.C., Tenorio, G., Kurata, H., Smith, P.A., Kerr, B.J. (2019) Sensory neurons of the dorsal root ganglia become hyperexcitable in a T-cell mediated MOG-EAE model of multiple sclerosis. *eNeuro*. 6(2).

I was responsible for concept formation, data collection, analysis, and manuscript composition. M.N., T.F., K.Z., and J.C.J. collected data. G.T. assisted with sample preparation and data collection. H.K. was involved with editing the manuscript. P.A.S. and B.J.K. were the supervisory authors involved with concept formation and manuscript edits.

Chapter 2 of this thesis has been published as:

- Yousuf, M.S., Zubkow, K., Tenorio, G., Kerr, B.J. (2017) The chloride co-transporters, NKCC1 and KCC2, in experimental autoimmune encephalomyelitis (EAE). *Neuroscience*. 344: 178-186.

I was responsible for concept formation, data collection, analysis, and manuscript composition. K.Z. collected data. G.T. assisted with sample preparation and data collection. B.J.K. was the supervisory author involved with concept formation and manuscript edits.

Chapter 3 of this thesis is currently submitted for peer-review at *PNAS* as:

- Yousuf, M.S., Samtleben, S., Lamothe, S.M., Catuneanu, A., Friedman, T., Thorburn, K., Desai, M., Tenorio, G., Schenk, G., Ballanyi, K., Kurata, H. T., Simmen, T., Kerr, B.J. (2019) Endoplasmic reticulum stress in the periphery contributes to pain in a model of multiple sclerosis.

I was responsible for concept formation, data collection, analysis, and manuscript composition. S.S., S.M.L., A.C., T.F., K.T., and M.D. collected data. G.T. assisted with sample preparation and data collection. G.S. was involved with sample preparation and manuscript editing. K.B. provided equipment for experiments and assisted with Ca²⁺ imaging. H.K., T.S., and B.J.K. were the supervisory authors involved with concept formation and manuscript edits.

بِسْمِ اللَّهِ الرَّحْمَنِ الرَّحِيمِ

To my dear parents,
Dr. Mohammad and Salma Yousuf
For your love, sacrifice, and guidance.

رَبِّ اَرْحَمُهُمَا كَمَا رَبَّيَانِي صَغِيرًا
“My lord, bestow upon them Thy Mercy
As they cherished me in childhood.”

And

To my beautiful wife, *Muniba*
For being my better half

وَخَلَقْنَاكُمْ اَزْوَاجًا
“We created you in pairs.”

مِنْهَا خَلَقْنَاكُمْ وَفِيهَا نُعِيدُكُمْ وَمِنْهَا نُخْرِجُكُمْ تَارَةً أُخْرَى

Acknowledgements

This thesis is not just endeavour over the past seven year but rather the result of my entire life's experiences. As such, it would be impossible to carry this work out without the generous support of my supervisor and mentor, Dr. Bradley Kerr. I cannot thank you enough for all your support and guidance throughout this time. When I left Toronto and came to a new city, you made me feel at home. I started as an MSc student and you convinced me to stay on to complete a PhD. I am glad that you did. Your guidance has inspired me to be a better scientist and, above all, a better person.

Considering the innumerable hours I spent at the lab, my colleagues became my family. To Curtis, Liam, Katherine, Kevin, Timo, Gustavo, Kasia, Eszter, John, Rei, Jen, David, Erica, Danny, Jyoti, Sam, Melanie, Haecy, and Shawn, I would like to say thank you. Thank you for your support. Thank you for being there when I needed you. Thank you for the stimulating conversations. I could not have completed this work without your support.

I would like to thank my supervisory committee, Dr. Satya Kar, Dr. Chris Power, and Dr. Thomas Simmen for their invaluable advice and guidance in making this thesis possible. I would like to specially thank Dr. Christine Webber and Dr. Peter Smith for their continuous support throughout my PhD. Your powerful reference letters enabled me to secure prestigious external funding throughout my graduate studies. Also, I am ever grateful to you for giving me the opportunity to deliver lectures in your undergraduate courses.

Outside the lab, I would like to thank the Faculty of Graduate Studies Outreach Team: Dr. Renee Polzeihn, Charity Slobod, Dr. Fred Mills, Andreea Mohora, and Valerie Miller. My experience working with you has been priceless. I have learned many skills from our time together. You allowed me to disseminate my knowledge and give back to the community.

Last but not least, I would like to thank my family without whom I would not be here. Your love and support means the world to me. I am grateful to my parents, Mohammad and Salma, for being ever supportive of my dreams and endeavours and for believing in me. I would not be here if it were not for your unconditional love and countless sacrifices. Thank you for being with me on this educational journey since I was only a year and a half old. I would also like to thank my brothers, Ahmed and Saud, who are less like brothers and more like my best friends. I know I can always count on you guys to have my back. To my beautiful wife, Muniba, thank you for being so supportive and putting up with my long, erratic schedules. Thank you for riding this roller coaster with me. I could not have accomplished this without you by my side. To my adorable daughter, Sumayyah, you might be too young to appreciate this yet but you have renewed my sense of affection and motivated me to work harder and go above and beyond my limits.

Over the past several years, I have been fortunate to have such a supportive group of people around me. Your support, mentorship, and encouragements has had an everlasting effect on me.

Thank you.

Table of Contents

ABSTRACT	II
PREFACE	IV
DEDICATION	VI
ACKNOWLEDGEMENTS	VII
LIST OF TABLES	XII
LIST OF FIGURES	XIII
LIST OF SUPPLEMENTARY FIGURES	XIII
ABBREVIATIONS AND SYMBOLS	XIV
INTRODUCTION	1
MULTIPLE SCLEROSIS	1
<i>Epidemiology</i>	<i>1</i>
<i>Pathogenesis of MS</i>	<i>2</i>
PAIN	7
<i>Anatomical substrates of pain</i>	<i>8</i>
<i>Neuronal plasticity and pain</i>	<i>11</i>
<i>Descending modulation</i>	<i>12</i>
<i>Animal models of pain</i>	<i>13</i>
EXPERIMENTAL AUTOIMMUNE ENCEPHALOMYELITIS	17
<i>Pain in EAE</i>	<i>18</i>
<i>Central mechanisms of pain in EAE</i>	<i>19</i>
<i>Peripheral mechanisms of pain in EAE</i>	<i>21</i>
CHLORIDE HOMEOSTASIS	23
<i>Chloride co-transporters</i>	<i>23</i>
<i>Implications for pain</i>	<i>26</i>
ENDOPLASMIC RETICULUM HOMEOSTASIS	28
<i>Unfolded protein response</i>	<i>29</i>
<i>Ca²⁺ regulation</i>	<i>33</i>
SUMMARY AND PURPOSE	37
AIM 1: PERIPHERAL SENSITIZATION	37
<i>Hypothesis 1:</i>	<i>37</i>
AIM 2: CHLORIDE HOMEOSTASIS	38
<i>Hypothesis 2:</i>	<i>38</i>
AIM 3: ENDOPLASMIC RETICULUM STRESS	38
<i>Hypothesis 3:</i>	<i>38</i>
CHAPTER 1 : SENSORY NEURONS OF THE DORSAL ROOT GANGLIA BECOME HYPEREXCITABLE IN A T-CELL MEDIATED MOG-EAE MODEL OF MULTIPLE SCLEROSIS	39
INTRODUCTION	39
METHODS AND MATERIALS	42
<i>EAE Induction and Scoring</i>	<i>42</i>
<i>Tissue Harvesting and Storage</i>	<i>42</i>

<i>Polymerase Chain Reaction</i>	43
<i>Western Blotting</i>	43
<i>Immunohistochemistry</i>	44
<i>Dissociated DRG cultures for electrophysiology</i>	44
<i>Electrophysiological recording</i>	45
<i>Experimental Design and Statistical Analysis</i>	46
RESULTS	47
<i>Immune activation and inflammation in the DRG of MOG-EAE mice</i>	47
<i>Myelin dysregulation</i>	48
<i>Cellular injury and cytoskeletal disruption</i>	49
<i>Larger diameter ($\geq 26 \mu\text{m}$) neurons are hyperexcitable in MOG-EAE</i>	50
TABLES:	59
<i>Table 1.1. qRT-PCR primers used in this study</i>	59
<i>Table 1.2. Antibodies used in this study</i>	60
<i>Table 1.3. Various spike parameters of small ($< 26 \mu\text{m}$) and large ($\geq 26 \mu\text{m}$) diameter DRG neurons obtained from CFA, EAE onset, and EAE chronic mice</i>	61
<i>Table 1.4. Statistical analyses performed in this study</i>	62
FIGURES:.....	64
<i>Figure 1.1. EAE-induced complement and inflammasome activation in the DRG</i>	64
<i>Figure 1.2. Immune cells infiltrate the DRG in EAE</i>	65
<i>Figure 1.3. Myelin protein transcripts in the periphery are not significantly altered in EAE</i>	66
<i>Figure 1.4. Cellular injury marker, ATF3, is upregulated in the DRG of EAE animals</i>	68
<i>Figure 1.5. Cytoskeletal disruption of DRG neurons occurs late in the EAE disease course</i>	69
<i>Figure 1.6. Larger diameter ($\geq 26 \mu\text{m}$) dissociated DRG neurons exhibit hyperexcitability</i>	72
CHAPTER 2 : THE CHLORIDE CO-TRANSPORTERS, NKCC1 AND KCC2, IN EXPERIMENTAL AUTOIMMUNE ENCEPHALOMYELITIS (EAE)	73
INTRODUCTION	73
EXPERIMENTAL PROCEDURES.....	75
<i>EAE Induction</i>	75
<i>Behavioural Assays</i>	76
<i>Tissue Harvesting</i>	76
<i>Western Blotting</i>	76
<i>Reverse Transcription and qRT-PCR</i>	77
<i>Bumetanide Administration</i>	77
<i>Statistical Analysis</i>	78
RESULTS	78
<i>EAE Disease Course</i>	78
<i>Chloride co-transporters in the DRG and dorsal spinal cord</i>	79
<i>Bumetanide Treatment</i>	80
DISCUSSION	82
TABLES:	88
<i>Table 2.1. Primers used in qRT-PCR reactions</i>	88
FIGURES:.....	89
<i>Figure 2.1. Mice with EAE show evidence of mechanical allodynia</i>	89
<i>Figure 2.2. NKCC1 and KCC2 mRNA expression in the DRG and dSC</i>	90
<i>Figure 2.3. Western blot analysis reveals a dysregulation of NKCC1 and KCC2 in the DRG and the dSC</i>	91
<i>Figure 2.4. Bumetanide treatment does not alleviate mechanical allodynia</i>	93
<i>Figure 2.5. Bumetanide treatment modifies the expression of chloride cotransporters in the DRG and the dSC</i>	94

CHAPTER 3 : ENDOPLASMIC RETICULUM STRESS IN THE PERIPHERY CONTRIBUTES TO PAIN IN A MODEL OF MULTIPLE SCLEROSIS.....	96
INTRODUCTION	96
MATERIALS AND METHODS	98
<i>Human Tissue</i>	98
<i>EAE induction and scoring</i>	99
<i>Behavioural assessments</i>	100
<i>4-PBA administration in vivo</i>	100
<i>Immunohistochemistry</i>	101
<i>Western blotting</i>	101
<i>Quantitative real-time PCR</i>	102
<i>Dissociated DRG cultures</i>	102
<i>Live cell Ca²⁺ imaging in DRG neurons</i>	103
<i>Perforated patch whole-cell recordings</i>	104
<i>Experimental Design and Statistical Analysis</i>	106
<i>Data availability</i>	106
RESULTS	107
<i>Inflammation and ER stress in the post-mortem MS DRG</i>	107
<i>EAE mice develop pain hypersensitivity</i>	108
<i>ER stress in the DRG of EAE mice</i>	108
<i>4-PBA treatment alleviates mechanical and facial hypersensitivity</i>	109
<i>4-PBA treatment does not alter inflammation and ER stress in the spinal dorsal horn</i>	110
<i>4-PBA treatment reduces ER stress in the DRG</i>	111
<i>4-PBA dampens Ca²⁺ responses in small diameter neurons</i>	111
<i>Knockdown of Ddit3 and Xbp1 mRNA does not alter evoked Ca²⁺ rises</i>	112
<i>The PERK inhibitor, AMG44, reduces Ca²⁺ signalling in small diameter neurons</i>	113
<i>BK channel current is rescued by 4-PBA and AMG44 treatment</i>	113
DISCUSSION	115
TABLES:	122
<i>Table 3.1. Demographics of MS patients and non-demented controls</i>	122
<i>Table 3.2. Antibodies used in this study</i>	123
FIGURES:.....	125
<i>Figure 3.1. Human DRGs undergo inflammation, immune activation, and ER stress in MS</i>	126
<i>Figure 3.2. ER stress-associated proteins are dysregulated in the DRG of EAE mice</i>	128
<i>Figure 3.3. Daily 4-PBA treatment alleviates EAE-induced mechanical hypersensitivity</i>	129
<i>Figure 3.4. 4-PBA treatment does not alter spinal inflammation and ER stress</i>	131
<i>Figure 3.5. 4-PBA treatment reduces the expression of UPR-associated proteins in the DRG</i>	133
<i>Figure 3.6. 4-PBA diminishes cellular Ca²⁺ responses in small-diameter DRG neurons</i>	134
<i>Figure 3.7. Gene knockdown of XBP1 and CHOP did not alter Ca²⁺ transients in small-diameter DRG neurons</i>	135
<i>Figure 3.8. AMG44 treatment dampens cytosolic Ca²⁺ responses in small-diameter DRG neurons</i>	137
<i>Figure 3.9. ER stress modulators rescues EAE-mediated changes in Ca²⁺-sensitive BK channel properties</i>	139
<i>Supplementary Figure 3.1. 4-PBA and AMG44 treatment, in vitro, alters gene expression of UPR-associated transcripts</i>	141
CONCLUSIONS:.....	142
REFERENCES	146

List of Tables

Table 1.1. qRT-PCR primers used in this study.	59
Table 1.2. Antibodies used in this study.	60
Table 1.3. Various spike parameters of small (<26 μm) and large ($\geq 26 \mu\text{m}$) diameter DRG neurons obtained from CFA, EAE onset, and EAE chronic mice.	61
Table 1.4. Statistical analyses performed in this study.	62
Table 2.1. Primers used in qRT-PCR reactions.	88
Table 3.1. Demographics of MS patients and non-demented controls.	122
Table 3.2. Antibodies used in this study.	123

List of Figures

Figure 1.1. EAE-induced complement and inflammasome activation in the DRG.....	64
Figure 1.2. Immune cells infiltrate the DRG in EAE.	65
Figure 1.3. Myelin protein transcripts in the periphery are not significantly altered in EAE.	66
Figure 1.4. Cellular injury marker, ATF3, is upregulated in the DRG of EAE animals.	68
Figure 1.5. Cytoskeletal disruption of DRG neurons occurs late in the EAE disease course.	69
Figure 1.6. Larger diameter ($\geq 26 \mu\text{m}$) dissociated DRG neurons exhibit hyperexcitability.	72
Figure 2.1. Mice with EAE show evidence of mechanical allodynia.	89
Figure 2.2. NKCC1 and KCC2 mRNA expression in the DRG and dSC.	90
Figure 2.3. Western blot analysis reveals a dysregulation of NKCC1 and KCC2 in the DRG and the dSC.....	91
Figure 2.4. Bumetanide treatment does not alleviate mechanical allodynia.....	93
Figure 2.5. Bumetanide treatment modifies the expression of chloride cotransporters in the DRG and the dSC.....	94
Figure 3.1. Human DRGs undergo inflammation, immune activation, and ER stress in MS.	126
Figure 3.2. ER stress-associated proteins are dysregulated in the DRG of EAE mice.....	128
Figure 3.3. Daily 4-PBA treatment alleviates EAE-induced mechanical hypersensitivity.	129
Figure 3.4. 4-PBA treatment does not alter spinal inflammation and ER stress.	131
Figure 3.5. 4-PBA treatment reduces the expression of UPR-associated proteins in the DRG.	133
Figure 3.6. 4-PBA diminishes cellular Ca^{2+} responses in small-diameter DRG neurons.	134
Figure 3.7. Gene knockdown of XBP1 and CHOP did not alter Ca^{2+} transients in small-diameter DRG neurons.	135
Figure 3.8. AMG44 treatment dampens cytosolic Ca^{2+} responses in small-diameter DRG neurons.....	137
Figure 3.9. ER stress modulators rescues EAE-mediated changes in Ca^{2+} -sensitive BK channel properties.....	139

List of Supplementary Figures

Supplementary Figure 3.1. 4-PBA and AMG44 treatment, in vitro, alters gene expression of UPR-associated transcripts.	141
---	-----

Abbreviations and Symbols

MS	Multiple sclerosis
SPMS	Secondary progressive MS
PPMS	Primary progressive MS
RRMS	Relapsing remitting MS
HLA	Human leukocyte antigen
IL	Interleukin
CD	Cluster of differentiation
TYK	Tyrosine kinase
STAT	Signal transducer and activator of transcription
TNF	Tumor necrosis factor
TNFRSF	TNF receptor superfamily
CNS	Central nervous system
EAE	Experimental autoimmune encephalomyelitis
FoxP3	Forkhead box P3
Treg	Regulatory T-cell
IFN	Interferon
GMCSF	Granulocyte macrophage colony stimulating factor
Breg	Regulatory B-cell
GFAP	Gilial fibrillary acid protein
Nav	Voltage-gated sodium channel
NCX	Na ⁺ /Ca ²⁺ exchanger
MCT1	Monocarboxylate transporter 1
CGRP	Calcitonin gene-related peptide
IB4	Isolectin B4
TRPV1	Transient receptor potential cation channel subfamily V member 1
TRPA1	Transient receptor potential cation channel subfamily A member 1
P2X	ATP-gated P2X receptor cation channel family
TRPM8	Transient receptor potential cation channel subfamily M member 8
S1	Primary somatosensory cortex
AMPA	α -amino-3-hydroxy-5-methyl-4-isoxazolepropionic acid
NMDA	N-Methyl-d-aspartic acid
ERK	extracellular signal–regulated kinases (also known as classical MAP kinases)
5HT	5-hydroxytryptamine (commonly known as serotonin)
NA	Noradrenaline (also known as norepinephrine)
DA	Dopamine
DAT	DA transporter
DXMP	Dextromethorphan
MOG₃₅₋₅₅	Myelin oligodendrocyte glycoprotein peptide 35-55

PLP₁₃₉₋₁₅₁	Proteolipid protein peptide 139-151
Th	T-helper cell
TGF	Transforming growth factor
TREZ	Trigeminal root entry zone
TG	Trigeminal ganglia
DRG	Dorsal root ganglia
CXCL1	chemokine (C-X-C motif) ligand 1
CX3CL1	chemokine (C-X ₃ -C motif) ligand 1 (commonly known as fractalkine)
BDNF	Brain-derived neurotrophic factor
SGC	Satellite glial cell
NKCC1	Na-K-Cl cotransporter 1
KCC2	K-Cl transporter 5
ATP	Adenosine triphosphate
GABA	Gamma-aminobutyric acid
PNS	Peripheral nervous system
PAD	Primary afferent depolarization
DRR	Dorsal root reflexes
TrkB	Tropomyosin receptor kinase B
BiP	Binding immunoglobulin protein (also known as glucose regulated protein 78 (GRP78) or heat shock protein 5 (HSPA5))
ER	Endoplasmic reticulum
RNA	Ribonucleic acid
PERK	PKR-like ER kinase
ATF	Activating transcription factor
IRE1	inositol-requiring enzyme 1
uORF	Upstream open reading frame
GCN2	general control nonderepressible 2
PKR	Protein kinase RNA-activated
HRI	Heme-regulated inhibitor kinase
ISR	Integrated stress response
UPR	Unfolded protein response
tRNA^{Met}	Initiator transfer RNA-methionine
eIF2	eukaryotic initiation factor 2
Bcl2	B-cell lymphoma 2
Bak	Bcl-2 homologous antagonist/killer
Bax	Bcl-2-associated X protein
CHOP	C/EBP homologous protein (also known as DNA damage-inducible transcript 3 (Ddit3))
PP1	Protein phosphatase 1
XBP1	X-box binding protein 1
RIDD	Regulated IRE1-dependent decay of mRNA

TRAF	TNF receptor associated factor
ASK	Apoptosis signal-regulating kinase
JNK	c-Jun N-terminal kinase
NFκB	nuclear factor kappa-light-chain-enhancer of activated B cells
RIPK	Receptor-interacting serine/threonine-protein kinase
CBP	Calcium binding protein
RyR	Ryanodine receptor
IP3R	IP3 receptor
IP3	Inositol trisphosphate
BK Channel	Calcium-sensitive large conductance potassium channel
SERCA	sarco/endoplasmic reticulum Ca ²⁺ -ATPase
MCU	mitochondrial calcium uniporter
Iba1	ionized calcium-binding adapter molecule 1
NLRP3	NACHT, LRR and PYD domains-containing protein 3
NFH	Neurofilament, heavy
CFA	Complete Freund's adjuvant
SC	Spinal cord
BMT	Bumetanide
CNX	Calnexin
4-PBA	4-phenylbutyric acid
CICR	Calcium induced calcium release
HDAC	Histone deacetylase
uORF	Untranslated open reading frame
ISRIB	ISR inhibitor

Introduction

Multiple Sclerosis

Epidemiology

Multiple sclerosis (MS) is an immune-mediated neurodegenerative disorder often characterised by demyelinating plaques, or sclerae, in the central nervous system. Symptoms of MS can vary from person to person, however, patients typically have problems with coordination, muscle weakness, vision/sight impairments, and sensory abnormalities (Howard et al., 2016). The disease is estimated to affect 2.3 million individuals globally with increasing distribution of the disease with increasing distance from the equator, albeit with some reservations (Howard et al., 2016; Thompson et al., 2018). About 85% of MS cases present as relapsing-remitting MS (RRMS) where clinical episodes (or relapses) are interspersed with relatively normal periods (Faissner et al., 2019). Majority of these individuals will proceed to developing a single progressive disease known as secondary progressive MS (SPMS) (Howard et al., 2016; Faissner et al., 2019). The remaining 15% of MS patients develop a more aggressive, progressive condition at the time of diagnosis described as primary progressive MS (PPMS) (Faissner et al., 2019). The disease is known to disproportionately affect about three times more females than males (3.2:1) (Orton et al., 2006).

Although MS was first described as a distinct disease by Jean-Martin Charcot in 1868 over a century ago, the exact cause of MS is still unknown (Stys et al., 2012; Lehmann et al., 2018). Considering the geographic distribution of the disease, vitamin D deficiency, due to a lack of sun exposure, is predicted to play a role in developing MS (Ascherio et al., 2010). In addition, smoking and obesity are prominent risk factors of the disease (Thompson et al., 2018). The hygiene hypothesis proposes that exposure to infections early in life leads to a reduced risk of

autoimmune and allergic diseases (Thompson et al., 2018). However, Epstein-Barr virus infection in adolescence can significantly increase the risk of developing MS (Levin et al., 2005). Certain genetic factors have also been identified as risk factors of MS. Most prominent genetic association arises from variations within the HLA (human leukocyte antigen) locus which accounts for 20-30% of genetic susceptibility to the disease (Haines et al., 1998). Non-HLA associations have recently been described and include genes involved in immune response such as *IL2RA*, *IL7RA*, *CD58*, *TYK2*, *STAT3*, and *TNFRSF1A* (Thompson et al., 2018). In total, over 200 genetic risk factors of MS have been identified (Thompson et al., 2018).

Pathogenesis of MS

The pathogenesis of MS is currently contended in the literature. Competing hypotheses place the initiating factor of the disease either outside or within the CNS. The CNS extrinsic or “outside-in” hypothesis suggests that the initiating factor such as an infection happens outside the CNS and this leads to an aberrant immune response against molecules in the CNS (Stys et al., 2012). On the contrary, the CNS intrinsic or “inside-out” model proposes that some injury or inflammation takes place in the CNS which allows for the extrusion of CNS antigens and subsequent immune reaction against the CNS, particularly myelin (Stys et al., 2012). In either case, it is clear that both the peripheral and central immune responses are key to the progression of MS pathology (Stys et al., 2012; Van Kaer et al., 2019).

The innate and the adaptive immune systems function in concert in the pathogenesis of MS. T-cells and B-cells are thought to initiate the immune response against the CNS by recruiting and activating phagocytic cells of the body, including macrophages and microglia (Thompson et al., 2018). Specifically, CD4+ T-cells have received the most attention particularly

because of their presence in MS lesions in the CNS as well as their modulatory role in preclinical models of MS, particularly experimental autoimmune encephalomyelitis (EAE) (Van Kaer et al., 2019). Furthermore, CD4⁺ T-cells from MS patients show impaired functionality including reduced production of anti-inflammatory cytokines, such as IL10, suggesting a reduction in regulatory CD4⁺ T-cells (CD4⁺ Foxp3⁺ Tregs) in MS as compared to T-cells from healthy controls (O'Connor and Anderton, 2008; Cao et al., 2015). Genetic studies have also identified cytotoxic CD8⁺ T-cells as important mediators of MS pathology (Van Kaer et al., 2019). Interestingly, CD8⁺ T-cells are found in greater numbers in MS lesions than CD4⁺ T-cells (Hauser et al., 1986; Van Kaer et al., 2019). These cells express cytotoxic granzyme B as well as a plethora of proinflammatory cytokines such as IL-17 and IFN γ (Ifergan et al., 2011). CD8⁺ T-cells have also been shown to be required for preclinical models of MS implying that CD4⁺ and CD8⁺ T-cells interact with each other for the pathogenesis of the disease (Sun et al., 2001; Ankathatti Munegowda et al., 2011; Huber et al., 2013). Counterintuitively, depleting CD8⁺ T-cells from preclinical models of MS prior to the onset of signs of the disease worsens disease progression, further suggesting that CD8⁺ T-cells may also have a protective, regulatory role in the disease (Ortega et al., 2013).

B-cells have also been implicated in MS as well as preclinical models of MS (for an excellent review, see Michel et al., 2015). Antibody producing B-cells are found in MS lesions and are known to present CNS antigen to T-cells in the periphery which can in turn lead to further activation and infiltration of T-cells in the CNS (Harp et al., 2008; Henderson et al., 2009). B-cells contribute to the inflammatory milieu in the CNS by secreting proinflammatory cytokines such as TNF α , IL-6, and GM-CSF (Van Kaer et al., 2019). In MS, impaired regulatory B cell (Breg) function has been reported (Michel et al., 2015). In fact, loss of IL-10 secreting

Bregs exacerbates animal models of MS and adoptive transfer of Bregs reduces the time of disease onset in rodents but not the disease course (Matsushita et al., 2008, 2010). Hence, the role of B cells in the pathogenesis of MS is well appreciated however many questions remain unanswered (Michel et al., 2015).

Central immune responses are also important mediators of MS pathology. Microglia are the resident immune cells of the CNS and are critical to defending the CNS from invading infections. Microglial populations, even in normal-appearing white matter and gray matter, are activated early in the disease signifying widespread neurodegeneration (Kutzelnigg et al., 2005). Once activated these cells produce proinflammatory cytokines as well as reactive oxygen species which further exacerbate the disease (Ohl et al., 2016; Faissner et al., 2019). As with other immune cells, microglia can take pro- and anti-inflammatory phenotypes over a continuum (Ransohoff, 2016). In preclinical MS models, microglia adopt a more proinflammatory phenotype while later disease stages is characterised by anti-inflammatory microglia (Herder et al., 2015). It should be noted though, microglia and macrophage populations are harder to distinguish in an inflammatory environment and thus, prior studies on microglia may be riddled with macrophage contamination (Faissner et al., 2019).

Astrocytes perform a variety of essential functions in the CNS ranging from maintaining the blood brain barrier to metabolic support of neurons (Ponath et al., 2018). In this regard, the astrocytes also function as immune modulators primarily by contributing to the inflammatory milieu via the production of soluble mediators such as chemokines, cytokines, and reactive oxygen species (Faissner et al., 2019). Activated, hypertrophic GFAP+ astrocytes are noted in acute MS lesions and the immediate surrounding normal appearing white and gray matter, suggesting that astrocytes may contribute to the development and progression of the lesion

(Ponath et al., 2018). Furthermore, astrogliosis at the glia limitans near MS lesions is hypothesized to cause a breakdown of the blood brain barrier resulting in the infiltration of CNS-targeting peripheral immune cells (Ponath et al., 2018). GFAP immunoreactivity in astrocytes is reduced in chronic lesions and astrocytes are primarily restricted to the lesion border where they contribute to the formation of an “astroglial scar” (Ponath et al., 2018). As with other glial cells, astrocytes have recently been described to adopt multiple inflammatory (A1 vs. A2) phenotypes in response to injury or disease (Liddelow and Barres, 2017). Activated astrocytes are found in proximity to activated macrophages and microglia in an acute MS lesion (Ponath et al., 2018). Further investigation revealed that astrocytes and myeloid cells, such as microglia and macrophages, occupy distinct regions within acute lesions while chronic lesions are characterized by more diffuse expression of astrocytes and myeloid cells (Park et al., 2019). Loss of astrocytes in early EAE exacerbates the disease while ablation of astrocytes in chronic EAE is protective (Mayo et al., 2014).

The most predominant feature of MS is the loss of myelin sheaths and subsequent axonal damage and degeneration. Myelinating oligodendrocytes are largely considered to be passive targets of the immune system primed against myelin in the CNS (Thompson et al., 2018). However, recent data suggest that oligodendrocyte progenitor cells and mature oligodendrocytes actively contribute to the inflammatory environment in the CNS including T-cell proliferation and phagocytising debris (Falcão et al., 2018; Kirby et al., 2019). In this respect, using single-cell RNA-sequencing approach, considerable heterogeneity of oligodendrocytes is observed in human CNS tissue in response to MS (Falcão et al., 2018; Jäkel et al., 2019). Nevertheless, it is clear that myelin is crucial for salutatory conduction and the lack of myelin severely hampers action potential propagation along axons (Waxman, 2006). In myelinated axons, Nav1.6 is

concentrated in the nodes of Ranvier while Nav1.2 is found largely on premyelinated and unmyelinated axons in the CNS (Caldwell et al., 2000; Boiko et al., 2001). After the loss of myelin, some axons compensate for failed conduction across the demyelinated region by increasing the number of Nav1.6 channels as well as expressing Nav1.2 channels (Craner et al., 2004). Nav1.6 and Nav1.2 activity directly contributes to neurodegeneration by increasing neuronal energy demands (Waxman, 2006; Schattling et al., 2016). Furthermore, persistent Na⁺ current through Nav1.6 coupled with the reversal of Na⁺-Ca²⁺ exchanger (NCX) increases intracellular Ca²⁺ which in turn initiates secondary detrimental processes such as calcium-induced calcium release, activation of proteases and lipase, and mitochondrial dysfunction (Waxman, 2006). Indeed, acute MS lesions show increased expression of Nav1.6, Nav1.2, and NCX along demyelinated axons (Craner et al., 2004). Beyond their role in action potential propagation, oligodendrocytes provide metabolic support to axons by shuttling lactate through oligodendrocyte monocarboxylate transporter 1 (MCT1) (Lee et al., 2012). Perturbation in oligodendrocyte MCT1 in animal and in vitro models causes axonal degeneration, despite axons being myelinated, suggesting that metabolic coupling between oligodendrocytes and axons are necessary for axonal integrity (Lee et al., 2012).

Pain

Pain is an adaptive response to noxious stimuli that causes tissue injuries, or at least has the potential to cause injuries (Loeser and Treede, 2008). It is the most common symptom across various medical various diseases ranging from autoimmune disorders, such as rheumatoid arthritis, to traumatic nerve injury (Calvo and Bennett, 2012; Sarzi-Puttini et al., 2014) and a major reason for seeking physician consultation (Yousuf and Ali, 1997; Debono et al., 2013). When pain loses its adaptive value and becomes persistent even after the initial cause has healed, it becomes a disease in its own capacity. As such, The International Association of Pain (IASP) defines neuropathic pain as pain caused by a lesion or disease of the somatosensory nervous system (Loeser and Treede, 2008). It further has the capacity to severely affect one's quality of life and general activities of daily living (Leadley et al., 2014). While the prevalence of neuropathic pain is hard to assess, a recent meta-analysis concluded that 6.9% to 10% of the general population experiences neuropathic pain (Van Hecke et al., 2014). The economic burden of chronic pain in the United States is estimated to be as high as \$635 billion, which is greater than the annual cost associated with heart disease, cancer, and diabetes, combined (Gaskin and Richard, 2012).

The Gate Control Theory of Pain (Melzack and Wall, 1965) proposes that local interneurons in the spinal cord modulate incoming pain signals from the periphery and then, relay that information to the brain where the perception of pain occurs. Although the neural networks responsible for pain signalling are more complicated than initially proposed by Melzack and Wall, the Gate Theory of Pain highlights the three components of the pain pathway: the periphery, the spinal cord (and brainstem), and the brain. Complex circuitry of the spinal cord allows for integration of incoming sensory information across modalities, such as touch, temperature, and pain (Sandkuhler, 2009). These sensations can be further modulated by top-

down processing from various areas of the brain (Ossipov et al., 2014). Neuropathic pain is postulated to occur because of sensitization, or enhanced signalling, along this pain pathway. Of particular interest are neurons of the superficial laminae of the spinal dorsal horn which receive bulk of the nociceptive afferent inputs and contain projection neurons extending to the cortical regions such as the thalamus and the somatosensory cortex (Zeilhofer et al., 2012).

Anatomical substrates of pain

Nociceptors are a specialized class of neural cells in the periphery that encode painful stimuli across various modalities such as noxious heat, chemicals, and mechanical stimulation. In concert with other sensory neurons, nociceptors inform the central nervous system about the nature, location, and intensity of the painful stimulus (Basbaum et al., 2009). Primary afferents are classified according to combinations of myelination, modalities, response characteristics, and specific molecular markers. Among these, nociceptors are generally classified as thinly myelinated A δ fibres or unmyelinated C-fibres which respond to multiple sensory modalities to produce highly localized fast pain (A δ fibres) and poorly localized slow pain (C-fibres) (Basbaum et al., 2009; Woller et al., 2017). Furthermore, the role of highly myelinated A β fibres in pain processing has also been implicated (Xu et al., 2015). Sensory neurons may also be characterized by the expression of certain neuropeptides, such as substance P or calcitonin gene related peptide (CGRP), or their reactivity to *Griffonia simplicifolia* isolectin B4 (IB4) (Basbaum et al., 2009). As such, distinctions are made between peptidergic (expressing neuropeptides) and non-peptidergic neurons. Furthermore, nociceptors express various transducer proteins, like TRPV1, TRPA1, P2X3, TRPM8, and Piezo2 (or a combination thereof), which respond to a variety of stimuli including heat, noxious chemicals, cold, and mechanical stimulation (Emery et

al., 2016; Moehring et al., 2018). This may be used further to delineate the sensory neuron population. Since considerable overlap among these characteristics exist, sensory neurons should be classified using a combination of these criteria (for example, TRPV1+ IB4+ neurons). Recent single cell RNA-sequencing experiments of mouse DRGs have identified 11 subtypes of sensory neurons, each with their distinct molecular characteristics (Usoskin et al., 2015). Enhancement of the response properties of sensory neurons, known as peripheral sensitization, due to inflammation, injury, or a lesion often leads to hyperalgesia (increased sensitivity to painful stimulus) and allodynia (pain from a previously non-noxious stimulus) (Woller et al., 2017).

Rexed (1954) organized cells in the cat spinal cord based on their size and packing density. He identified ten distinct regions, or laminae, of the spinal cord of which the first six (lamina I-VI) are considered to make up the dorsal horn while laminae VII-IX comprise the ventral horn. Lamina X consists of cells surrounding the central canal (Rexed, 1954). The dorsal horn receives majority of the primary afferent input. Superficial dorsal horn (lamina I and II) neurons particularly receive input from high threshold nociceptors while deep dorsal horn (lamina III-VI) neurons predominantly receive input from low threshold mechanoreceptors and proprioceptors (Moehring et al., 2018). Spinothalamic projection neurons in lamina I integrate nociceptive and mechanosensitive information through a complex network of inhibitory and excitatory interneurons which extend throughout the dorsal horn (Basbaum et al., 2009; Woller et al., 2017). Dorsal column projection neurons in the deeper laminae receive most of their input from spinal interneurons and transmit touch information to the brainstem (Basbaum et al., 2009; Woller et al., 2017). The heterogeneity of spinal interneurons allows the spinal cord to integrate, process, and modulate incoming sensory information. Recent single cell RNA sequencing approaches have identified roughly 30 different neuronal populations in the dorsal horn (Häring

et al., 2018). Interestingly, same cell types are clustered together along Rexed's laminar organization suggesting that function of these cells is correlated with their location (Häring et al., 2018; Moehring et al., 2018). Interneurons of the dorsal horn also connect to motor neurons in the ventral horn giving rise to spinal reflexes (Koch et al., 2018).

Once nociceptive information from the periphery is processed, it is transmitted to the brain via the ascending spinal tracts (Basbaum et al., 2009). Somatotopic organization is preserved throughout the somatosensory nervous system (Wilson et al., 1986). Projection neurons of the spinothalamic tract synapse onto the thalamus and third-order neurons carry signals from the thalamus to their respective location in the somatosensory cortex (S1) based on the somatotopic representation on the cortex (i.e. sensory homunculus in humans) (Vierck et al., 2013). Activation of these cortical neurons allows for the localization of pain as well as the discrimination of the pain intensity (Basbaum et al., 2009). The S1 is highly modulated by the frontal cortex based on cognitive factors such as attention and prior experience with the stimulus (Price et al., 2006a). The postcentral gyrus of the S1 consists of 3 Brodmann areas: areas 1, 2 and 3 (subdivided into 3a and 3b) (Vierck et al., 2013). Area 3a primarily receives input originating in high threshold C-fibres while information from myelinated ($A\beta$ and $A\delta$) fibres terminate in areas 1 and 3b (Vierck et al., 2013). Extensive synaptic connectivity between these areas of the S1 allows the cortex to modulate its own activity by consolidating multiple sensory modalities through a network of excitatory and inhibitory neurons (Vierck et al., 2013). In addition to the S1, other brain regions also receive nociceptive information branching out from the thalamus and various brainstem nuclei (Basbaum et al., 2009). The limbic system, including the hippocampus, amygdala, and the anterior cingulate cortex, is thought to be important for the affective

component of pain such as the unpleasant, aversive, and memorable nature of a painful stimulus (Price et al., 2006a).

Neuronal plasticity and pain

Plasticity in the peripheral nervous system occurs via the modulation and/or modification of sensory neurons. Modulation involves transient changes in the expression of transducer proteins including their phosphorylation states as well as the presence of associated proteins which may alter the functional properties of signal transducers, themselves (Woolf and Salter, 2000). For example, activation of protein kinase C ϵ by a sensitizing stimulus leads to the phosphorylation of Nav1.8 further reducing its threshold of activation and enhancing its electrophysiological properties (Wu et al., 2012). Modification of the sensory neurons entails altering the expression of voltage gated ion channels which are ultimately responsible for action potential initiation, propagation, and neurotransmitter release (Woolf and Salter, 2000). Modification processes are also associated with altered connectivity such as collateral sprouting, increased fibre sprouting in the skin, and long term potentiation of afferent terminals in the spinal cord (Woolf and Salter, 2000). In essence, peripheral sensitization represents a reduction in the threshold of nociceptors and an increase the gain of neurotransmission.

A key mechanism of neuropathic pain is the sensitization of central circuits particularly in the spinal cord. Central processes of plasticity involve facilitation, potentiation, augmentation, and amplification of neuronal output (Latremoliere and Woolf, 2009). These processes are mediated by phosphorylation of neurotransmitter receptors, such as the phosphorylation and insertion of glutamatergic AMPA and NMDA receptors, as well as alterations in ion channel properties over the short term (Chen and Huang, 1992; Tingley et al., 1997; Latremoliere and

Woolf, 2009). Longer lasting changes are transcription-dependent and are mediated by increases in intracellular calcium (Ji et al., 2009). Windup is a well-known phenomenon of activity-dependent synaptic facilitation (Mendell and Wall, 1965). It occurs when a relatively mild noxious stimulus is repeated in close temporal proximity such that each subsequent activation of the nociceptor leads to a heightened post-synaptic response in second-order spinal neurons (Latremoliere and Woolf, 2009). Windup is a product of temporal summation allowing the removal of Mg^{2+} block from NMDA receptors and further enhancing the post-synaptic response (Chen and Huang, 1992; Sivilotti et al., 1993). Moreover, glutamatergic receptors are coupled with ER calcium channels which upon stimulation lead to a dramatic rise in cytosolic calcium (Latremoliere and Woolf, 2009). Through Ca^{2+} sensing proteins (e.g. CaMKII, PKC), intracellular Ca^{2+} alters gene expression by activating ERK signalling and downstream transcription factors (e.g. CREB) (Xu et al., 2008; Ji et al., 2009). In this regard, Ca^{2+} modulates ion channel function by insertion, phosphorylation, and changes in voltage gradients (Latremoliere and Woolf, 2009). It is proposed that calcium may also mediate polysynaptic sensitization in dorsal horn neurons contributing to mechanical allodynia, a key behavioural outcome of central sensitization (Latremoliere and Woolf, 2009).

Descending modulation

The most widely studied descending modulatory circuits involve the release of monoamine neurotransmitters, such as serotonin (5HT) and noradrenaline (NA), from the brainstem nuclei. As such, noradrenergic projections to the dorsal horn from the locus coeruleus (LC) play a key role in endogenous analgesia (Nakajima et al., 2012; Hoshino et al., 2014). The effects of 5HT in the spinal cord depends largely on the receptor subtype it activates. When

bound to 5HT-1A, 5HT-1B, and 5HT-1D receptors, 5HT inhibits nociception while activation of the 5HT-3 receptors facilitates nociceptive input (Ossipov et al., 2014). Anti-depressants, such as selective serotonin reuptake inhibitors and duloxetine, treat chronic pain by exploiting descending modulatory neurotransmitter levels in the spinal cord (Jann and Slade, 2007; Dharmshaktu et al., 2012). These medications are modest, at best, in treating chronic pain notwithstanding their severe side effects upon chronic use (Jann and Slade, 2007; Dharmshaktu et al., 2012).

A third descending circuit comes from the A11 nucleus of the hypothalamus and supplies dopamine (DA) to the spinal cord (Fleetwood-Walker et al., 1988). These neurons have not been as widely studied as descending NA or 5HT neurons but they are known to produce analgesia in naïve animals via activation of dorsal horn D2 receptors (D2Rs) (Taniguchi et al., 2011). While A11 neurons have classically been considered as the only source of DA in the spinal cord, recent data shows that a subset of DA transporter (DAT) expressing neurons are found in the outer lamina of the spinal cord (Kim et al., 2015; Megat et al., 2018). These neurons form elaborate rostral-caudal projections that penetrate deeper lamina of the spinal cord. The function of these newly identified DAT neurons is completely unknown.

Animal models of pain

The definition of an animal model is obscure in the literature. Some use it to define aspects of the subject (e.g. species, strain etc.) while others use it to define an assay used to induce pain (e.g. etiology of pain, time course of study etc.) (Mogil, 2009). Yet others consider an animal model to refer to an outcome measure (e.g. reflexes, operant behaviours etc.) (Mogil, 2009). A consistent definition is important since each of these interpretations may involve

distinct molecular mechanisms leading to pain hypersensitivity. The researcher, mainly based on the purpose of a study, chooses the most apt definition. To mimic clinical presentation of painful conditions, studies must use various subjects across a battery of assays to measure multiple pain-dependent behaviours.

Individual differences observed across patients and animals in their response to painful stimuli warrants the optimal choice of subjects for an experiment. This includes a careful consideration of a number of variables such as the genetic makeup of the test subjects, the sex of the subjects being examined as well as the subject's age. For example, while the chronic pain patient population consists primarily of ethnically diverse, middle-aged females, most basic science experiments commonly use young-adult, male Sprague-Dawley rats (Mogil and Bailey, 2010). It is now recognised that sex and genetic differences between strains of rodents may lead to different outcomes, thus demonstrating that there can be fundamentally different pathways of pain processing. For instance, peripheral injection of calcitonin-gene related peptide (CGRP) in C57BL/6 mice produces no significant thermal hypersensitivity while substantial hypersensitivity is noted in the AKR strain of mice (Mogil et al., 2005). In male mice, dextromethorphan (DXMP), a non-competitive NMDA blocker, potentiates the analgesic effects of morphine at low doses while attenuating analgesia at higher doses of morphine (Nemmani et al., 2004). The resulting large-scale clinical trial of Morphidex, a morphine sulphate-DXMP hydrobromide combination, did not reveal any significant effect of the drug. Later experiments revealed that DXMP administration leads to neither a potentiation nor an attenuation at any dose of morphine in female animals (Nemmani et al., 2004). While age may also play an important role in pain perception, housing animals for months or years to reach clinically relevant age may

not be practical and cost effective. Other subtle but important parameters such as husbandry must also be considered (Mogil, 2009).

Pain can be an overwhelming symptom of various diseases as well as be a disease in its own right. Assays assessing pain must also mirror such diverse etiology. Acute assays evaluate nociceptive pain by measuring simple pain behaviours, such as a reflex, following an acute noxious stimulus. Inflammatory assays are used to investigate supraspinal organization and their contribution to pain. These assays typically last longer due to their impact on the molecular milieu of a cell. As such, inflammatory assays may involve site appropriate induction with immune-activating compounds (e.g. carrageenan, complete Freund's adjuvant), and/or algesciogenic substances (e.g. pro-inflammatory cytokines, bradykinin) (Rang et al., 1991). Assays for neuropathic pain model pain caused by partial or complete damage to the somatosensory nerves. Partial injury to nerves are more common than complete transection injuries in a clinical setting (Mogil, 2009). In animal models, commonly used strategies involve constricting, cutting, ligating, freezing, inflaming, and depriving oxygen from nerves in the central or the peripheral nervous system (Mogil, 2009). Since many individuals face pain as a comorbid condition to an underlying syndrome, painful disease assays attempt to understand pain in a more clinically relevant context. This is achieved by modeling the fundamental disease or injury. Notable examples include low back pain (Shi et al., 2018), cancer pain (Lozano-Ondoua et al., 2013), multiple sclerosis pain (Khan and Smith, 2014), and spinal cord injury related pain (Kramer et al., 2017). The inability to fully recreate a disease state similar to humans in a model organism limits the functionality of these assays. Therefore, imitating pain in non-human subjects requires careful deliberation.

Measuring pain in an animal model is an inferential task. Behavioural correlates of pain seen in humans are only assumed to occur in non-human animals. Since these animals cannot speak, objectively measuring pain or more realistically, 'nociceptive' behaviours is a common strategy used to study pain and its therapeutics. Researchers commonly measure mechanical and thermal hypersensitivity employing evoked withdrawal paradigms as an indication of pain. However, these tests assess allodynia and hyperalgesia associated with pain (Mogil, 2009). The clinical prevalence of mechanical and thermal hypersensitivity in neuropathic pain is limited to 64% and 38%, respectively (Backonja and Stacey, 2004). Spontaneous pain is found universally in these patients but has largely been ignored in the basic scientific literature (Backonja and Stacey, 2004). A formalin injection to the hind paw leads to quantifiable spontaneous, long-lasting behaviours such as guarding, paw flinching, and licking (Tjølsen et al., 1992). Induction with inflammatory mediators and neuropathic injuries generate hypersensitivity in rodents but do not produce spontaneous behaviours, contrary to clinical presentation of neuropathic pain (Mogil, 2009). In addition, chronic pain patients often complain of negative affect, anxiety or depression, anhedonia, cognitive problems, sleep disruption, and functional disability (Turk et al., 2016). These complex states are less commonly studied in animal models and are not necessarily reliably replicated between experiments (Mogil, 2009). Accordingly, more clinically-relevant measures of pain need to be developed.

Experimental Autoimmune Encephalomyelitis

In order to study the pathophysiology of MS, the model of experimental autoimmune encephalomyelitis (EAE) is commonly used in research today (Iannitti et al., 2014). Although no model completely recapitulates all the features of the disease, EAE has been shown to be comparable with the immune-mediated effects of MS such as immune activation, myelin loss, gliosis, and axonal damage (Kipp et al., 2017). In addition, cognitive deficits in EAE have been noticed prior to the onset of motor symptoms similar to the clinical population (Olechowski et al., 2013). Thus, EAE may be used as a proxy for understanding the pathophysiology of MS.

EAE is generated by inoculating the animal, most commonly mice, with a peptide of a myelin protein emulsified in a strong adjuvant, such as complete Freund's adjuvant or CFA. In addition, inoculation with an immune activating factor (e.g. Pertussis toxin) enhances the chances of reliable EAE (Hofstetter et al., 2002). A combination of animal strain, the peptide used, emulsifying adjuvant, and immune stimulants largely determine the disease progression of EAE (Berard et al., 2010; Lu et al., 2012). As such, immunization of SJL mice with a fragment of myelin proteolipid protein (PLP₁₃₉₋₁₅₁) produces a relapsing-remitting disease course whereas C57BL/6 mice inoculated with myelin oligodendrocyte glycoprotein (MOG₃₅₋₅₅) generates a monophasic chronic disease course (Lu et al., 2012). However, a low dose of MOG₃₅₋₅₅ (50 µg) produces a monophasic relapsing-remitting form of EAE (Olechowski et al., 2009). Other models of EAE with variations of these factors have been reported in the literature (Iannitti et al., 2014; Wang et al., 2017a; Murphy et al., 2019). Since MS is a complex disorder that only affects humans, it is impossible to fully reproduce in animal models. Nonetheless, each variation on the EAE model hopes to capture multiple aspects of MS.

Couple weeks after inoculation with a myelin antigen, animals typically present with negative symptoms of the disease such as loss of muscle tone, paresis, paralysis, and hypoesthesia. Disease progression is usually scored from Grade 1 to Grade 5 (or a modified scale from 1 to 10), where each score increases with severity in paralysis ascending rostrally from the tail to the head (Olechowski et al., 2009; Lu et al., 2012). Although modified scales specific to each lab can also be found in the literature, the underlying criteria remains the same (Lu et al., 2012). This section will largely focus on myelin antigen induced rodent EAE models, particularly MOG₃₅₋₅₅ and PLP₁₃₉₋₁₅₁, because pain has predominantly been studied in these animals.

Pain in EAE

Rodents begin to show evoked pain behaviours before the onset of paralytic symptoms of EAE (Olechowski et al., 2009; Duffy et al., 2016; Thorburn et al., 2016). Common pain behaviours include mechanical allodynia, heat hyperalgesia, and noxious cold (Iannitti et al., 2014; Khan and Smith, 2014). Over the recent years, facial pain behaviours in EAE have been investigated using the grimace scale (Langford et al., 2010; Duffy et al., 2016), air puff test (Thorburn et al., 2016), and facial von Frey test (Duffy et al., 2016). Literature on spontaneous pain behaviours in EAE is limited (Duffy et al., 2016, 2019; Hu et al., 2018).

The combination of different EAE inocula and rodent strains produce different pain phenotypes in rodents. SJL mice inoculated with PLP₁₃₉₋₁₅₁ demonstrate a more profound heat hyperalgesic phenotype than MOG-induced C57BL/6 mice, in which thermal hyperalgesia is almost absent (Lu et al., 2012). On the other hand, evoked responses to von Frey filaments was more robust, indicative of mechanical allodynia, in MOG-C57 EAE mice than PLP-SJL mice. These signs correlated with stronger microglial activation and astrogliosis in the spinal cord in

SJL mice than C57 mice (Lu et al., 2012). Furthermore, MBP-inoculated rats also show heat and cold hyperalgesia before the onset of EAE signs of which heat hypersensitivity remains even after the motor symptoms have resolved (Thibault et al., 2011). Typically, pain in EAE precedes motor deficits similar to the MS population who complain of pain months to years before the onset of motor problems (Osterberg et al., 2005; Iannitti et al., 2014).

Sex differences in pain behaviours in EAE are not widely investigated. MOG-induced male EAE mice do not demonstrate mechanical and cold allodynia unlike female mice (Rahn et al., 2014). However, recent studies using a lower dose of MOG₃₅₋₅₅ peptide (50 µg) found that male and female EAE mice both develop mechanical hypersensitivity and cold allodynia (Catuneanu et al., 2019; Mifflin et al., 2019). Interestingly, over 80% of female mice develop mechanical hypersensitivity while roughly 60% of males develop this phenotype (Catuneanu et al., 2019). Of those that are hypersensitive to tactile stimulation, male EAE mice show mechanical allodynia in both hind paws while females have a unilateral response to von Frey stimulation (Catuneanu et al., 2019). These initial findings of sex differences in pain behaviours in EAE warrant further investigation.

Central mechanisms of pain in EAE

Pain in EAE is extensively linked to inflammation and damage in the spinal cord and the brain, particularly across the sensory/pain axis. Widespread inflammation is commonly noted in the CNS of EAE animals. In response to disease, peripherally-derived T-cells, notably CD25⁺ regulatory T-cells (Treg) and CD4⁺ Th1 and Th17 cells, infiltrate the spinal cord and the brain (Olechowski et al., 2009; Duffy et al., 2016, 2019; Catuneanu et al., 2019). These T-cells are reactive to myelin antigens used to induce EAE. Adoptive transfer of CD4⁺ myelin-reactive T-cells from EAE animals is sufficient to induce EAE symptoms in recipient animals (McPherson

et al., 2014). Th1 and Th17 subset of T-cells are pathogenic in EAE while regulatory T-cells are protective (Duffy et al., 2019; Van Kaer et al., 2019). A recent study found that adoptive transfer of Tregs or intrathecal administration of a Treg-derived cytokine, IL35, increased production of anti-inflammatory cytokine IL10 in lymphocytes, limited monocyte infiltration, and alleviated pain in EAE (Duffy et al., 2019). Macrophage and microglial activation is also observed in EAE (Olechowski et al., 2009; Duffy et al., 2016, 2019; Chu et al., 2018; Catuneanu et al., 2019). Activated macrophages and microglia contribute to the inflammatory milieu of the CNS by releasing a plethora proinflammatory cytokines. With the progression of the disease, microglia and macrophages assume a more protective role by producing anti-inflammatory mediators like IL-10 and TGF- β which may further suppress EAE disease (Weber et al., 2007). These cells are more phagocytic than their proinflammatory counterparts (Kocur et al., 2015). Moreover, anti-inflammatory microglia and macrophages can enhance Treg function and reduce Th1 activity, further dampening disease severity (Weber et al., 2007; Kong et al., 2016). Pain behaviours in EAE are also correlated with increased astrocyte activation (Olechowski et al., 2009; Duffy et al., 2016; Catuneanu et al., 2019). As immune regulators, astrocytes have both beneficial and harmful effects in EAE. Astrocytes form the blood-brain barrier and are among the first to be contacted by invading leukocytes (Brambilla, 2019). Reactive astrocytes also secrete chemokines and cytokines, reduce production of growth factors, release excessive glutamate, and generate reactive oxygen species all of which accelerates the disease process (Brambilla, 2019). Counterintuitively, ablating GFAP⁺ reactive astrocytes in EAE exacerbates the disease suggesting that astrocytes may also have a protective role in EAE (Voskuhl et al., 2009). Although various studies have investigated the role of peripheral and central immune-mediating cells in EAE disease course, the exact mechanism of how these cells contribute to pain

hypersensitivity in EAE still remains to be investigated. For an excellent review on central mechanisms of pain in EAE/MS please see Khan and Smith (2014).

Peripheral mechanisms of pain in EAE

T-cells are known to infiltrate peripheral tissue in EAE (Duffy et al., 2016; Frezel et al., 2016; Thorburn et al., 2016; Please see Chapter 1 for further discussion). However, literature on the macrophage composition of the sensory ganglia during EAE has been limited. Recent studies show an increase in Iba1+ macrophages in the TG and the DRG (see Chapter 1) only at the onset of EAE signs (Thorburn et al., 2016; Yousuf et al., 2019). The TREZ, however, hosts cells with increased Iba1 reactivity, both macrophages and microglia, with the onset of EAE extending into the peak and chronic phases (Duffy et al., 2016; Thorburn et al., 2016). Variations within the macrophage and monocyte populations in the sensory ganglia of EAE animals have not been thoroughly investigated. Although both DRG and TG form sensory ganglia in the peripheral nervous system, recent data suggests that both ganglia are transcriptionally different (Megat et al., 2019). Hence, it may be reasoned that each ganglia experiences a different flavour of inflammation as evident by the presence of certain immune cells, particularly T-cells, throughout the disease course (Duffy et al., 2016).

Molecular analyses of the dorsal root ganglia of EAE mice link increases in cytokines, such as TNF α (Begum et al., 2013) and IL1 β (Rodrigues et al., 2016), chemokines, including CXCL1 (Rodrigues et al., 2016) and CX3CL1 (Zhu et al., 2013), and neurotrophic factors, like BDNF (Zhu et al., 2012), to neuropathic pain in EAE. In this regard, subcutaneously administering blocking antibodies for IL1 receptor was able to reverse mechanical allodynia in EAE mice (Rodrigues et al., 2016). Since the administration of this antibody was performed

systemically, it is not known if its antinociceptive effects were solely due to its effect in the PNS. IL1 β and its receptor are known to be increased in the spinal cord as well (Rodrigues et al., 2016). Hence, a more rigorous analysis of immune factors in the sensory ganglia, particularly contributing to pain hypersensitivity is required to elucidate the contribution of peripheral immune mechanisms.

Activation of satellite glial cells (SGCs) in the sensory ganglia have previously been linked to neuropathic pain. Upon activation, satellite glial cells and astrocytes upregulate glial fibrillary acidic protein (GFAP). In the sensory ganglia of EAE mice, SGCs are activated with the onset of EAE signs (Warwick et al., 2014; Thorburn et al., 2016). By about day 35, the expression of GFAP normalizes to control levels in the TG (Thorburn et al., 2016). Further analysis of activated SGCs in EAE reveal an increased gap junction coupling between activated cells (Warwick et al., 2014). SGC activation and gap junction coupling has been associated in a variety of other pain models (Huang et al., 2010; Warwick and Hanani, 2013; Hanani et al., 2014). Whether SGC activation contributes to influx of immune cells and neuronal injury or is a by-product of these mechanisms in EAE remains to be investigated.

Chloride homeostasis

Ion transporters can use ATP to actively pump ions against their gradients or use the electrochemical potential of another ion (often referred to as ion exchangers). Since sodium and potassium are abundant ions in the body, they are commonly used as a driving ion to transport another ion (known as the driven ion) in the same direction (symporters) or in the opposite direction (antiporters). The nervous system has a plethora of different ion transporters. For brevity, this chapter will focus on chloride co-transporters, $\text{Na}^+\text{-K}^+\text{-2Cl}^-$ co-transporter 1 (NKCC1) and $\text{K}^+\text{-Cl}^-$ co-transporter 2 (KCC2), as they relate to GABAergic transmission and ultimately, to neuropathic pain.

Chloride co-transporters

NKCC1 and KCC2 are crucial for determining the strength and polarity of GABA (Price et al., 2005). NKCC1 actively transports sodium, potassium and chloride ions into the cell whereas KCC2 pushes potassium and chloride outwards. Phosphorylation of these transporters (pNKCC1, pKCC2) is proposed to enhance transporter activity by improving ion transport rate, cell surface stability and plasma membrane trafficking (Kahle et al., 2013; Alessi et al., 2014; Modol et al., 2014). Their activity is predominantly regulated through this process (Kahle et al., 2013; Modol et al., 2014). When GABA_A/glycine receptors are activated, chloride ions either leave or enter the cell. The influx or efflux of chloride is determined by its electrochemical gradient established by these chloride cotransporters (Price et al., 2005). When chloride leaves the cell, intracellular electrochemical potential becomes further depolarized. On the contrary, when chloride extrusion mechanisms are prevalent, chloride seeks to enter the cell leading to greater hyperpolarization. Since the DRG neurons express very little to no KCC2, the intracellular chloride levels are maintained predominantly by NKCC1 (Price et al., 2005; Modol

et al., 2014). This leads to an excitatory effect of GABA in the periphery as opposed to an inhibitory effect seen in CNS where KCC2 is abundant (Hasbargen et al., 2010).

Under normal conditions, a neuron's membrane potential is at or around -70 mV, although the exact value depends on a whole host of factors. The anion reversal potential (E_{anion}) of chloride ions is also around -70 mV (Price et al., 2009). In these conditions, opening of GABA_A receptors does not lead to chloride influx since the driving force for chloride ions is minimal, if any.

Simultaneous application of excitatory input is significantly dampened as chloride ions seek to maintain an E_{anion} of -70 mV through open GABA_A receptors (Price et al., 2009). This phenomenon is termed shunting and is contrasted with hyperpolarization in which a large driving force pushes K⁺ ions out of the cell. In the case of a neuron, the extracellular and intracellular E_{anion} is maintained by a balance of NKCC1 and KCC2 which regulate chloride homeostasis. At birth, NKCC1 levels are abundant in neurons leading to a relatively higher concentration of chloride inside the cell than outside. This makes GABA excitatory during this period. Around about the third week after birth, there is an active suppression of NKCC1 expression and an upregulation of KCC2 in the CNS. Thereby, chloride ions are removed from the cell and E_{anion} is reversed (Fitzgerald and Gibson, 1984; Falcon et al., 1996; Jiang and Gebhart, 1998; Teng and Abbott, 1998; Marsh et al., 1999). Neurons in the periphery do not experience such a shift and continue to experience GABAergic input as excitatory into adulthood (Price et al., 2005).

In the spinal cord, local GABAergic interneurons form axo-axonic synapses onto primary afferent terminals leading to primary afferent depolarization (PAD) (Zeilhofer et al., 2012). With abundance of NKCC1 on the primary afferent terminals, intracellular chloride concentration is high compared to the extracellular space. This leads an efflux of chloride ions in response to GABA and a small depolarization current is passed through the terminal (Price et al., 2005;

Zeilhofer et al., 2012). In contrast to depolarizations elsewhere in the nervous system, PAD leads to a decrease in neurotransmitter release by inactivating voltage-gated sodium and voltage-gated calcium channels, and by shunting through open GABA_A channels (Price et al., 2009; Zeilhofer et al., 2012; Price and Prescott, 2015). In this regard, PAD is seen as a form of presynaptic inhibition. However, sufficient increase in PAD may lead to propagation of antidromically conducting action potentials (known as dorsal root reflexes (DRR)) and further the release of neurotransmitters (Rees et al., 1994; Lin et al., 1999; Garcia-Nicas et al., 2001; Price et al., 2009; Chen et al., 2014a; Price and Prescott, 2015). Administration of GABA_A receptor antagonists (Lin et al., 1999, 2007a) and NKCC1 antagonist, bumetanide (Valencia-de Ita et al., 2006), prevent the development of DRRs. The exact mechanism of DRRs is not yet resolved.

KCC2 expression in dorsal horn neurons is important in maintaining the inhibitory tone of GABA. It helps maintain a relatively low intracellular chloride concentration such that GABAergic/glycinergic input leads to a chloride influx, hyperpolarization, and ultimately, inhibition (Gagnon et al., 2013; Price and Prescott, 2015). Local GABAergic interneurons synapse onto lamina I projection neurons and modulate its activity based on incoming sensory input from primary afferents, descending input from the brain, and complex local circuitry. Reduction of KCC2 expression forms the basis of disinhibition seen in various models of neuropathic pain (Nomura et al., 2006; Miletic and Miletic, 2008; Zhang et al., 2008; Hasbargen et al., 2010; Gagnon et al., 2013; Modol et al., 2014; Price and Prescott, 2015). Microglial activation has been shown to cause disinhibition in lamina I neurons (Beggs and Salter, 2013). After peripheral nerve injury, microglia release brain-derived neurotrophic factor (BDNF) as a result of P2X₄ receptor activation. BDNF then binds to TrkB receptors on lamina I neurons leading to a downregulation of KCC2. Through disinhibition, projection neurons become less

hyperpolarized in response to GABAergic transmission and more sensory and nociceptive information travels to the brain.

Implications for pain

Chloride co-transporters have the potential to alter the effects of GABA on primary afferent terminals and higher-order neurons of the spinal cord. In various neuropathic pain models, NKCC1 and KCC2 expression and post-translational modifications significantly change across injury and/or disease. In a contusion model of spinal cord injury in rats, NKCC1 levels were shown to increase while KCC2 levels decreased by day 7 post-injury, coinciding with observed hyperalgesia (Hasbargen et al., 2010). In a recent study, peripheral nerve injury lead to an upregulation of NKCC1 in the DRG, a downregulation of KCC2 in the spinal cord, and a temporally later decrease in KCC2 expression in the thalamus and the somatosensory cortex (Modol et al., 2014). Similarly, chronic constriction injury resulted in increased NKCC1 levels in the DRG and decreased KCC2 expression in the dorsal horn 2 days post-injury (Chen et al., 2014a). These changes are largely transient and disappear with time even though pain behaviours persist. This indicates that initial response to a neuropathic insult may be due to transient non-synaptic plasticity while pain at later, chronic stages may be a result of long lasting synaptic plasticity.

Earlier studies using NKCC1 knockout mice discovered that these mice had impaired noxious heat processing (Sung et al., 2000). Although NKCC1 is crucial for development but not necessary, NKCC1 knockout mice have a mortality rate of 30% before weaning (Sung et al., 2000). Those mice that do survive face various comorbidities ranging from poor motor coordination to severe cognitive impairments (Sung et al., 2000). Due to potential confounds in

this methodology, later studies have focused on using pharmacological agents, such as bumetanide, to inhibit NKCC1 in neurons. Although bumetanide has been shown to be effective in dampening pain across various models of neuropathic pain (Sung et al., 2000; Valencia-de Ita et al., 2006; Pitcher et al., 2007; Modol et al., 2014), it is a poor agent to study the role of NKCC1 in neurons due to its lack of specificity for NKCC1 and the widespread expression of NKCC1 throughout the body (Price et al., 2009). Intraperitoneal administration of bumetanide not only affects NKCCs (NKCC1 and NKCC2) in the PNS but also in the kidneys and exocrine glands (Hannaert et al., 2002). Any effects observed after a systemic injection of bumetanide must be subjected to these confounding factors.

Efforts to identify a pharmacological agent for enhancing KCC2 in the spinal cord have mainly been hindered by lack of specificity. Recent research has however identified CLP257 and CLP290 as a selective KCC2 activators (Gagnon et al., 2013). As a prodrug of CLP257, CLP290 was designed to protect its hydroxyl group from glucuronidation. CLP257 generated from the body's metabolism of CLP290 is more potent and longer lasting than CLP257 given intraperitoneally. Regardless, administration of both these compounds has been reported to enhance Cl⁻ transport and increase recruitment of KCC2 to the plasma membrane (Gagnon et al., 2013). Behaviourally, this alleviates pain hypersensitivity in rats with peripheral nerve injury (Gagnon et al., 2013). Since KCC2 is only found in neurons of the central nervous system, administration of CLP257 and CLP290 are not subjected to the same confounding factors as bumetanide for inhibiting NKCC1. The effects of these compounds have not been widely studied in pain models due to their novelty.

Endoplasmic Reticulum Homeostasis

The endoplasmic reticulum (ER) is perhaps the largest tubular organelle in the cell (Verkhatsky, 2005). In neurons, the ER is continuous throughout the cell extending from the dendritic arbors to the cell soma, across the axon and into the presynaptic terminals (Terasaki et al., 1994). The ER has classically been subdivided into rough ER (containing ribosomes), smooth ER (without ribosomes) and the nuclear envelope (Verkhatsky, 2005). The ER performs a variety of functions. Particularly, it is the site of protein synthesis and maturation with the help of a plethora of luminal and transmembrane chaperones and foldases (Hetz and Mollereau, 2014). In addition to protein synthesis, the ER is also important for lipid synthesis. As such, the smooth ER synthesizes phospholipids, glycolipids, and cholesterol which are used for various functions such as synthesizing steroid hormones from cholesterol (Stevenson et al., 2016). The ER also contains many detoxifying enzymes which particularly metabolize lipid soluble molecules by converting them into polar, water-soluble compounds that are then secreted from the cell and the body (Jacquemyn et al., 2017). The ER is also the cell's largest dynamic repository of Ca^{2+} (Krebs et al., 2015). Many of the ER's chaperones (e.g. BiP, calreticulin, calnexin, etc.) are low-affinity, high-capacity Ca^{2+} binding proteins essentially functioning as Ca^{2+} binding proteins (Krebs et al., 2015). Their function as chaperones also heavily depends on the luminal concentration of Ca^{2+} (Suzuki et al., 1991). Since the ER extends throughout the cell, it also serves as a highway for RNAs, proteins, lipids, and ions (Verkhatsky, 2005). Changes in the intraluminal environment of the ER, such as increased protein synthesis and altered Ca^{2+} homeostasis, may lead to ER stress which is initially protective but detrimental in the long-term (Hetz et al., 2019). Therefore, the ER is a versatile organelle capable of responding to environmental stimuli allowing the cell to react accordingly.

Unfolded protein response

Protein synthesis, folding, and quality control are canonical functions of the ER. Upon increased protein demand, the ER responds to an accumulation of unfolded or misfolded proteins by initiating a series of cellular processes collectively known as the unfolded protein response (UPR) (Martínez et al., 2018). The goal of the UPR is to reduce translation of proteins, increase the expression of chaperones, and degrade misfolded proteins. This response is mediated by three downstream transducers: Protein kinase RNA-like ER kinase (PERK), inositol-requiring enzyme 1 α (IRE1 α), and activating transcription factor 6 (ATF6) (Martínez et al., 2018). Each of these ER resident proteins contains a single transmembrane domain and a single luminal domain (Diehl and McQuiston, 2017). Under stressed conditions, binding immunoglobulin protein (BiP; also known as heat shock protein A 5, HSPA5, and glucose response protein 78, GRP78) dissociates from ATF6, PERK, and IRE1 α activating their respective arm of the UPR (Martínez et al., 2018). BiP actively folds unfolded proteins using its allosteric ATPase activity and prevents the formation of protein aggregates by binding and restraining unfolded proteins (Fujimori et al., 2017; Wang et al., 2017b).

Once BiP is sequestered from PERK's luminal domain, PERK autophosphorylates and oligomerizes as either a dimer or a transient tetramer (Ma et al., 2002). It may be further postulated that the extent of oligomerization of PERK may represent the degree of unfolded proteins in the ER since the tetramer configuration is a more potent kinase than the dimer (Carrara et al., 2015). Upon activation, PERK phosphorylates eukaryotic initiation factor 2 α (eIF2 α) reducing general translation of proteins while enhancing translation of select mRNAs particularly those that encode an upstream open reading frame (uORF) (Khoutorsky and Price, 2018). In particular, eIF2 α phosphorylation enhances the expression of activating transcription

factor 4 (ATF4) which in turn increases the expression of the proapoptotic transcription factor C/EBP homologous protein (CHOP) (Martínez et al., 2018).

PERK-mediated phosphorylation of eIF2 α in UPR is just one aspect of a larger translational regulation pathway known as the integrated stress response (ISR) (Khoutorsky and Price, 2018). Stressful conditions such as amino acid deprivation, viral infection, heme deficiency, and accumulation of unfolded proteins lead to the activation of general control nonderepressible 2 kinase (GCN2), protein kinase R (PKR), heme-regulated eIF2 α kinase (HRI), and PERK, respectively (Pakos-Zebrucka et al., 2016). As part of the ISR, these kinases converge onto the phosphorylation of eIF2 α regulating its translational control and allowing the cell to aptly react to the stressor (Tahmasebi et al., 2018).

eIF2 α is a subunit of the larger eIF2 complex consisting of additional β and γ subunits (Khoutorsky and Price, 2018). The eIF2 complex binds to guanosine triphosphate (GTP)-methionine bound transfer RNA (tRNA^{Met}), and the 40S ribosomal subunit to create a pre-initiation complex. GTP hydrolysis to GDP mediates the initiation of mRNA translation. Conversion of the now inactive eIF2-GDP complex to the active eIF2-GTP is mediated by eIF2B, a guanine nucleotide exchange factor (Khoutorsky and Price, 2018). Under conditions of cellular stress, phosphorylation of eIF2 α stabilizes the inactive eIF2-GDP-eIF2B complex preventing the recycling of GDP and reducing the ability of eIF2 to further initiate translation (Khoutorsky and Price, 2018). Ultimately, this leads to a reduction in general translation while ironically increasing the translation of mRNAs with a uORF in their 5' untranslated region (5' UTR). Many of these genes allow the cell to appropriately respond to stress, such as ATF4, while other genes may code for other translational repressors (Martínez et al., 2018). ATF4, the most thoroughly studied transcription factor induced by eIF2 α , increases the expression of ER

chaperones to mitigate ER stress (Diehl and McQuiston, 2017). It also induces the expression of CHOP, a proapoptotic transcription factor, which in turn enhances the expression of more apoptotic genes (Harding et al., 2000). CHOP directly mediates apoptosis by inducing the expression of Bim and Puma which inhibit the activity of Bcl-2, a protective protein localized to the outer membrane of the mitochondria (Puthalakath et al., 2007). Under normal conditions, Bcl-2 actively prevents the activation of proapoptotic Bak and Bax proteins which seeks to permeablize the mitochondria and release cytochrome C and reactive oxygen species (Ning et al., 2019). However, inhibition of Bcl-2 releases this braking mechanism allowing for the permeablization of the mitochondria and consequent cell death (Diehl and McQuiston, 2017). ATF4 and CHOP expression also negatively regulates the phosphorylation of eIF2 α through the expression of protein phosphatase 1 (PP1) allowing the cell to recover general translation (Han et al., 2013). In this manner, stressors, like accumulation of unfolded proteins, may shape the translome, and hence the fate, of a cell (Tahmasebi et al., 2018).

IRE1 α was first discovered in yeast cells and has been shown to be the most evolutionarily conserved ER protein (Nikawa and Yamashita, 1992; Junjappa et al., 2018). As a result, IRE1 α plays an important role in variety of cellular signalling pathways ranging from ER stress to inflammation (Junjappa et al., 2018). IRE1 α consists of a luminal domain, a transmembrane domain, and an enzymatic cytosolic domain with both kinase and endoribonuclease activity (Cox et al., 1993). Under physiological conditions, BiP is bound to the luminal domain of IRE1 α preventing its activation (Okamura et al., 2000). Upon accumulation of misfolded or unfolded proteins in the ER lumen, BiP dissociates from IRE1 α allowing it to dimerize and autophosphorylate its cytosolic domain which in turn initiates its enzymatic activity (Shamu and Walter, 1996). In a non-canonical fashion, misfolded proteins themselves could

directly activate IRE1 α (Karagöz et al., 2017). Further oligomerization of IRE1 α enhances its response to ER stress (Korennykh et al., 2009). The endoribonuclease activity of IRE1 α splices X-box binding protein 1 (XBP1) mRNA giving rise to a spliced isoform of XBP1 (XBP1s) (Calfon et al., 2002). As a potent transcription factor, XBP1s induces the expression of various genes including those involved in the alleviation of ER stress such as Hspa5 (BiP) and heat shock proteins (like DnaJ) (Lee et al., 2003). In addition to splicing XBP1 mRNA, IRE1 α also cleaves other mRNA in a process called regulated IRE1-dependent decay (RIDD) (Hollien et al., 2009). Degradation of mRNA alleviates ER stress by reducing protein synthesis. Cleaved and degraded mRNA fragments may also contribute to inflammation (Lencer et al., 2015).

UPR-mediated IRE1 α activation is protective under physiological conditions, however, chronic activation of IRE1 α initiate more detrimental, apoptotic pathways (Junjappa et al., 2018). In particular, the cytosolic domain of phosphorylated IRE1 α bind TNF receptor-associated factor 2 (TRAF2) and apoptosis signalling kinase 1 (ASK1) which phosphorylate c-Jun N-terminal kinase (JNK) (Zhang et al., 2016). Activated JNK induces apoptosis by inhibiting the anti-apoptotic Bcl-2 while activating proapoptotic BaX and BaD proteins (Yamamoto et al., 1999; Wang et al., 2007). Mitochondrial localization of these proteins then increases cytosolic release of ROS and cytochrome C which further contribute to inflammation and caspase activation (Yoneda et al., 2001; Win et al., 2014). Inflammation and cell death may also be induced by activation of AP1 and NF κ B which enhance the expression of proinflammatory cytokines (like TNF) and proapoptotic genes (Kaneko et al., 2003; Hu et al., 2006). Inflammatory cytokines further activate their receptors, particularly in immune cells, in an autocrine, feedforward manner (Hu et al., 2006). Receptor-interacting serine/threonine protein kinase 1 (RIPK1) is also known

to bind to IRE1 α stimulating caspase 8 activity and ultimately contributing to downstream caspase 9 and caspase 3 mediated cell death (Estornes et al., 2015).

Another resident ER stress transducer is ATF6 which is less well researched than the other two arms. Two homologs of ATF6 exist: ATF6 α and ATF6 β . More is known about the former ATF6 α than the latter (Hillary and FitzGerald, 2018). ATF6 α is a more potent transcription factor than ATF6 β (Thuerauf et al., 2007). ATF6 belongs to a basic leucine zipper (bZIP) family of transcription factors (Hillary and FitzGerald, 2018). With the accumulation of misfolded proteins in the ER, BiP dissociates from ATF6 exposing two Golgi-localization sequences on the protein (Chen et al., 2002). ATF6, then, translocates to the Golgi apparatus where it is cleaved at two locations on the N-terminal removing the transmembrane domain and releasing a cleaved 50 kilo-Dalton ATF6 fragment (ATF6f) (Shen et al., 2002). As a transcription factor, ATF6f contributes to the IRE1 α arm by increasing the transcription of the Xbp1 gene as well as genes for chaperones such as BiP (Lee et al., 2002). It also induces the expression of ER proteins associated with misfolded protein degradation such as ER degradation enhancing α -mannosidase-like protein 1 (EDEMI) and protein disulphide isomerase-associated 6 (PDIA6) (Vekich et al., 2012).

Ca²⁺ regulation

The ER is the largest repository for intracellular Ca²⁺ (Verkhatsky, 2005). Since Ca²⁺ is a multifunctional molecule involved in a variety cellular processes, the ER can directly impact gene expression, bioenergetics, ion channel physiology, and even enzyme function (Verkhatsky, 2005). With the presence of Ca²⁺ transporters on the ER membrane, the ER can be excited to release or sequester Ca²⁺ tightly regulating the concentration of available cytosolic Ca²⁺. In the

ER, Ca^{2+} is stored as bound to Ca^{2+} binding proteins (CBPs), many of which are chaperones, like calnexin, calreticulin, and BiP (Verkhatsky, 2005; Krebs et al., 2015). By and large, each CBP binds to many Ca^{2+} molecules in a low-affinity, high capacity manner such that the opening of a Ca^{2+} exporters allows for the immediate dissociation of Ca^{2+} from the CBPs (Krebs et al., 2015). Ca^{2+} efflux from the ER is mediated by Ca^{2+} -sensitive ryanodine receptors (RyRs) and inositol triphosphate receptor (IP3Rs) while the influx of Ca^{2+} into the ER is mediated sarco(endo)plasmic reticulum Ca^{2+} -ATPase (SERCA) pumps.

RyRs are named after their antagonist, ryanodine, which was originally used as an insecticide. RyRs are one of the largest membrane proteins consisting of four-identical subunits arranged in a four-leaf clover-shaped structure (Inui et al., 1987; Zalk et al., 2015). There are three variants of RyRs (RyR1, RyR2, and RyR3) all of which can be activated by free Ca^{2+} in the cytosol in a process known as Ca^{2+} -induced Ca^{2+} release or CICR (Verkhatsky, 2005). RyR1 is the most sensitive to cytosolic Ca^{2+} followed by RyR2 and then RyR3 (Chen et al., 1997; Murayama and Ogawa, 1997). RyR3s were classically known as the “brain” isoform however all three isoforms can be detected in the nervous tissue spanning across different cell types, being expressed in virtually every cellular compartment (Murayama and Ogawa, 1996; Rossi et al., 2002; Krebs et al., 2015). RyRs have poor selectivity for Ca^{2+} , instead they also counter-conduct other ions such as Mg^{2+} , Li^+ , Na^+ , and K^+ (Gillespie et al., 2012). This allows the channel to release Ca^{2+} without largely affecting the membrane potential (Gillespie et al., 2012). RyRs can associate with other proteins to further enhance a cellular Ca^{2+} response (Van Petegem, 2015). Voltage-gated calcium channels and Ca^{2+} -sensitive big K^+ (BK) channels are functionally coupled to RyRs (Tully and Treistman, 2004; Irie and Trussell, 2017). As a result, cytosolic Ca^{2+} increase due to neuronal activity can enhance Ca^{2+} release from the ER which in turn readily

affects action potential dynamics via Ca^{2+} sensitive channels (Irie and Trussell, 2017). A growing number of diseases and conditions are linked to impaired RyR function such as genetic RyR mutations in malignant hyperthermia, central core disease, and catecholaminergic polymorphic ventricular tachycardia (Rosenberg et al., 2007; Manotheepan et al., 2016; Chen et al., 2017). Aberrant RyR function has been implicated in neurodegenerative disorders, like Alzheimer's disease (Del Prete et al., 2014).

IP3Rs are another class of ER Ca^{2+} release channel. IP3Rs respond to inositol triphosphate (IP3) which is catalyzed by phospholipase C (PLC) typically after the activation of plasmalemmal G-protein coupled receptors (GPCRs) such as metabotropic glutamate receptors (Krebs et al., 2015). Like the RyRs, there are 3 types of IP3Rs: IP3R1, IP3R2, and IP3R3. The channel may form as homo- or hetero-tetramers (Krebs et al., 2015). IP3Rs could be further modulated by (de)phosphorylation by various kinases, like protein kinase A, B, and C, and phosphatases like calcineurin (Vanderheyden et al., 2009). Further splice variations in the IP3R genes allow for even more channel functional diversity despite 60-80% shared homology among IP3R isotypes (Krebs et al., 2015). IP3Rs open when both IP3 and Ca^{2+} bind to the receptor (Taylor and Tovey, 2010). It is believed that IP3 primes the receptor to cytosolic Ca^{2+} which allows for the opening of the channel in a Ca^{2+} -dependent manner (Taylor and Tovey, 2010). IP3R1s are maximally activated around 300-400 nM of Ca^{2+} beyond which they lose their sensitivity to intracellular Ca^{2+} (Bezprozvanny et al., 1991). In contrast, IP3R2s and IP3R3s are not inhibited by high Ca^{2+} concentration (Hagar et al., 1998). Activation of the IP3Rs may lead to widespread Ca^{2+} waves or be confined to microdomains depending on the sensitivity of IP3Rs to IP3, the density of IP3Rs, degradation of IP3, and the buffering capacity for IP3 (Verkhatsky, 2005). Since IP3Rs are co-activated by intracellular Ca^{2+} , RyR mediated CICR enhances Ca^{2+}

release from IP3Rs (and vice-versa) possibly contributing to widespread Ca^{2+} waves in the ER (Verkhatsky, 2005; Taylor and Tovey, 2010).

Cytosolic Ca^{2+} concentrations are tightly regulated by SERCA pumps. These channels belong to a class of P-type Ca^{2+} ATPases that respond to increases in intracellular Ca^{2+} levels by actively sequestering the ion from the cytosol into the ER (Krebs et al., 2015). Like other ER Ca^{2+} transporters, there are three paralogs of SERCA: SERCA1, SERCA2, and SERCA3. SERCA2 is further differentiated by its spliced isoforms, SERCA2a and SERCA2b. Of particular interest is SERCA2b which is ubiquitously expressed in nervous tissue (Verkhatsky, 2005). SERCA2b activity is modulated by Ca^{2+} -sensitive calreticulin and ER resident protein 57 (ERp57), both of which also function as chaperones (John et al., 1998; Li and Camacho, 2004). When Ca^{2+} decreases in the ER lumen, calreticulin binds to SERCA2b increasing its activity while ERp57 functions as a thiol oxidoreductase, catalyzing disulfide bridges and enhancing Ca^{2+} uptake. Hence, luminal Ca^{2+} concentration inversely determines the rate of Ca^{2+} uptake by SERCA such that channel activity peaks at low luminal Ca^{2+} concentrations and wanes at higher concentrations (Verkhatsky, 2005). With drastic increase in cytosolic Ca^{2+} (e.g. during an action potential), other transporters with a greater capacity for Ca^{2+} such as mitochondrial calcium uniporter (MCU) and $\text{Na}^+/\text{Ca}^{2+}$ exchanger (NCX), can further support Ca^{2+} homeostasis (Krebs et al., 2015).

Summary and Purpose

Multiple sclerosis (MS) is an immune-mediated disorder characterised by inflammation, demyelination, and neurodegeneration. Among a variety of symptoms, chronic pain afflicts majority of the MS population at some point in their disease. Pain in MS is a debilitating condition, severely impacting an individual's quality of life. Neuropathic pain is described as pain due to an injury or disease of the somatosensory nervous system. The pain axis consists of sensory neurons in the periphery, the spinal cord, and the brain. Pain is thought to arise as a result of increased excitability along the pain pathways. The experimental autoimmune encephalomyelitis (EAE) model is typically employed to investigate immune-mediated effects of MS. Traditionally, pain in MS and EAE have been studied in the context of the pathology observed in the CNS. However, the contribution of the PNS remains to be thoroughly investigated. This dissertation aims to implicate sensory neurons of the DRG in EAE and MS in mediating pain hypersensitivity.

Aim 1: Peripheral Sensitization

In Chapter 1, I characterized immune cell infiltration, inflammation, and cytoskeletal disruption in the DRGs of EAE mice. Using whole-cell patch clamp recordings, I also assessed the electrophysiological properties of diseased versus control dissociated DRG neurons.

Hypothesis 1:

DRG neurons from EAE mice undergo inflammation and injury as well as sensitization, contributing to pain hypersensitivity.

Aim 2: Chloride homeostasis

In Chapter 2, I explored the contribution of chloride co-transporters, NKCC1 and KCC2, in mediating pain in EAE. Using molecular techniques, I established the expression of NKCC1 and KCC2 in the DRG and the spinal cord. Bumetanide, an NKCC1 inhibitor, was used to further investigate the role of NKCC1 in sensory neurons.

Hypothesis 2:

Levels of chloride co-transporters will be altered in the state of pain in EAE and bumetanide treatment will reduce nociceptive behaviours associated with EAE.

Aim 3: Endoplasmic reticulum stress

In Chapter 3, I investigated the cellular mechanisms of pain hypersensitivity in the DRG. As such, I explored the role of ER stress in altering Ca²⁺ dynamics and excitability of sensory neurons. I also assessed immune activation, inflammation, and ER stress in the DRGs obtained from post-mortem MS patients.

Hypothesis 3:

ER stress will enhance Ca²⁺ responsiveness and excitability of sensory neurons in EAE.

Chapter 1 : Sensory neurons of the dorsal root ganglia become hyperexcitable in a T-cell mediated MOG-EAE model of multiple sclerosis

Introduction

Multiple sclerosis (MS) is an autoimmune disorder that is characterized by inflammation and demyelinating lesions that target the brain and spinal cord (SC), ultimately leading to neurodegeneration (Hemmer et al., 2015). Common symptoms of MS involve visual, motor, and sensory changes including neuropathic pain (Benson and Kerr, 2014). Over half of MS patients will experience neuropathic pain at some point during the course of their disease (Drulovic et al., 2015). Neuropathic pain is associated with disability, depression, and anxiety which ultimately contribute to a poorer quality of life (Drulovic et al., 2015). Current therapies to alleviate pain in this population have largely been ineffective (Truini et al., 2013).

While the pathological features of MS and EAE are focused in the CNS, sensory neurons residing in the dorsal root and trigeminal ganglia (DRG, TG) also undergo significant changes in response to chronic, concomitant CNS inflammation (Duffy et al., 2016; Thorburn et al., 2016; Yousuf et al., 2017). A significant body of literature emerging from the rodent model of MS, myelin oligodendrocyte glycoprotein-induced experimental autoimmune encephalomyelitis (MOG-EAE), demonstrates that the DRG and TG undergo major pathological changes with disease progression (Duffy et al., 2016; Thorburn et al., 2016; Yousuf et al., 2017). Indeed, there is evidence of leukocyte invasion and increased pro-inflammatory cytokine expression in the sensory ganglia of rats and mice with EAE (Melanson et al., 2009; Begum et al., 2013; Duffy et

al., 2016; Frezel et al., 2016; Rodrigues et al., 2016). It is unclear, however, how the physiological properties of the primary sensory neurons of the DRG are affected in the diseased state.

Neuropathic pain is postulated to involve sensitization, or enhanced signalling, along the primary afferent pain pathway. Nociceptors are a specialized class of neural cell in the PNS that encode painful stimuli across various modalities such as noxious heat, chemicals, and mechanical stimulation. In concert with other sensory neurons, nociceptors inform the central nervous system about the nature, location, and intensity of the painful stimulus. Primary afferents are classified across various combinations of myelination status, response characteristics, cell soma size, and specific molecular markers (Basbaum et al., 2009). Among these, nociceptors are generally classified as unmyelinated, small-diameter C-fibres or lightly myelinated, medium-diameter A-delta fibres that respond to multiple modalities to produce slow pain (C-fibres) and fast pain (A-delta fibres) (Davis et al., 1993; Slugg et al., 2000). In contrast, mechanoreceptors and proprioceptors are heavily myelinated, have a larger diameter, and respond to touch and position in space. Recent attempts to classify sensory neurons based on molecular signatures have revealed 11 different subsets (Usoskin et al., 2015). Enhancement of the response properties of sensory neurons, known as peripheral sensitization, due to inflammation or injury can often lead to hyperalgesia (increased sensitivity to painful stimulus) and allodynia (pain from a non-noxious stimulus) (Abdulla and Smith, 2001a; Ma et al., 2003; Stemkowski et al., 2015; Moy et al., 2017).

In this study, we aimed to study the impact of the MOG-EAE disease on the primary sensory neurons of the lumbar DRG in mice. We find that at the onset of disease, DRGs become inflamed with immune cell invasion followed by cytoskeletal disruption at more chronic time

points. Electrophysiological analysis reveals that medium-to-large diameter neurons become hyperexcitable. They exhibit increased action potential firing, reduced rheobase, and decreased cumulative spike latencies in the diseased condition. Altogether, this study demonstrates that there are significant functional alterations in the DRG in response to MOG-EAE contesting the commonly held notion that the pathology of MOG-induced EAE is limited to the CNS.

Methods and Materials

EAE Induction and Scoring

MOG-EAE was elicited by subcutaneously injecting 50 μ g of myelin oligodendrocyte glycoprotein (MOG₃₅₋₅₅; Peptide Synthesis Facility, Stanford University), emulsified in complete Freund's adjuvant (CFA; 1.5 mg/ml) in the hind flank. 8-10 week-old female C57BL/6 mice were used in this study (n=90; Charles River). Mice were examined daily for clinical signs of the disease and classified using the following criteria: Grade 0, no signs; Grade 1, paralyzed tail; Grade 2, mild hindlimb weakness; Grade 3, severe hindlimb weakness; Grade 4, complete hindlimb paralysis; Grade 5, moribund. MOG-EAE mice were grouped according to their disease progression: EAE onset (at appearance of clinical symptoms, Grade 1), and chronic (day 21 post-induction; average disease score: 2.67 ± 0.22). A set of CFA-only administered mice were used as control for EAE induction. Two intraperitoneal injections of pertussis toxin, *Bordatella pertussis*, (List Biological Labs) were also administered to all mice on the day of induction and 48 hours thereafter.

All animal experiments were performed according to the national Council on Animal Care's Guidelines and Policies with approval from the institute's Health Sciences Animal Care and Use Committee.

Tissue Harvesting and Storage

Mice were euthanized by intraperitoneal pentobarbital overdose (Euthansol, 0.1 mL of 340 mg/mL) followed by intracardiac flush with 0.9% saline. For immunohistochemical (IHC) experiments, the cadaver was transcardially perfused with 4% paraformaldehyde (PFA) in 0.1M phosphate buffer (PB). Otherwise, lumbar DRGs (L3-L6) were extracted from euthanized

animals promptly and snap frozen in liquid nitrogen. Similarly, the lumbar SC was extracted and the dorsal (dSC) and ventral halves dissected using a scalpel blade.

Polymerase Chain Reaction

Total RNA was extracted from tissue samples using Qiazol (Qiagen, 79306) and RNeasy Lipid Tissue Mini Kit (Qiagen, 74804). 200 ng of total RNA were subjected to DNase I treatment (Invitrogen, 18068-015) followed by Superscript III reverse transcription (Invitrogen, 18080-044) using oligo-dT₁₂₋₁₈ primers (Invitrogen, 18418-012). PCR reactions (20 μ L) were performed using Fast SYBR Green MasterMix (Applied Biosystems, 4385612) on BioRad CFX96 thermocycler with *Ppia* as a housekeeping gene. Primers have been summarized in **Table 1**.

Western Blotting

Western blotting was performed as previously described (Yousuf et al., 2017) with slight modifications. Briefly, tissue samples were homogenized and diluted to 1 μ g/ μ l in RIPA (25 mM Tris, 150 mM NaCl, 0.1% SDS, 0.5% Na deoxycholate, 1% NP-40) with protease (cOmplete EDTA-free, Roche, 04693159001) and phosphatase inhibitors (PhosSTOP, Roche, 04906837001). Samples were diluted in 4X Laemmli buffer (Biorad, 1610747) with dithiothreitol (50 mM final concentration, Biorad, 1610610) and boiled for 10 min prior to loading 16 μ g of sample onto 4-20% Mini-PROTEAN TGX precast gels (Biorad, 4561093DC). Gels were run at 150V for 60 min and transferred onto PVDF membranes with 300 mA over 60 min. Membranes were blocked in 5% BSA in PBS-Tween (0.5% Tween20 in 1X PBS) followed by overnight incubation at 4°C with primary antibody dissolved in 1% BSA in PBS-Tween. Membranes were further washed with PBS-Tween (3x, 10 min per wash) and incubated with

secondary antibody in 1% BSA in PBS-Tween for 1 hour at room temperature. Membranes were then washed with PBS-Tween (3x, 10 min per wash) and visualized using electrochemiluminescence (ECL, GE, 45000875) with Biorad ChemiDoc XRS+ system. Membranes were stained with Coomassie Brilliant Blue (Biorad, 1610400) to obtain total protein levels as loading control. Antibodies are summarized in **Table 2**.

Immunohistochemistry

A previously established protocol from our lab was used (Benson et al., 2015). Briefly, fixed tissue was immersed in 4% PFA in 0.1M PB overnight at 4°C and then transferred into 30% sucrose in 0.1M PB for two nights at 4°C. Tissue was embedded in optimum cutting temperature compound (TissueTek OCT, Sakura Finetek, 4583). DRGs were cryosectioned (Leica CM1950) at -20°C with a thickness of 10 microns on glass slides. Tissue sections were blocked in 10% normal goat serum for 1 hour and incubated in primary antibody overnight. Slides were washed in PBS-tween (0.5% tween20 in 1X PBS) and incubated in secondary antibody for 45 minutes. Slides were counterstained with Vectashield mounting medium with DAPI (Vector Laboratories, H-1200). Using a Zeiss AxioCam MRm camera and Zeiss Observer Z1 inverted fluorescence microscope, 20X fluorescent images were obtained for analysis. Representative confocal images (63X) were acquired using Leica CTR6000 and PerkinElmer UltraView Vox confocal imaging system.

Dissociated DRG cultures for electrophysiology

Immediately after extraction, lumbar DRGs (L3-L6) from CFA (n=5), onset (n=3), and chronic (n=5) mice were immersed in ice-cold dissection solution [118mM NaCl, 2.5mM KCl, 1.3μM

MgSO₄, 1.2mM NaH₂PO₄, 5mM MgCl₂·6H₂O, 25mM D-glucose, 26mM NaHCO₃, and 1.5mM CaCl₂]. Shortly thereafter, DRGs were digested with 0.5 mg/ml trypsin (Sigma, cat no. T-9201), 1 mg/ml collagenase type IV (Cedarlane, cat no. LS004186), and 0.1mg/ml deoxyribonuclease I (Sigma, cat no. D-5025) dissolved in DMEM supplemented with GlutaMax (Invitrogen, cat no. 10569044) for 40 minutes in a shaking water bath set at 35°C. Dissociated cells were plated onto 35x10mm plates (VWR, cat no. CA25382331) that were pretreated with 3µg/ml poly-DL-ornithine (Sigma, cat no. P-8638) dissolved in HPLC water (Sigma) and 2µg/ml laminin (Sigma, cat no. L-2020) dissolved in HBSS [138 mM NaCl, 5.33mM KCl, 0.44mM KH₂PO₄, 0.5mM MgCl₂·6H₂O, 0.41mM MgSO₄·7H₂O, 4mM NaHCO₃, 0.3mM Na₂HPO₄, 5.6mM D-glucose, and 1.26mM CaCl₂]. Each 35x10mm dish was immersed in 2ml of culture medium (20ml total), which contained 18ml DMEM+GlutaMax (Invitrogen, cat no. 10569044), 2ml heat-inactivated horse serum (Sigma, cat no. H-1138), 200µl antibiotic-antimycotic 100x (Invitrogen, cat no. 15240-096), and 20µl antimetabolic [cytosine β-D-arabinofuranoside (Ara-C), uridine, 5-fluoro-2'-deoxyuridine all at 10µM (Sigma, cat nos. C1768, U3003, and F0503)]. Finally cells were incubated at 36.5°C, 95% air-5% CO₂ for 2-6 hours.

Electrophysiological recording

As described previously (Abdulla and Smith, 2001b), whole-cell patch-clamp experiments were done at room temperature (22°C) in bridge balance current-clamp mode using an NPI (model SEC 05 LX) amplifier (NPI Electronic GmbH, Tamm, Germany). Whole-cell recording was established using a glass patch electrode (4-6 MΩ) containing internal solution comprised of (in mM) 130 K Gluconate, 4 Mg-ATP, 0.3 Na-GTP, 10 EGTA, 2 CaCl₂ and 10 HEPES (adjusted to pH 7.2 with KOH; osmolarity 310-320 mOsm). The petri dish was superfused with external

solution containing (in mM) 127 NaCl, 2.5 KCl, 1.2 NaH₂PO₄, 26 NaHCO₃, 2.5 CaCl₂, 1.3 MgSO₄ and 25 D-glucose saturated with 95% O₂ - 5% CO₂ at approximately 2 ml/min. All cells during current-clamp experiments were held at -60 mV. Neurons with resting membrane potential (RMP) less negative than -40 mV were rejected. DRG neuron excitability was assessed by counting total number of action potentials (AP) discharged in response to a 450 ms depolarizing current ramp to +2nA. Rheobase was determined by measuring the amplitude of a 5ms square wave depolarizing current pulse that was required to generate a single action potential. Other spike parameters (**Table 3**) were measured as previously described (Stemkowski and Smith, 2012; Stemkowski et al., 2015). Data were obtained and analysed using pCLAMP 10 (Axon Instruments).

Experimental Design and Statistical Analysis

Mice were randomly assigned to each experimental group. All statistical analyses were performed using GraphPad Prism 6. Data were subjected to one-way ANOVAs followed by Tukey's test for pairwise comparisons. A Student's t-test was used when comparing only 2 groups. PCR and Western blot data were log₂ transformed and then analysed in order to fulfill the normality and homogeneity of variance assumption for ANOVAs. Log-transformed data are back-transformed on a linear scale and graphed accordingly for the ease of the reader. An alpha-value of 0.05 was used throughout the study. Statistical analyses are summarized in **Table 4**.

Results

Immune activation and inflammation in the DRG of MOG-EAE mice

Since the activation of the immune system is an integral part of EAE pathogenesis, we examined lumbar DRGs for indications of immune activation and inflammation. Innate immune responses including complement system activation and subsequent initiation of the NLRP3 inflammasome are important mediators that activate and recruit adaptive immune cells (Hemmer et al., 2015; Arbore et al., 2016). Using PCR, we assessed the mRNA levels of complement components and receptors (C3, C3aR1, C5aR1) each of which were significantly altered throughout the disease course ($F_{C3}(2, 12)=17.78, p=0.0003$; $F_{C3aR1}(2, 12)=4.217, p=0.0410$; $F_{C5aR1}(2, 12)=8.126, p=0.0059$, One-way ANOVA) (Fig. 1A-C). Post-hoc analysis using the Tukey's multiple comparisons test indicated that C3, C3aR1 and C5aR1 mRNA expression was increased at the onset of disease in the DRG as compared to CFA controls. In addition, C3 mRNA expression was significantly elevated in samples from chronic time points as compared to CFA controls, however, these levels were significantly lower when compared to samples from the 'onset' time point. Furthermore, the mRNA expression of the NLRP3 inflammasome components, NLRP3, caspase-1, and the inflammatory cytokines, IL-1 β and IL-18, were significantly upregulated over the entire disease course ($F_{NLRP3}(2, 12)=34.37, p<0.0001$; $F_{Caspase-1}(2, 12)=42.74, p<0.0001$; $F_{IL-1\beta}(2, 12)=42.83, p < 0.0001$; $F_{IL-18}(2, 12)=9.410, p=0.0035$, One-way ANOVA) (Fig. 1D). NLRP3, caspase-1, and IL-1 β transcript levels were increased at MOG-EAE onset and, to a lesser extent, at the chronic phase of MOG-EAE as compared to CFA samples. On the other hand, IL-18 transcript levels increased only at disease onset and then normalized back to non-diseased, CFA levels at the chronic time point.

Initial IHC analysis of C5aR1 revealed that this receptor, based on morphology, was transiently present in non-neuronal cells in the DRG at disease onset ($F_{C5aR1}(2, 11)=17.51$, $p=0.0004$, One-way ANOVA) (Liang et al., 2012). This is consistent with reports suggesting that macrophages are the primary source of C5aR1 in the DRG (Shutov et al., 2016). Further analysis of CD4+ T-cells and Iba1+ macrophages also showed a transient expression of infiltrating immune cells in the lumbar DRGs from mice with MOG-EAE ($F_{CD4}(2, 10)=6.254$, $p=0.0173$; $F_{Iba1}(2, 10)=6.361$, $p=0.0165$, One-way ANOVA) (Fig. 2A-C). The number of these cells increased dramatically in the DRG at disease onset only to return to non-disease, CFA control levels at the chronic time point. Taken together, these results demonstrate that immune infiltration in the DRG of mice with MOG-EAE is a transient phenomenon that accompanies the onset of clinical signs of the disease.

Myelin dysregulation

Since demyelination is another hallmark feature of MS, we investigated myelin disruption in the sciatic nerve (SN), DRG, and dorsal horn of the spinal cord (dSC) by assessing mRNA transcripts of important myelin structural proteins. In the SN and DRG, mRNA transcripts of myelin basic protein (MBP), peripheral myelin protein 22 (PMP22), and myelin protein zero (MPZ) were not significantly altered with the progression of MOG-EAE (SN: $F_{MBP}(2, 7)=0.9470$, $p=0.4325$; $F_{PMP22}(2, 7)=2.747$, $p=0.1317$; $F_{MPZ}(2, 7)=0.9616$, $p=0.4276$; DRG: $F_{MBP}(2, 12)=0.7474$, $p=0.4944$; $F_{PMP22}(2, 12)=1.770$, $p=0.2120$; $F_{MPZ}(2, 12)=0.8078$, $p=0.4687$, One-way ANOVA) (Fig. 3). Since MOG expression in the PNS has recently been implicated in MOG-EAE pathology (Wang et al., 2017a), we also performed qRT-PCRs for MOG transcripts in the DRG and the SN (data not shown) but were unable to reliably detect MOG transcripts,

especially in the SN. In contrast, there was a significant downregulation of MBP, PMP22, and myelin oligodendrocyte glycoprotein (MOG) mRNA in the dorsal horn at disease onset ($F_{\text{MBP}}(2, 12)=10.52, p=0.0023$; $F_{\text{PMP22}}(2, 12)=9.242, p=0.0037$; $F_{\text{MOG}}(2, 12)=12.56, p=0.0011$, One-way ANOVA) (Fig. 3). These transcript levels rebound at the chronic stage. Taken together, these results establish that disruption of myelin occurs in the dorsal horn while not being significantly impacted in the PNS over the disease course.

Cellular injury and cytoskeletal disruption

Activating transcription factor 3 (ATF3) is a commonly used marker for assessing cellular injury in neurons (Frezel et al., 2016). In our study, we observed a marked upregulation of ATF3 in the DRG of MOG-EAE animals at the onset of disease signs ($t(12.41)=3.237, p=0.0069$, Two-tailed unpaired t-test with Welch's correction) (Fig 4). A common feature of MS is axonal damage and subsequent neurodegeneration in response to demyelination in the CNS (Haines et al., 2011). To assess whether cellular architecture was also affected in the PNS of EAE animals, we examined the levels of select cytoskeletal proteins (non-phosphorylated neurofilament-H (NFH), tau, kinesin, α -tubulin, and β -actin) over the disease course (Fig. 5A-F). Although cytoskeletal proteins from the PNS remained intact at the onset of disease, chronic disease lead to significant dysregulation of these cytoskeletal proteins ($F_{\text{NFH}}(2, 10)=10.73, p=0.0032$; $F_{\text{tau}}(2, 10)=29.40, p < 0.0001$; $F_{\text{kinesin}}(2, 10)=4.361, p=0.0435$; $F_{\alpha\text{-tubulin}}(2, 10)=25.80, p=0.0001$; $F_{\beta\text{-actin}}(2, 9)=15.92, p=0.0011$, One-way ANOVA). Of note, there was a significant decrease in tau, kinesin, α -tubulin, and β -actin as compared to CFA controls. In contrast, NFH was increased dramatically at the chronic time point implicating axonal damage at this stage of disease progression (Fig. 5A). Further immunohistochemical analysis revealed that the average fluorescence intensity of

phosphorylated NFH (p-NFH, NF200) was only reduced in the DRGs of chronically diseased animals ($F_{p\text{-NFH}}(2, 13)=7.750$, $p=0.0061$, One-way ANOVA) (Fig. 5G, H). Upon visual inspection, p-NFH in the soma of chronic DRG neurons displayed irregular morphology with increased compaction and reduced fascicular staining indicating cytoskeletal disruption at this later time point in the disease.

Larger diameter ($\geq 26 \mu\text{m}$) neurons are hyperexcitable in MOG-EAE

To assess the functional consequence of the disease in the DRG of EAE mice, we next carried out an electrophysiological assessment of the sensory neurons. p-NFH (also known as neurofilament 200) has previously been used to identify larger-diameter, putative myelinating cells (Ruscheweyh et al., 2007; Usoskin et al., 2015; Xu et al., 2015). Labeling of control, non-EAE DRG tissue with p-NFH revealed a spectrum of DRG neurons, 90% of which were greater than or equal to $26\mu\text{m}$ in diameter, making $26\mu\text{m}$ a good benchmark for delineating smaller and larger cells (Fig 6A, B). The minimal amount of current required to elicit an action potential, also known as rheobase, of smaller diameter neurons ($<26\mu\text{m}$) remained unchanged while larger diameter neurons ($\geq 26\mu\text{m}$) exhibited a reduced rheobase with the onset of MOG-EAE as compared to CFA cells ($F_{<26\mu\text{m}}(2, 61)=1.849$, $p=0.1660$, $F_{\geq 26\mu\text{m}}(2, 219)=5.274$, $p=0.0058$, One-way ANOVA) (Fig. 6C). Smaller diameter ($<26\mu\text{m}$) dissociated neurons from this cohort revealed no difference in number of action potentials on current ramps as compared to cells from non-diseased, CFA mice (Fig. 6D, E). In contrast, larger diameter neurons ($\geq 26\mu\text{m}$) from EAE mice at the onset and chronic time points fire more action potentials in response to current ramps of 1.5 nA and 2.0 nA ($H_{1.5 \text{ nA}}(2)=7.448$, $p=0.024$; $H_{2.0 \text{ nA}}(2)=9.943$, $p=0.007$, Kruskal-Wallis H test) (Fig. 6D, E). Deeper analysis of individual action potentials demonstrated

transient changes in spike parameters in both smaller and larger diameter neurons in the disease (Fig. 6F, I, further summarized in Table 3). Spike width was unaltered in both size categories with the progression of disease ($F_{<26\mu\text{m}}(2, 61)=1.238, p=0.2971, F_{\geq 26\mu\text{m}}(2, 219)=1.832, p=0.1625$, One-way ANOVA) (Fig 6G, J). Larger diameter DRG neurons from MOG-EAE animals, both at onset and chronic time points, also fire consecutive action potentials much quicker than CFA controls, as measured by their cumulative latencies (Disease: $F_{\geq 26\mu\text{m}}(2, 708)=38.03, p<0.0001$, Spike number: $F_{\geq 26\mu\text{m}}(7, 708)=11.82, p<0.0001$, Interaction: $F_{\geq 26\mu\text{m}}(14, 708)=0.6171, p=0.8522$, Two-way ANOVA) (Fig. 6K). These results indicate that DRG neurons $\geq 26\mu\text{m}$ become hyperexcitable in MOG-induced EAE.

Discussion

Multiple sclerosis and its commonly used animal model, MOG-EAE, has traditionally been viewed as a disorder affecting the CNS. Here, we provide evidence in addition to that notion, suggesting that the DRG of mice with MOG-EAE also undergo various pathological changes. Sensory neurons experience inflammation and cellular injury with progression of the disease. Electrophysiological analysis of neurons from the lumbar DRG of MOG-EAE mice also reveals a lasting functional consequence of MOG-EAE as demonstrated by an increased excitability of medium-to-large diameter neurons.

While the cause of MS is not known, it is accepted that the disorder involves the activation of the immune system (Dendrou and Fugger, 2017). Even though the EAE-inducing antigen is predominantly expressed in the CNS (i.e. MOG₃₅₋₅₅ peptide), pathological features of the disease are also found in the PNS. Immunohistochemical and molecular analyses of the sensory ganglia reveal an infiltration of immune cells and an increase in cytokines, chemokines, and neurotrophic factors with disease progression. Infiltrating T-cells and macrophages have been observed in the DRG (Duffy et al., 2016; Frezel et al., 2016) and the TG (Duffy et al., 2016; Frezel et al., 2016; Thorburn et al., 2016) with the onset of EAE. In particular, the trigeminal nerve and ganglia experience an influx of CD3⁺ T-cells early on in the presymptomatic phase of the disease (~day 8) followed by an increase in CD4⁺ T-cells at disease onset and peak (~day 16) (Duffy et al., 2016; Frezel et al., 2016; Thorburn et al., 2016). CD4⁺ T-cells remain elevated in the TG and the trigeminal root entry zone (TREZ) chronically (~day 35) (Thorburn et al., 2016). The DRG on the other hand does not experience immune cell infiltration to the same extent as the trigeminal system. Although CD4⁺ T-cells infiltrate the lumbar DRG at peak disease (~day 16), these immune cells dissipate with the progression of the

disease (Duffy et al., 2016; Wang et al., 2017a). Very few CD3⁺ T-cells are found in the diseased DRG (Duffy et al., 2016). Consistent with previous accounts, this study demonstrates a transient increase in CD4⁺ T-cells in the DRG of MOG-EAE mice, peaking at the onset of disease. Literature on the monocyte composition of the sensory ganglia during EAE has been limited. A recent study showed an increase in Iba1⁺ macrophages in the TG at the onset of MOG-EAE signs (Thorburn et al., 2016). Similarly, here we report for the first time an increase in Iba1⁺ macrophages in the DRG at the onset of MOG-EAE signs, only to normalize by the chronic time point.

Upon infection, the innate immune system is often the first to respond to a foreign substance by recruiting immune cells to the site of injury, initiating the complement cascade, and by activating the adaptive immune system (Turvey and Broide, 2010; Hemmer et al., 2015). In this regard, activation of innate immune cells, such as resident macrophages, can lead to the production of complement components and NLRP3-mediated cytokines including IL-1 β and IL-18 (Turvey and Broide, 2010; Hemmer et al., 2015; Mathern and Heeger, 2015). Complement components C3a and C5a are known as anaphylatoxins and, as such, cause a local inflammatory response by binding to their receptors C3aR1 and C5aR1 (Griffin et al., 2007; Liang et al., 2012; Mathern and Heeger, 2015). C3a, C5a, and IL-1 β have also previously been linked to nociceptor sensitization (Ho et al., 2010; Liang et al., 2012; Stemkowski et al., 2015). Our results provide the first evidence of a prolonged activation of the NLRP3 inflammasome and a transient activation of the complement system in the DRG of MOG-EAE mice. Despite the reduced presence of immune cells in the DRG at the chronic time point, increased *NLRP3*, *Casp1*, and *I11b* transcripts may be produced by resident cells including neurons and satellite glial cells.

Demyelination is a canonical feature of MS and EAE. Early studies that examined the coccygeal dorsal roots in a rat model of EAE demonstrated that tail paralysis progressively coincided with demyelination and conduction block of lightly myelinated afferents (Pender, 1986; Pender and Sears, 1986). As a result, these rats displayed hypoesthesia with reduced vocalization upon noxious mechanical stimulation of the tail (Pender, 1986). Many CNS myelin proteins, including MBP and PLP, are also found in the PNS (Nave and Werner, 2014) and thus induction with whole spinal cord lysates or MBP may lead to peripheral myelin reactive T-cells. In mice, Wang et al (2017a) noted myelin decompaction and dissociation in the sciatic nerve of both MOG-induced EAE and in MOG-EAE that was generated without pertussis toxin (EAEnp). Using nested qRT-PCRs, these authors confirmed that MOG transcripts are found in the peripheral nerves, speculating that this is the target of immune attack in the periphery. However, since no myelin loss was observed in the peripheral nerve and protein expression of MOG in the PNS *in vivo* was undetected (Pagany et al., 2003; Nave and Werner, 2014), it remains to be determined whether MOG transcripts in the PNS are indeed transcribed into proteins that can be targeted by immune cells.

Neurodegeneration is another hallmark pathological feature of MS. In this regard, we observed a reduction in various cytoskeletal-associated proteins including tau, kinesin, α -tubulin, and β -actin in PNS samples at the chronic time point of MOG-EAE. Of note, non-phosphorylated NFH was significantly elevated while the phosphorylated isoform of NFH was downregulated. NFHs are the most phosphorylated protein in the nervous system (Kirkcaldie and Collins, 2016). A complex balance of phosphorylation and dephosphorylation of NFH, in collaboration with microtubule associated proteins (e.g. tau), actin, tubulin, and motor proteins (e.g. kinesin), allows for efficient movement across the axon and supports the survival of the

neuron. We also observed that p-NFH in chronic samples had an irregular morphology with increased fragmentation and a loss of regular, round lattice structures. This is characteristic of p-NFH in injured cells (Siedler et al., 2014; Kirkcaldie and Collins, 2016). ATF3, a stress-induced transcription factor, is present presymptomatically (Frezel et al., 2016) and upregulated at onset of motor signs (Fig. 5). It is interesting to note that ATF3 expression can be induced by only CFA and pertussis toxin inoculation without the MOG peptide while the peptide is required for T-cell infiltration into the DRG (Frezel et al., 2016). ATF3 expression in our MOG-EAE model was found to be dramatically increased as compared to CFA-controls albeit to a much lesser degree than models of peripheral nerve injury (Tsuji no et al., 2000; Hunt et al., 2012). Furthermore, evidence suggests that secondary injury pathways such as Ca^{2+} dysregulation and mitochondrial dysfunction precede cytoskeletal disruption (Siedler et al., 2014). We did not observe neuronal apoptosis, as measured by cleaved caspase-3 immunoreactivity (data not shown), in our cohort. However, activation of the NLRP3 inflammasome is known to induce another form of cell death, pyroptosis, via caspase 1 rather than caspase 3 (Man et al., 2017). This hypothesis will need to be addressed in future studies.

The Gate Control Theory of Pain (Melzack and Wall, 1965) proposes that local interneurons of the spinal cord modulate pain perception by integrating nociceptive and innocuous stimulation from the primary afferents prior to relaying information to the higher-order structures of the brain. Injury or disease can lead to sensitization of peripheral and/or central neurons facilitating, augmenting, potentiating, and amplifying their response, ultimately contributing to abnormal and persistent sensory processing (Latre moliere and Woolf, 2009). Here, we describe the first account of aberrant electrophysiological responses of DRG neurons in MOG-induced EAE. Electrophysiological analysis has revealed an increase in the excitability of

small-diameter putative nociceptive neurons in other models of neuropathic pain (Garrison et al., 2014; Ratté and Prescott, 2016; Moy et al., 2017; Mule et al., 2017). In contrast, we find that larger diameter neurons ($\geq 26 \mu\text{m}$) in the DRG of MOG-EAE mice fire more action potentials at higher current ramps, have a lower rheobase, and reduced cumulative latency, all indicative of hyperexcitability. Previous electrophysiological studies in the PNS of EAE animals have focused largely at the chronic time point during which, as shown here, immune cell activation subsides and cytoskeletal disruption prevails (Pender and Sears, 1982, 1986; Lu et al., 2012). In fact, one of the first studies investigating the involvement of the DRG in EAE noted demyelination-induced nerve conduction block in rats and rabbits up to 7 days post disease onset. It should be noted however that the inoculum used by Pender and Sears (1982, 1986) was a whole guinea pig spinal cord. As discussed in their original paper, the inoculum may contribute to peripheral demyelination since some myelin antigens that are present in the CNS are also present in the periphery (Pender and Sears, 1982, 1986; Nave and Werner, 2014). Just as the purpose of this study was to highlight novel mechanisms of sensory dysfunction in MOG-EAE, by performing those initial electrophysiological studies on whole spinal cord induced EAE, Pender and Sears (1982, 1986) brought into question the peripheral component of EAE and hence, its relevance to MS. More recently, Lu and colleagues (2012) demonstrated increased excitability of large-diameter A β primary afferents using skin-nerve preparations in SJL-PLP₁₃₉₋₁₅₁ EAE mice albeit at the chronic time point (35-45 days post induction). Along with our current study, Lu et al., identify a disease-mediated effect on large diameter mechanoreceptors rather than small diameter nociceptors. In this regard, we consistently observe mechanical hypersensitivity in MOG₃₅₋₅₅ induced EAE which may require heightened input from mechanoreceptors, as previously suggested (Xu et al., 2015; Xie et al., 2016; Sun et al., 2017a). Of note, we do not reliably

observe heat hyperalgesia in our model (data not shown) further corroborating the lack of electrophysiological changes in smaller diameter neurons ($< 26 \mu\text{m}$) which are known to possess heat-sensing TRPV1 channels. Aberrant firing properties of larger diameter afferents ($\geq 26 \mu\text{m}$) may therefore be a driver of central sensitization that can maintain chronic mechanical hypersensitivity (Baron et al., 2013).

Inflammatory mediators, such as IL-1 β (Binshtok et al., 2008; Stemkowski et al., 2015; Alles and Smith, 2018) and TNF α (Czeschik et al., 2008; Leung and Cahill, 2010; Wang et al., 2018), that are induced in EAE (Melanson et al., 2009; Rodrigues et al., 2016) can modulate ion channel expression and/or activity and induce neuronal hyperexcitability. The electrophysiological changes remaining into the chronic phase of MOG-EAE suggest that transient immune cell infiltration and activation in the DRG inherently alters neuronal properties into the chronic phase of MOG-EAE. In this regard, long-term IL-1 β exposure (5-6 days) to dissociated rat DRG neurons increases the excitability of medium-sized sensory neurons in a potassium-channel dependent manner (Stemkowski and Smith, 2012; Stemkowski et al., 2015). At the chronic time-point in our model, slightly elevated levels of IL-1 β (Fig 1) in concert with altered ion channels may contribute to electrophysiological changes (Fig 6). Various models of neuropathic pain have reported changes in sensory neuron excitability. After peripheral nerve injury, sensory neurons have been consistently reported to have a reduced rheobase and increased excitability (Abdulla and Smith, 2001b, 2001a). However, the cell-specific changes in neurophysiological properties of sensory neurons typically vary with the model of study. Spinal nerve ligation in rats induces mechanical hyperalgesia and allodynia and this phenomenon coincides with hyperexcitability of medium and large diameter DRG neurons (Ma et al., 2003). In comparison, partial rhizotomy reduces mechanical threshold (hyperalgesia) but does not

induce allodynia in rats. Unlike spinal nerve ligation, partial rhizotomy does not significantly alter sensory neuron electrophysiology, suggesting involvement of central mechanisms to modulation pain (Ma et al., 2003). Other axotomy models have noted increased action potential amplitude and reduced rheobase in mainly small unmyelinated C-fibres (Zhang et al., 1997). Small-diameter neurons in our model have increased afterhyperpolarization amplitude (Table 3) which may allow these cells to fire multiple action potential in response to increasing stimulus frequency, as previously suggested (Villière and McLachlan, 1996). Differences between our study and the literature may also be attributed to differences in animals, strains, and even sexes.

Sensory axons projecting into the CNS encounter an inflammatory milieu which may initiate retrograde stress responses causing an infiltration of leukocytes to mitigate cellular injury or damage. Myelinated axons of sensory neurons are especially susceptible to EAE inflammation due to the active demyelination in the CNS. We describe here the first account of aberrant electrophysiology of DRG neurons in MOG₃₅₋₅₅ induced EAE. Electrophysiological analysis have revealed increased excitability of putative nociceptive neurons in various models of neuropathic pain (Garrison et al., 2014; Ratté and Prescott, 2016; Moy et al., 2017; Mule et al., 2017). Contrary to this, we find that medium-to-large diameter neurons in the DRG of MOG-EAE mice fire more action potentials at higher current ramps and have a lower rheobase, indicative of hyperexcitability. Pharmacologically blocking medium to large diameter afferents from the DRG using a combination of flagellin and QX-314 alleviates mechanical allodynia but not heat hyperalgesia in multiple models of neuropathic pain (Xu et al., 2015). Our electrophysiology data support this notion and demonstrate that large diameter neurons are the most affected in the PNS of MOG-EAE mice.

Tables:

Table 1.1. qRT-PCR primers used in this study.

Gene ID	FWD/REV	Sequence (5'-3')
<i>Ppia</i>	FWD	GAGCTGTTTGCAGACAAAGTTC
	REV	CCCTGGCACATGAATCCTGG
<i>C3</i>	FWD	GAGGCACATTGTCCGGTGGTG
	REV	CCAGGATGGACATAGTGGCG
<i>C3ar1</i>	FWD	CTCAGCAACTCGTCCAATGC
	REV	CCATGGCTCAGTCAAGCACA
<i>C5ar1</i>	FWD	CTTCCTTCAGAAGAGTTGCCTG
	REV	AGCTGCTGTTATCTATGGGGTC
<i>Nlrp3</i>	FWD	ATTACCCGCCCCGAGAAAGG
	REV	TCGCAGCAAAGATCCACACAG
<i>Casp1</i>	FWD	ACAAGGCACGGGACCTATG
	REV	TCCCAGTCAGTCCTGGAAATG
<i>Il1b</i>	FWD	GCAACTGTTCTGAACTCAACT
	REV	ATCTTTTGGGGTCCGTCAACT
<i>Il18</i>	FWD	ACTTTGGCCGACTTCACTGT
	REV	GGGTTCACTGGCACTTTGAT
<i>Mbp</i>	N/A	Qiagen, PPM04745F
<i>Pmp22</i>	N/A	Qiagen, PPM05053F
<i>Mpz</i>	N/A	Qiagen, PPM41824A
<i>Mog</i>	N/A	Qiagen, PPM33328B

Table 1.2. Antibodies used in this study.

Antibody	Host	Source	Dilution Factor
CD4	Rt	Biorad, MCA2691	1:200
CD88 (C5aR1)	Rt	Biorad, MCA2456GA	1:500
IBA-1	Rb	Wako, 019-19741	1:500
p-NFH (IHC)	Ck	ThermoFisher, PA1-10002	1:5,000
ATF3 (IHC)	Rb	Santa Cruz, SC-188	1:200
NFH (WB)	Ms	Covance, 14974402	1:1,000
Tau	Rb	Abcam, ab64193	1:200
Kinesin	Ms	Millipore, MAB1614	1:500
α -tubulin	Rb	Cell Signalling, 2125	1:1,000
β -actin	Ms	Sigma, A1978	1:2,000
Goat anti-mouse IgG HRP	Gt	Abcam, ab6789	1:10,000
Goat anti-rabbit IgG HRP	Gt	Abcam, ab6721	1:10,000
Goat anti-rabbit IgG AF488	Gt	Life Technologies, A11008	1:200
Goat anti-chicken IgY AF594	Gt	Life Technologies, A11042	1:200
Goat anti-rat IgG AF488	Gt	Life Technologies, A11006	1:200

Table 1.3. Various spike parameters of small (<26 μm) and large ($\geq 26 \mu\text{m}$) diameter DRG neurons obtained from CFA, EAE onset, and EAE chronic mice.

Spike Parameter	<26 μm			$\geq 26 \mu\text{m}$		
	CFA	Onset	Chronic	CFA	Onset	Chronic
Peak Amplitude (mV)	116.4 \pm 2.159	112.5 \pm 2.437	116.2 \pm 2.42	104.9 \pm 1.796	102.2 \pm 2.066	108.9 \pm 1.362 [#]
Afterhyperpolarization Amplitude (mV)	-14.38 \pm 0.927	-10.22 \pm 1.223 ^{**}	-13.65 \pm 0.525 [#]	-13.84 \pm 0.598	-12.18 \pm 0.657	-12.38 \pm 0.483
Half Width (ms) ^{&}	3.959 \pm 0.421	5.165 \pm 0.915	4.213 \pm 0.348	1.18 \pm 0.104	1.474 \pm 0.141	1.233 \pm 0.083
Rise Slope (mV/ms)	175.3 \pm 22.55	83.64 \pm 6.219 ^{**}	143.1 \pm 10.36 ^{###}	236.7 \pm 14.12	108.5 \pm 4.298 ^{***}	218.8 \pm 12.5 ^{####}
Decay Slope (mV/ms)	-62.46 \pm 6.376	-45.32 \pm 8.131	-55.19 \pm 5.451	-134.4 \pm 5.835	-96.5 \pm 5.518 ^{***}	-120.4 \pm 4.876 [#]
Rheobase (nA) ^{&}	0.2625 \pm 0.017	0.3 \pm 0.023	0.3074 \pm 0.018	0.4697 \pm 0.028	0.349 \pm 0.027 ^{**}	0.4138 \pm 0.022

Mean \pm SEM. One-way ANOVA followed by Tukey's test performed within each group. *p<0.05, **p<0.01, ***p<0.001, in comparison to CFA; #p<0.05, ##p<0.01, ###p<0.001 in comparison to Onset. &Graphed in Fig 6.

Table 1.4. Statistical analyses performed in this study.

Figure	Data structure	Statistical test	Sample size	Statistical data
1	Log2-transformed to normalize data	One-way ANOVA (Tukey's post-hoc test)	CFA: 5 Onset: 5 Chronic: 5	A: F(2, 12)=17.78, p=0.0003 B: F(2, 12)=4.217, p=0.0410 C: F(2, 12)=8.126, p=0.0059 D (i) : F(2, 12)= 34.37, p<0.0001 D (ii) : F(2, 12)=42.74, p<0.0001 D (iii): F(2, 12)=42.83, p<0.0001 D (iv): F(2, 12)=9.410, p=0.0035
2a	Normal	One-way ANOVA (Tukey's post-hoc test)	CFA: 4 Onset: 5 Chronic: 5	F(2, 11)=17.51, p=0.0004
2b	Normal	One-way ANOVA (Tukey's post-hoc test)	CFA: 5 Onset: 5 Chronic: 3	F(2, 10)=6.254, p=0.0173
2c	Normal	One-way ANOVA (Tukey's post-hoc test)	CFA: 4 Onset: 5 Chronic: 4	F(2, 10)= 6.361, p=0.0165
3a-c	Log2-transformed to normalize data	One-way ANOVA (Tukey's post-hoc test)	CFA: 4 Onset: 3 Chronic: 3	A: F(2, 7)=0.9470, p=0.4325 B: F(2, 7)=2.747, p=0.1317 C: F(2, 7)=0.9616, p=0.4276
3d-i	Log2-transformed to normalize data	One-way ANOVA (Tukey's post-hoc test)	CFA: 5 Onset: 5 Chronic: 5	D: F(2, 12)=0.7474, p=0.4944 E: F(2, 12)=1.770, p=0.2120 F: F(2, 12)=0.8078, p=0.4687 G: F(2, 12)=10.52, p=0.0023 H: F(2, 12)= 9.242, p=0.0037 I: F(2, 12)=12.56, p=0.0011
4c	Non-normal	Two-tailed unpaired t-test with Welch's correction	CFA: 5 EAE: 13	t(12.41)=3.237, p=0.0069
5a-e	Log2-transformed to normalize data	One-way ANOVA (Tukey's post-hoc test)	CFA: 5 Onset: 4 Chronic: 4	A: F(2, 10)=10.73, p=0.0032 B: F(2, 10)=29.40, p < 0.0001 C: F(2, 10)=4.361, p=0.0435 D: F(2, 10)=25.80, p=0.0001 E: F(2, 10)=15.92, p=0.0011
5h	Normal	One-way ANOVA (Tukey's post-hoc test)	CFA: 4 Onset: 6 Chronic: 6	F(2, 13)=7.750, p=0.0061
6c	Non-parametric	Kruskal-Wallis H test	<26 μ m: CFA: 33 Onset: 17 Chronic: 27 \geq 26 μ m: CFA: 76	<26 μ m: H _{0.5 nA} (2)=0.3138, p=0.8548 H _{1.0 nA} (2)=0.1677, p=0.9196 H _{1.5 nA} (2)=0.8715, p=0.2750 H _{2.0 nA} (2)=0.9634, p=0.6177 \geq 26 μ m:

			Onset: 51 Chronic: 94	$H_{0.5 \text{ nA}}(2)=1.498, p=0.4728$ $H_{1.0 \text{ nA}}(2)=3.924, p=0.1406$ $H_{1.5 \text{ nA}}(2)=7.448, p=0.0241$ $H_{2.0 \text{ nA}}(2)=9.943, p=0.0069$
6d	Normal	One-way ANOVA (Tukey's post-hoc test)	<26 μm : CFA: 24 Onset: 13 Chronic: 27 $\geq 26 \mu\text{m}$: CFA: 76 Onset: 51 Chronic: 94	$F_{<26\mu\text{m}}(2, 61)=1.849, p=0.1660$ $F_{\geq 26\mu\text{m}}(2, 219)= 5.274, p=0.0058$
6g	Normal	One-way ANOVA (Tukey's post-hoc test)	CFA: 24 Onset: 13 Chronic: 27	$F(2, 61)=1.238, p=0.2971$
6h	Normal	Two-way ANOVA (Tukey's post-hoc test)	CFA: 31 Onset: 17 Chronic: 25	Disease: $F(2, 444)=2.740, p=0.0657$ Spike number: $F(7, 444)=25.00, p<0.0001$ Interaction: $F(14, 444)=0.1811, p=0.9996$
6j	Normal	One-way ANOVA (Tukey's post-hoc test)	CFA: 76 Onset: 52 Chronic: 94	$F(2, 219)=1.832, p=0.1625$
6k	Normal	Two-way ANOVA (Tukey's post-hoc test)	CFA: 40 Onset: 27 Chronic: 44	Disease: $F(2, 708)=38.03, p<0.0001$ Spike number: $F(7, 708)=11.82, p<0.0001$ Interaction: $F(14, 708)=0.6171, p=0.8522$
Table 3	Normal and non-normal	One-way ANOVA (Tukey's post-hoc test) or Kruskal-Wallis H test	<26 μm : CFA: 24 Onset: 13 Chronic: 27 $\geq 26 \mu\text{m}$: CFA: 76 Onset: 51 Chronic: 94	Peak Amplitude: $F_{<26\mu\text{m}}(2, 61) = 0.6022, P = 0.5508$ $F_{\geq 26\mu\text{m}}(2, 219) = 3.883, P = 0.0220$ Afterhyperpolarization Amplitude: $F_{<26\mu\text{m}}(2, 61) = 5.211, P = 0.0081$ $F_{\geq 26\mu\text{m}}(2, 219) = 2.481, P = 0.0860$ Half Width (as plotted in Fig 6): $F_{<26\mu\text{m}}(2, 61) = 1.238, P = 0.2971$ $F_{\geq 26\mu\text{m}}(2, 219) = 1.832, P = 0.1625$ Rise Slope: $H_{<26\mu\text{m}}(2) = 14.44, p=0.0007$ $H_{\geq 26\mu\text{m}}(2) = 50.99, p<0.0001$ Decay Slope: $F_{<26\mu\text{m}}(2, 61) = 1.423, P = 0.2488$ $F_{\geq 26\mu\text{m}}(2, 219) = 10.08, P < 0.0001$ Rheobase (as plotted in Fig 6): $F_{<26\mu\text{m}}(2, 61)=1.849, p=0.1660$ $F_{\geq 26\mu\text{m}}(2, 219)= 5.274, p=0.0058$

Figures:

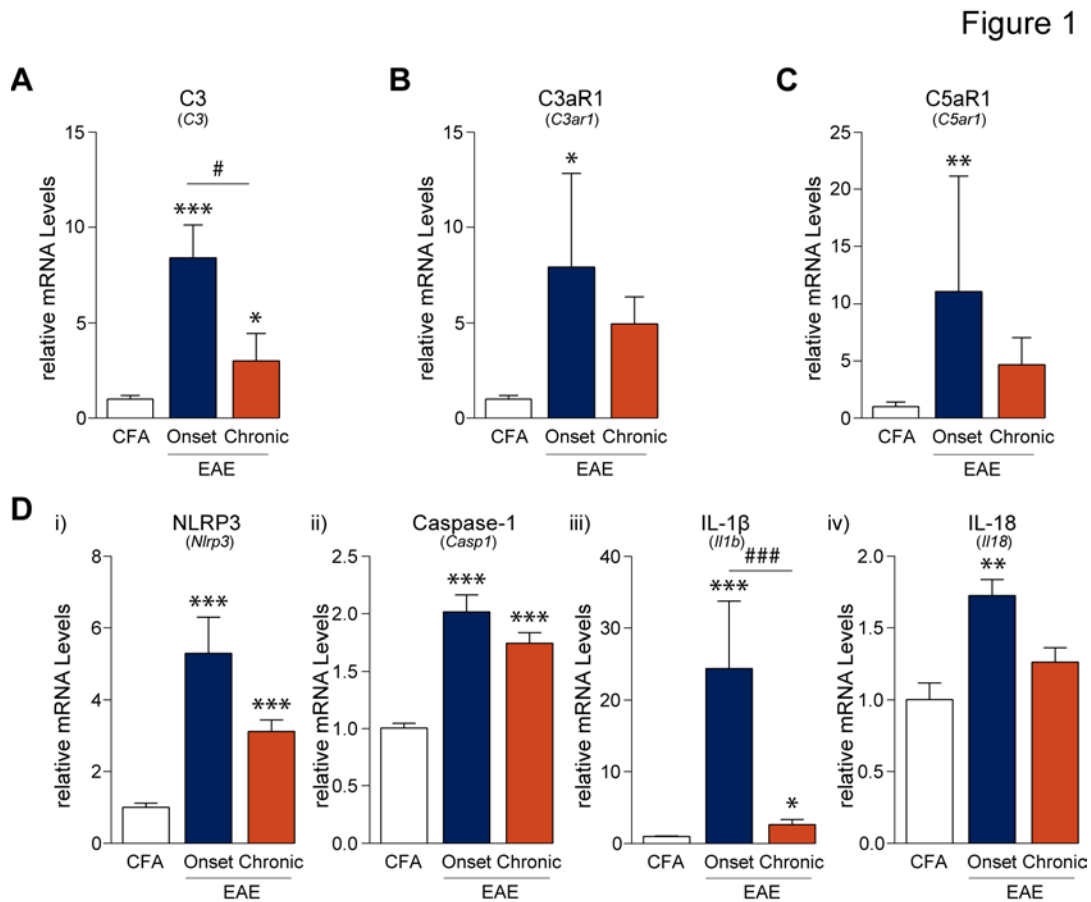


Figure 1.1. EAE-induced complement and inflammasome activation in the DRG.

(A-C) PCR analysis of lumbar DRGs from EAE animals revealed that the complement component 3 (C3), its receptor C3aR1, and component 5a receptor (C5aR1, also known as CD88) are transiently upregulated at the onset of disease as compared to CFA control samples. (D) Similarly, mRNA transcripts of NLRP3, caspase-1, IL-1 β , and IL-18 are also upregulated at disease onset only to taper off at the chronic time point 21 days post-induction. NLRP3 = NACHT, LRR and PYD domains-containing protein 3, IL = interleukin. Bars indicate mean \pm standard error of mean (SEM). *, # p<0.05, **, ### p<0.01, ***, ### p<0.001, one-way ANOVAs with Tukey's post-hoc analysis. CFA, n=5; Onset, n=5; Chronic, n=5.

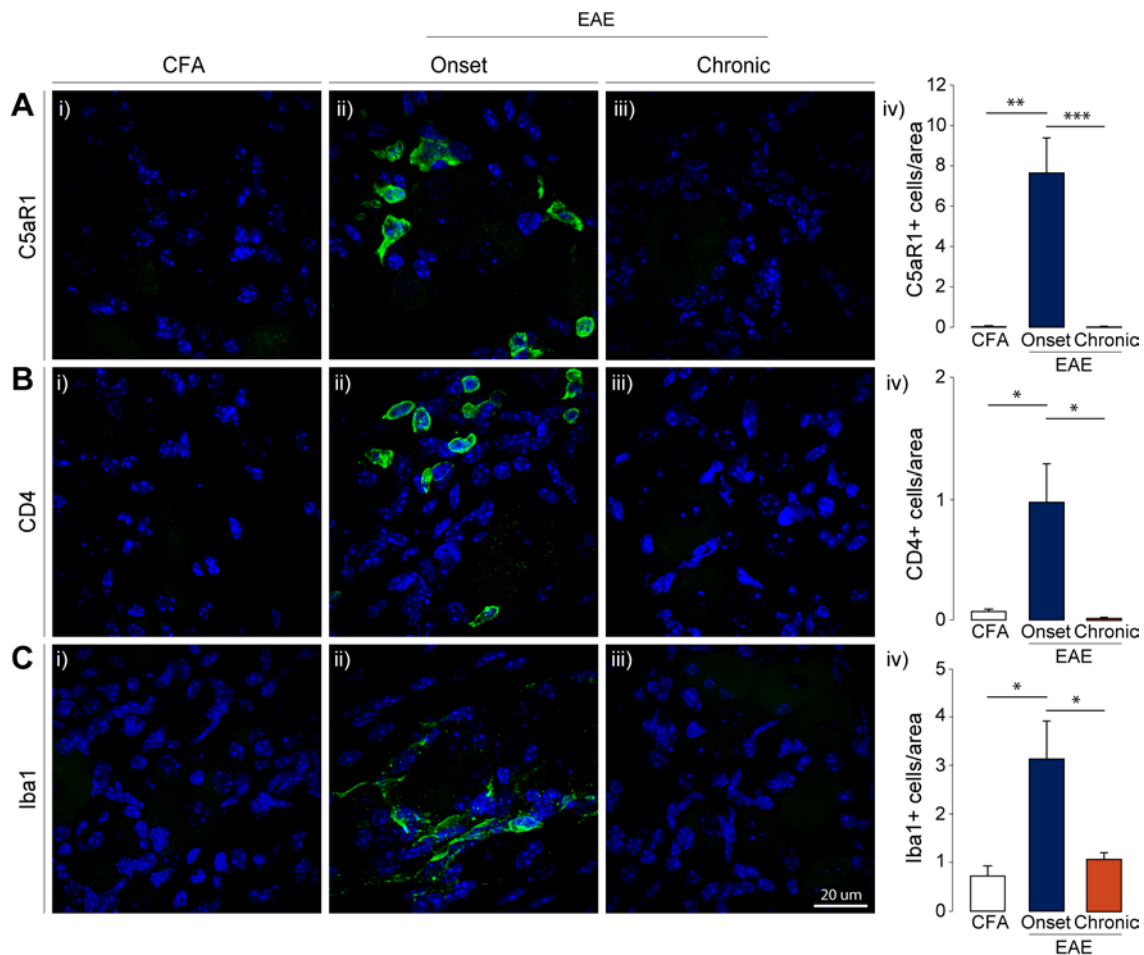


Figure 1.2. Immune cells infiltrate the DRG in EAE.

(A-C) IHC analysis further confirmed that C5aR1+ immune cells, CD4+ T-cells, and Iba1+ macrophages infiltrate the DRG at EAE onset and retreat at the later, chronic disease stage. C5aR1 = Complement 5a receptor, CD4 = cluster of differentiation 4, Iba1 = ionized calcium binding adapter molecule 1. Bars indicate mean \pm standard error of mean (SEM). * $p < 0.05$, ** $p < 0.01$, *** $p < 0.001$, one-way ANOVAs with Tukey's post-hoc analysis. CFA, $n=5$; Onset, $n=5$; Chronic, $n=5$.

Figure 3

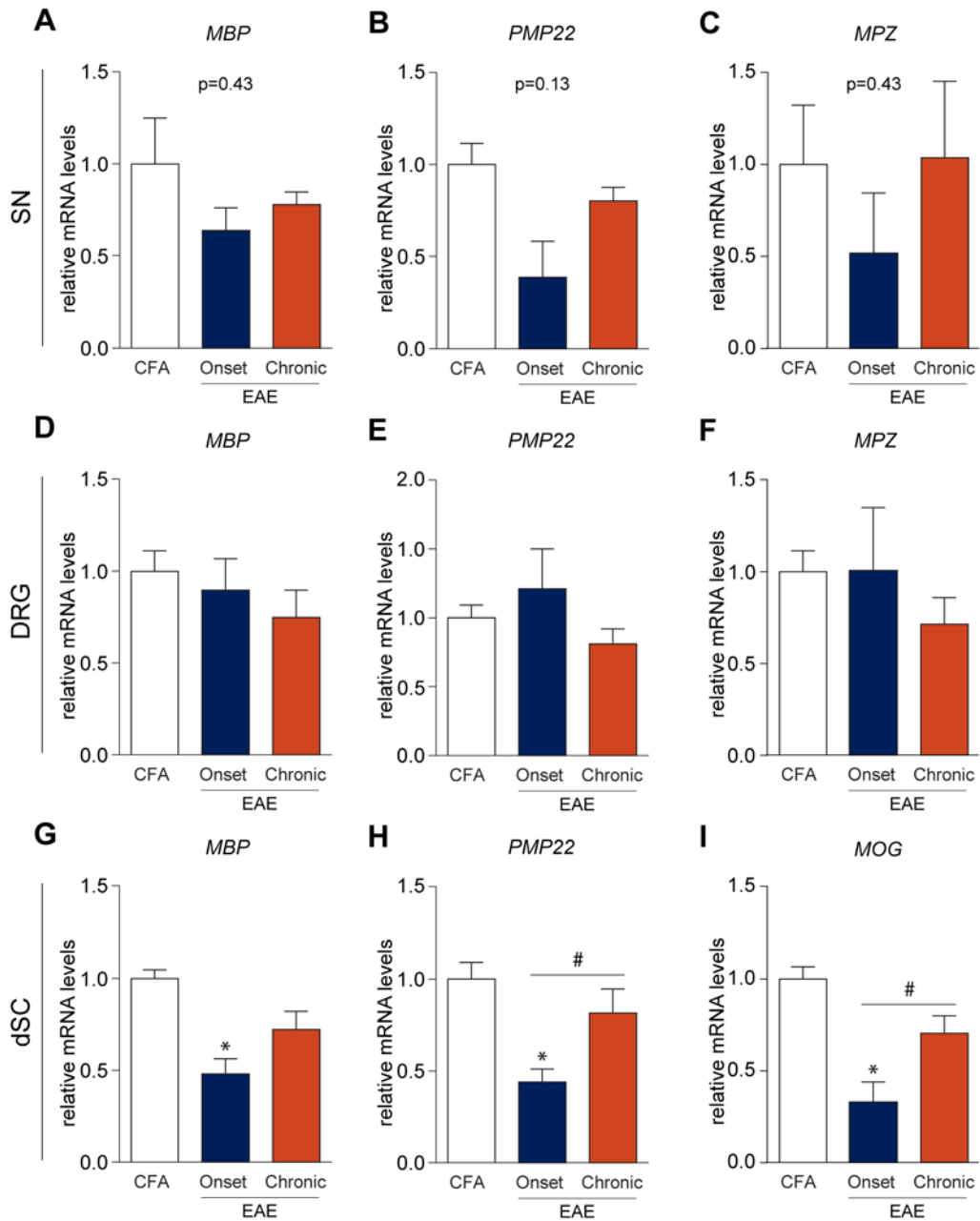


Figure 1.3. Myelin protein transcripts in the periphery are not significantly altered in EAE.

(A-F) mRNA transcripts of myelin basic protein (MBP), peripheral myelin protein 22 (PMP22), and myelin protein zero (MPZ) were not significantly altered in EAE. (G-I) MBP, PMP22, and myelin oligodendrocyte glycoprotein (MOG) transcripts were reduced at EAE onset in the dorsal

spinal cord (dSC) suggesting myelinopathy. Normalization of these transcripts was also observed chronically which may indicate repair mechanisms. *, # $p < 0.05$, one-way ANOVAs with Tukey's post-hoc analysis. (A-C) CFA, n=4; Onset, n=3; Chronic, n=3. (D-I) CFA, n=5; Onset, n=5; Chronic, n=5.

Figure 4

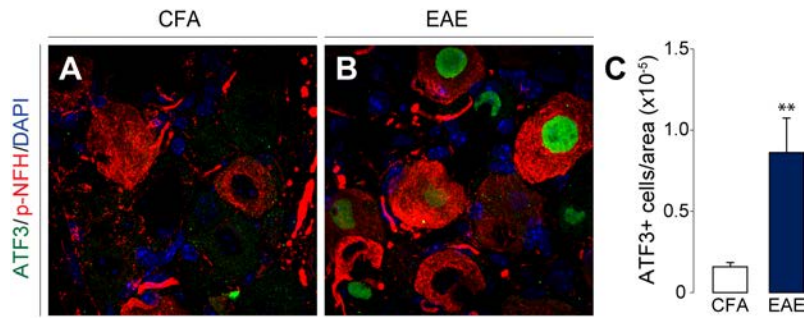


Figure 1.4. Cellular injury marker, ATF3, is upregulated in the DRG of EAE animals.

(A-C) Activating transcription factor 3 (ATF3) expression in the nucleus of DRG neurons is induced with the onset of disease signs. P-NFH staining is used to identify neurons. (C) The number of ATF3-positive neurons in the DRG were normalized to the area (in pixels) of the entire DRG. Bars indicate mean \pm standard error of mean (SEM). ** $p < 0.01$, Two-tailed unpaired t-test with Welch's correction. CFA, $n=5$; EAE, $n=13$.

Figure 5

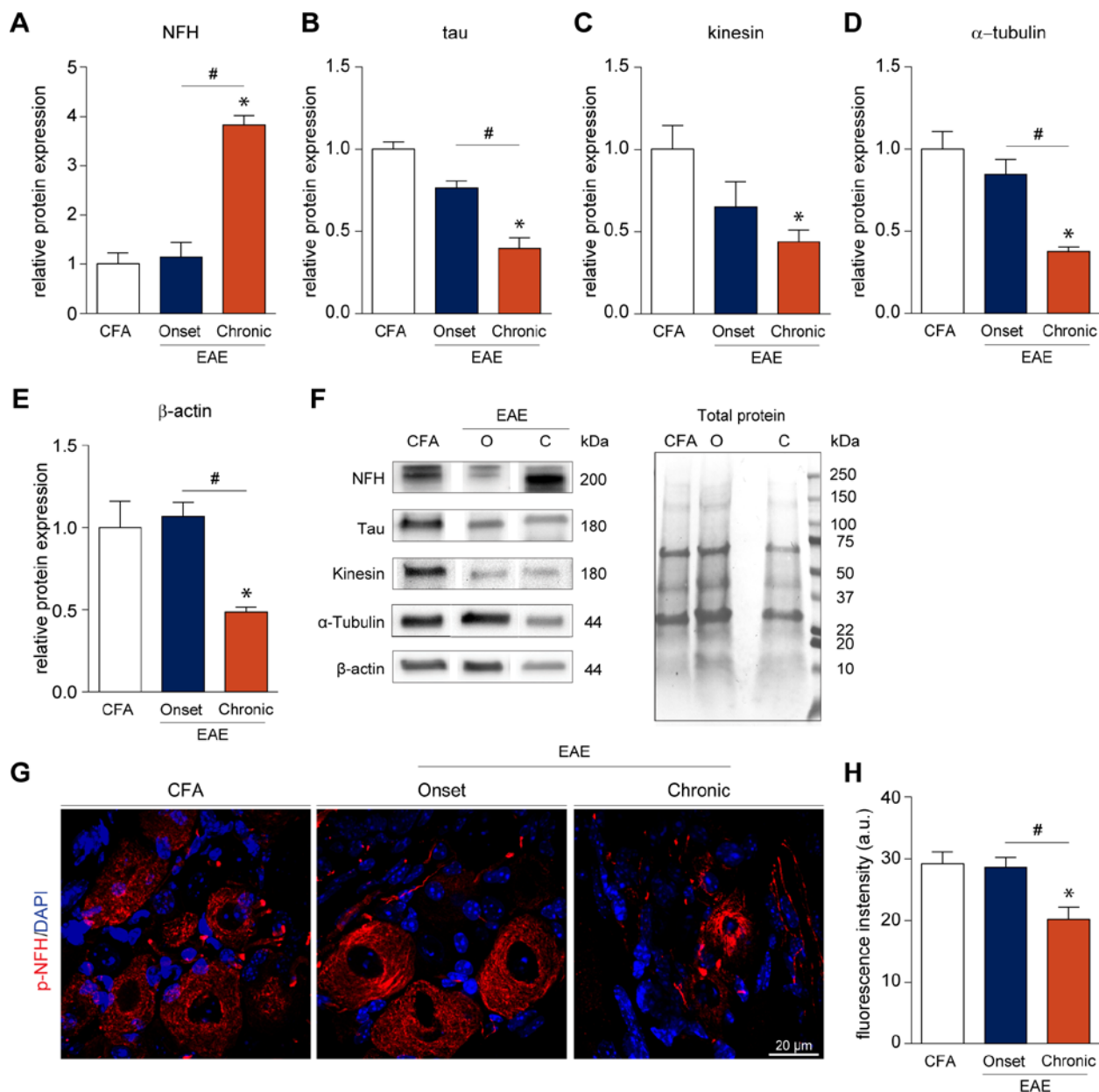


Figure 1.5. Cytoskeletal disruption of DRG neurons occurs late in the EAE disease course.

(A-F) Western blot data suggest that cytoskeletal proteins remain intact at the onset of EAE symptoms and become impaired at the chronic timepoint. We observe a significant elevation in the level of the non-phosphorylated isoform of heavy-chain neurofilament (NFH) at the chronic stage. On the contrary, a significant reduction in the levels of tau, kinesin, α -tubulin, and β -actin

was detected chronically. (G-H) Immunofluorescence staining of lumbar DRGs for the phosphorylated isoform of NFH (p-NFH) revealed a significant reduction in fluorescence intensity in chronic samples (20.23 ± 1.976 a.u.) as compared to CFA control (29.26 ± 1.951 a.u.) and EAE onset samples (28.68 ± 1.581 a.u.). Furthermore, p-NFH staining in the soma of chronic DRG neurons displays aberrant morphology. a.u. = arbitrary units. Bars indicate mean \pm standard error of mean (SEM). O = Onset, C = Chronic. *, # $p < 0.05$, one-way ANOVAs with Tukey's post-hoc analysis. (A-F) CFA, n=5; Onset, n=4; Chronic, n=4. (G,H) CFA, n=4; Onset, n=6; Chronic, n=6.

Figure 6

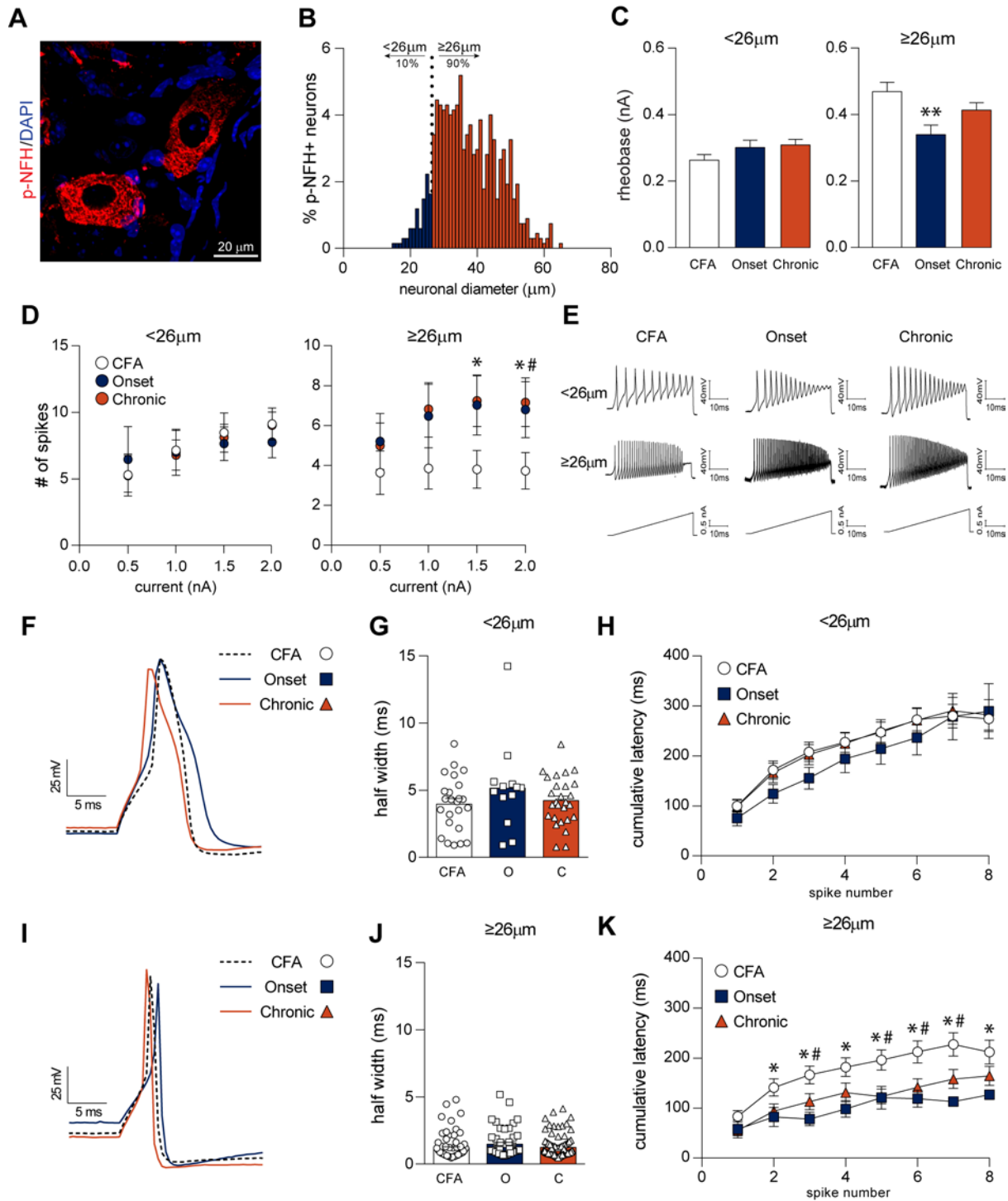


Figure 1.6. Larger diameter ($\geq 26 \mu\text{m}$) dissociated DRG neurons exhibit hyperexcitability.

(A, B) Labeling DRG sections from non-diseased control mice with p-NFH (also known as NF200) demonstrates that 90% of p-NFH+ cells are $\geq 26 \mu\text{m}$, delineating smaller and larger cells.

(C, D) Dissociated DRG neurons from these animals exhibit aberrant firing properties under current ramp analysis. In particular, larger diameter ($\geq 26 \mu\text{m}$) EAE sensory neurons at disease onset have reduced rheobase and fire more action potentials with a current ramp of 1.5 nA and 2.0 nA than their CFA counterparts. EAE chronic DRG neurons also exhibit increased firing pattern at a current ramp of 2.0 nA but show an insignificant reduction in their rheobase. (E) Sample 2.0 nA current ramp traces of dissociated DRG neurons. (F-H) Half width of smaller diameter neurons ($< 26 \mu\text{m}$) as well as cumulative latencies of action potentials remain relatively unchanged with EAE disease. (I-K) Although spike width is unaffected in larger diameter neurons ($\geq 26 \mu\text{m}$), cumulative latencies are reduced with EAE disease indicating that action potentials fire quicker in succession with the onset of EAE. Other spike parameters are summarized in Table 3. (C) *, # $p < 0.05$, Kruskal-Wallis H-test. * CFA vs. Onset, # CFA vs. Chronic. (D) ** $p < 0.01$, one-way ANOVAs with Tukey's post-hoc analysis. (K) *, # $p < 0.05$, two-way ANOVA with Tukey's post-hoc analysis. (A,B) $n=5$, 674 of 1055 cells were p-NFH+. (C,D) $< 26 \mu\text{m}$: CFA, $n=33$; Onset, $n=17$; Chronic, $n=27$. $\geq 26 \mu\text{m}$: CFA, $n=76$; Onset, $n=51$; Chronic, $n=94$. (G) CFA, $n=24$; Onset, $n=13$; Chronic, $n=27$. (H) CFA, $n=31$; Onset, $n=17$; Chronic, $n=25$. (J) CFA, $n=76$; Onset, $n=52$; Chronic, $n=94$. (K) CFA, $n=40$; Onset, $n=27$; Chronic, $n=44$.

Chapter 2 : The chloride co-transporters, NKCC1 and KCC2, in experimental autoimmune encephalomyelitis (EAE)

Introduction

Multiple sclerosis (MS) is an autoimmune inflammatory disorder of the central nervous system (CNS) characterised by demyelination and focal lesions (Compston and Coles, 2008). Common symptoms of MS include visual, motor, and sensory abnormalities. It is becoming increasingly more recognized that nearly half of MS patients will also experience neuropathic pain during their disease course (Foley et al., 2013). The International Association of Pain defines neuropathic pain as, “pain caused by a lesion or disease of the somatosensory nervous system” (Loeser and Treede, 2008). Despite such a high incidence of pain in MS, research on the biological foundation of these abnormal pain states in MS is limited.

Maintaining a balance in the levels of excitatory and inhibitory neurotransmitters such as glutamate (Glu) and GABA at the synapse, is critical for regulating sensory processing in the CNS. Major changes in sensory function can occur when the nervous system is perturbed and the balance of excitatory and inhibitory signaling is disrupted, leading to hypersensitivity and often neuropathic pain (Coull et al., 2003; Chen et al., 2014a). The Gate Control Theory of Pain (Melzack and Wall, 1965) proposes that local inhibitory interneurons of the spinal cord act as “gates” to either dampen or allow nociceptive inputs to reach the brain. Within the spinal cord, interneurons can form inhibitory or excitatory synapses with projection neurons and other interneurons, creating a sophisticated network (Sandkuhler, 2009). This network can further be modulated by regulating the polarity and strength of GABA, in particular by Na⁺-K⁺-2Cl⁻ co-transporter 1 (NKCC1) and K⁺-Cl⁻ co-transporter 2 (KCC2). When GABA_A/glycine receptors are activated, chloride either leaves (depolarizes) or enters (hyperpolarizes) the cell. The influx

or efflux of chloride is determined by its electrochemical gradient established by the chloride cotransporters (Price et al., 2005; Price and Prescott, 2015). Since the dorsal root ganglion (DRG) expresses very little to no KCC2, the intracellular chloride levels in primary sensory neurons are maintained predominantly by NKCC1 (Price et al., 2006b). This leads to an excitatory effect of GABA in the periphery as opposed to the classical, inhibitory effects in the CNS, where KCC2 is abundant. Various models of peripheral neuropathy (Hasbargen et al., 2010; Beggs and Salter, 2013; Gagnon et al., 2013; Modol et al., 2014) have noted a decrease in KCC2 in the dorsal spinal cord and an increase in NKCC1 in the DRG. A loss or reduction of KCC2 expression on projection neurons can lead to disinhibition resulting in an amplification of nociceptive signals reaching the brain (Coull et al., 2003; Gagnon et al., 2013). Increased levels of NKCC1 in the primary afferents has been proposed to amplify peripheral stimulation by increasing primary afferent depolarization beyond shunting capabilities, resulting in a GABA_AR-mediated action potential and increased neurotransmitter release (Cervero and Laird, 1996; Cervero et al., 2003; Price et al., 2009; Chen et al., 2014a).

The animal model of experimental autoimmune encephalomyelitis (EAE) has been used widely to study the pathophysiology of MS as it mimics the T-cell mediated inflammation seen in MS (Robinson et al., 2014). The clinical course of disease, histopathology of lesions, gliosis, demyelination, and axonal damage are similar in EAE and patients with MS (Schreiner et al., 2009). Although EAE is not a perfect recapitulation of MS, it does offer researchers a model to understand MS pathophysiology and suggest potential treatment measures. As such, EAE has been previously used to study pain in MS (Olechowski et al., 2009; Benson et al., 2013; Olechowski et al., 2013; Benson and Kerr, 2014; Khan and Smith, 2014). In this study, we aimed to investigate whether the expression of the chloride co-transporters NKCC1 and KCC2 were

affected in the EAE model in areas involved in sensory processing and pain, the DRG and dorsal spinal cord. Using PCR and Western Blot analysis, we examined the changes in transcript and protein levels throughout the EAE disease course. We also assessed the effects of blocking NKCC1 with bumetanide, a well characterised antagonist of NKCC on pain hypersensitivity in the disease.

Experimental Procedures

EAE Induction

Subcutaneous injection (50µg) of myelin oligodendrocyte glycoprotein (MOG₃₅₋₅₅; Peptide Synthesis Facility, University of Calgary) emulsified in complete Freund's adjuvant (CFA) was used to elicit EAE in 8-10 week-old female C57BL/6 mice (n=50; Charles River). Only female mice were used in this study. Mice were examined daily for clinical signs of the disease and classified using the following criteria: Grade 0, no symptoms; Grade 1, paralyzed tail; Grade 2, mild hindlimb weakness; Grade 3, severe hindlimb weakness; Grade 4, complete hindlimb paralysis; Grade 5, moribund. EAE mice were grouped according to their disease progression: pre-symptomatic (PS; day 7 post-induction), EAE onset (at appearance of clinical symptoms), peak (at the height of clinical symptoms, Grade 4), and chronic (day 28 post-induction). On average, EAE mice presented symptoms at day 14.1 ± 0.84 post-induction and reached peak disease 16.7 ± 1.09 days post-induction. A set of CFA-control mice were also used as control for EAE induction. Two intraperitoneal injections of pertussis toxin, *Bordetella pertussis*, (List Biological Labs) were also administered to all mice on the day of induction and 48 hours thereafter. Different animals were used for mRNA (n=25) and protein (n=22) expression experiments. Two animals failed to get sick and one animal died due to the disease.

All animal experiments were performed according to Canadian Council on Animal Care's Guidelines and Policies with approval from University of Alberta Health Sciences Animal Care and Use Committee.

Behavioural Assays

Von Frey filaments test were used to assess mechanical allodynia in mice. Mice were habituated in boxes for three days for 10 min prior to the day of testing. On the day of testing, mice were habituated in boxes for 10 min and then the plantar surface of the hind paws were stimulated gradually with filaments ranging from 0.04 g to 2.0 g. Each paw was tested 5 times and the bending force of each filament that elicited pain behaviours more than half of the time (3/5 trials) were recorded as the mechanical threshold. All animals were subjected to von Frey filaments test on three separate days to establish a baseline threshold. All von Frey analysis is compared to the baseline threshold of the individual mouse in order to control for individual differences.

Tissue Harvesting

Dorsal portion of the lumbar spinal cord (dSC), and lumbar DRGs (L4-L5) were be harvested and used for downstream Western blotting, and quantitative real-time polymerase chain reactions (qRT-PCR).

Western Blotting

A previously established protocol of Western blotting from our lab will be used (Olechowski et al., 2013). Protein samples (16 µg) were separated on a 4-20% TGX precast gels (BioRad) and

transferred onto a PVDF membrane (BioRad). After blocking with 5% BSA (Sigma) in PBS-Tween, membranes were incubated with primary antibodies overnight. NKCC1 was probed using a monoclonal mouse T4 antibody (Developmental Studies Hybridoma Bank, University of Iowa, Cat# t4) (Price et al., 2006b) and both oligo and monomeric forms of KCC2 were identified using polyclonal rabbit anti-KCC2 antibody (EMD Millipore, Cat# 07-432). Binding of secondary antibodies (goat anti-mouse HRP and goat anti-rabbit HRP) were detected using enhanced chemiluminescence (GE). Reprobing with monoclonal mouse anti-beta-actin (Sigma, Cat# A5441) was used as a loading control.

Reverse Transcription and qRT-PCR

Using the Superscript III Reverse Transcriptase (Invitrogen), 200 ng of total RNA were converted to cDNA using oligo (dT)₁₂₋₁₈ primers (Invitrogen). 1.0 µl of resulting cDNA were used in a 20.0 µl FAST Sybr Green (Applied Biosystems) qRT-PCR reaction on a StepOne Plus System (Life Technologies). Primer sequences for KCC2 and PPIA were obtained from PrimerBank (Wang and Seed, 2003; Spandidos et al., 2008, 2010). NKCC1 primer sequences were generated in the lab. Primers are presented in Table 1.

Bumetanide Administration

Bumetanide (30 mg/kg; Tocris) was completely dissolved in 4% PBS-Tween20 solution and injected intraperitoneally (n=10) daily post day 7 of EAE induction. Bumetanide was administered until the onset of disease which varied individually. A solution of 4% PBS-Tween20 (Fisher Scientific) was used as a vehicle control (n=10) and it has previously been shown to have no effect on behaviour (Castro et al., 1995). On average, bumetanide-treated mice

developed EAE 16.6 ± 1.39 (Mean \pm SEM) days post-induction while vehicle-treated mice developed EAE 15.3 ± 1.38 days post-induction. No significant difference in the time to disease onset was found (Two-sample t-test, $t(15) = 0.627$, $p=0.53996$). Von Frey filaments test baselines were obtained on 3 separate days prior to EAE induction.

Statistical Analysis

All statistical analyses were performed in IBM SPSS v 20. PCR data was analysed using the Pfaffl method (Pfaffl, 2001) and the REST2009 software (Qiagen) (Pfaffl et al., 2002) applying a pairwise fixed reallocation randomisation test. Western blot data was subjected to one-way ANOVAs with Dunnett's t-test as a post-hoc analysis. PCR and Western blot data were log₂ transformed in order to normalize data and fulfill the homogeneity of variance assumption for ANOVAs. An alpha-value of 0.05 was used throughout the study.

Results

EAE Disease Course

Mice inoculated with MOG₃₅₋₅₅ develop symptoms of EAE over a course of 28 days (Fig 1A). The disease tends to recede slightly after reaching peak disability around day 20 post immunization and plateaus until the end of the experiment. On average, these mice develop the initial clinical signs of EAE at day 15 post induction.

We next examined the development of mechanical hypersensitivity in mice with EAE using Von Frey hair filaments (Fig 1B, C). As we and others have shown in previous studies, mice with EAE exhibit a characteristic hypersensitivity to tactile stimulation that is evident at the first clinical signs of the disease (Paired samples t-test, $t(5) = 6.158$, $p=0.002$, $M_{baseline} = 0.5889 \pm$

0.06536, $M_{onset} = 0.2492 \pm 0.05736$). In contrast, mice immunized with CFA alone show no significant change in withdrawal thresholds (Paired samples t-test, $t(9) = -0.692$, $p=0.506$, $M_{baseline} = 0.6027 \pm 0.04064$, $M_{onset} = 0.6700 \pm 0.10858$). Since this behavioural assay is limited by functional motility of the hind limbs, Von Frey filament testing was only carried out up to this time point in the disease as motor ability degenerates rapidly after clinical grade 1 is reached (van den Berg et al., 2016).

Chloride co-transporters in the DRG and dorsal spinal cord

qRT-PCR analysis of dorsal root ganglion samples revealed no difference in the mRNA levels of NKCC1 over the disease course as compared to CFA control samples ($p>0.05$, $M_{CFA(log2)} = 0.00 \pm 0.22$, $M_{PS(log2)} = 0.40 \pm 0.62$, $M_{onset(log2)} = 0.29 \pm 0.48$, $M_{peak(log2)} = 0.15 \pm 0.48$, $M_{chronic(log2)} = 0.48 \pm 0.34$) (Fig 2A). KCC2 expression is negligible or not present at all in the peripheral nervous system (Price et al., 2006b) and as such we found that KCC2 expression was undetectable in the DRG samples.

In the dorsal spinal cord, NKCC1 mRNA expression is significantly reduced at disease onset and peak as compared to CFA controls ($p=0.024$, $M_{CFA(log2)} = 0.00 \pm 0.29$, $M_{onset(log2)} = -1.24 \pm 0.21$; $p=0.033$, $M_{peak(log2)} = -1.59 \pm 0.47$) (Fig 2B, C). Similarly, KCC2 mRNA levels are downregulated at onset and peak ($p=0.048$, $M_{CFA(log2)} = 0.00 \pm 0.29$, $M_{onset(log2)} = -1.10 \pm 0.10$; $p=0.049$, $M_{peak(log2)} = -1.40 \pm 0.49$). These effects in NKCC1 and KCC2 mRNA expression in dSC recuperate at the chronic stage (NKCC1: $p>0.05$, $M_{CFA(log2)} = 0.00 \pm 0.29$, $M_{chronic(log2)} = -0.23 \pm 0.41$; KCC2: $p>0.05$, $M_{CFA(log2)} = 0.00 \pm 0.29$, $M_{chronic(log2)} = -0.50 \pm 0.35$).

We next asked whether there are changes in the protein levels of the chloride co-transporters NKCC1 and KCC2 in the DRG and dorsal spinal cord in mice with EAE. In contrast to the PCR

results, NKCC1 protein levels in the DRG are significantly increased at disease onset and returned back to CFA control levels by the chronic stage (One-way ANOVA, $F(4, 16) = 3.666$, $p=0.027$, Dunnett's t-test post-hoc comparison to CFA) (Fig 3A). In the dSC, NKCC1 and KCC2 protein levels decreased significantly in mice with EAE at disease onset and peak disease (One-way ANOVA, NKCC1: $F(4, 17) = 14.673$, $p<0.001$; KCC2: $F(4,17) = 5.632$, $p = 0.004$; Dunnett's t-test post hoc comparison to CFA) (Fig 3B, C), in line with the mRNA expression. KCC2 oligomer levels were also significantly reduced at onset and peak (One-way ANOVA, $F(4, 17) = 4.884$, $p = 0.008$; Dunnett's t-test post hoc comparison to CFA, $p_{onset} = 0.005$, $p_{peak} = 0.036$) (Fig 3D).

Bumetanide Treatment

Given the increase in NKCC1 levels at disease onset in mice with EAE, we next assessed a second cohort of animals that were treated with bumetanide, an NKCC inhibitor, in order to investigate the relationship of NKCC1 and the tactile hypersensitivity we find in the disease. Other groups (Valencia-de Ita et al., 2006; Pitcher et al., 2007; Hasbargen et al., 2010; Pitcher and Cervero, 2010) have reported to have observed a reduction in hypersensitivity after bumetanide administration in their respective models. Non-diseased, CFA control mice did not exhibit any significant change in mechanical threshold in with either bumetanide (Paired samples t-test, $t(9)=0.663$, $p=0.524$, $M_{baseline} = 0.7767 \pm 0.04333$, $M_{CFA}=0.6920 \pm 0.13354$) or vehicle treatment (Paired samples t-test, $t(8)=0.081$, $p=0.938$, $M_{baseline} = 0.8200 \pm 0.11382$, $M_{CFA}=0.8067 \pm 0.13072$) (Fig. 4A, B). EAE mice treated with bumetanide exhibited a similar disease progression as the first, untreated cohort, with an average day of onset at day 16 post immunization. Bumetanide treated mice with EAE also showed evidence of tactile

hypersensitivity as compared to their baselines (Paired samples t-test, $t(6)=3.239$, $p=0.018$, $M_{baseline} = 0.6762 \pm 0.04286$, $M_{onset}=0.3914 \pm 0.05621$), similar to the allodynia observed in vehicle treated EAE mice (Paired samples t-test, $t(9)=6.561$, $p<0.001$, $M_{baseline} = 0.6867 \pm 0.05356$, $M_{CFA}=0.3635 \pm 0.04884$) (Fig 4C, D). Treatment with bumetanide did not reverse allodynia and was deemed ineffective at preventing the development of tactile hypersensitivity in mice with EAE.

This lack of behavioural response to bumetanide treatment was not the result of ineffective drug delivery or lack of biological action of bumetanide in EAE. We examined NKCC1 protein levels in the DRG after bumetanide treatment and found that the levels of NKCC1 were significantly reduced at disease onset (One-way ANOVA, $F(3, 16) = 3.891$, $p = 0.029$; Dunnett's t-test post hoc comparison, EAE-Veh vs EAE-BMT, $p = 0.023$) (Fig 5A). Vehicle treated EAE mice showed a significant elevation of NKCC1 in the DRG (Dunnett's t-test post hoc comparison, CFA-Veh vs EAE-Veh, $p = 0.031$) and a reduction in the dSC (One-way ANOVA, $F(3, 17) = 12.424$, $p<0.001$; Dunnett's t-test post hoc comparison, CFA-Veh vs EAE-Veh, $p = 0.002$), as expected (Fig 5B). Bumetanide treatment was found to be effective in significantly raising NKCC1 levels in the dSC to CFA vehicle levels (Dunnett's t-test post hoc comparison, CFA-Veh vs EAE-BMT, $p = 0.959$; EAE-BMT vs EAE-Veh, $p = 0.005$). Similarly, the levels of the monomeric form of KCC2 were normalized with bumetanide treatment (One-way ANOVA, $F(3, 17) = 10.686$, $p<0.001$; Dunnett's t-test post hoc comparison, CFA-Veh vs EAE-Veh, $p = 0.001$; EAE-BMT vs EAE-Veh, $p= 0.009$; EAE-BMT vs CFA-Veh, $p = 0.723$) (Fig 5C). However, levels of the oligomeric form of KCC2 were not fully restored in EAE mice treated with bumetanide (One-way ANOVA, $F(3, 17) = 20.198$, $p<0.001$; Dunnett's t-test post hoc

comparison, CFA-Veh vs EAE-Veh, $p = 0.004$; EAE-BMT vs EAE-Veh, $p = 0.094$; EAE-BMT vs CFA-Veh, $p = 0.335$) (Fig 5D).

Discussion

NKCC1 and KCC2 in the nervous system have the potential to regulate GABAergic transmission and hence, control the degree and extent of inhibition in the CNS and excitation in the PNS (Price et al., 2005; Pitcher and Cervero, 2010; Price and Prescott, 2015). Since GABAergic transmission is critical for maintaining normal nociceptive processing, we investigated whether the levels of these critical regulatory proteins are affected in the mouse model EAE to gain insight into potential underlying causes of the tactile hypersensitivity that we and others have reported develops in mice with the disease (Olechowski et al., 2009; Khan and Smith, 2014). We find that there is a transient dysregulation in the levels of NKCC1 and KCC2 at disease onset, the time point when heightened nociceptive behaviours are most pronounced in mice with EAE. NKCC1 expression in primary afferent terminals is crucial for primary afferent depolarization, a form of presynaptic inhibition (Zeilhofer et al., 2012). In effect, NKCC1 leads to an accumulation of chloride ions inside the cell leading to a high reversal potential of GABA (E_{GABA}). Physiologically, GABA_AR activation on these terminals causes a localized depolarizing current that is enough to inactivate voltage gated calcium and sodium channels and to produce a shunting conductance which eventually results in reduced glutamate release (Price et al., 2009; Zeilhofer et al., 2012; Chen et al., 2014a). A reduction of presynaptic inhibition via a change in E_{GABA} or G_{GABA} (GABAergic conductance) would compromise the inhibitory gate. Our results indicate that there is a significant decrease in NKCC1 levels in the dorsal spinal cord in mice with EAE. This, in turn, would reduce the effect of PAD and ultimately cause disinhibition of the

presynaptic terminal. Other studies have described an upregulation of NKCC1 levels in the dorsal horn using various models of neuropathic pain (Cramer et al., 2008; Hasbargen et al., 2010; Chen et al., 2014a, 2014b). It has been postulated that an increase in NKCC1 levels would cause sufficient depolarization via PAD leading to dorsal root reflexes and neurotransmitter release (Cervero and Laird, 1996; Cervero et al., 2003; Price et al., 2009; Chen et al., 2014a). This, in turn, would amplify sensory input arriving from the periphery onto second order neurons. However, a recent study has shown that an increase in NKCC1 expression after chronic constriction injury is not sufficient to lead to an action potential but rather it is enough to cause disinhibition at the afferent terminal (Chen et al., 2014a). Based on these observations, a reduction in levels of primary afferent derived NKCC1 in the dorsal horn of the spinal cord, as we observed in mice with EAE, would effectively reduce the ability of spinal GABAergic interneurons to inhibit incoming sensory signals.

The interplay of KCC2 and the neurotrophin, brain derived neurotrophic factor (BDNF), in neuropathic pain has been robustly described (Watanabe and Fukuda, 2015). Microglia that express the ATP receptor subtype, P2X4, release BDNF leading to a decrease in KCC2 expression on projection neurons via the activation of TrkB receptor (Coull et al., 2003, 2005; Trang et al., 2009, 2012; Beggs and Salter, 2013; Gagnon et al., 2013). A reduction in KCC2 on these neurons leads to a disinhibition allowing greater amount of nociceptive and allodynic stimulation to reach high order regions of the CNS. Our group and other have observed microglial activation (Olechowski et al., 2009; Lassmann, 2010; Khan et al., 2015) and an upregulation of P2X4 receptors in EAE (Tsuda et al., 2003; Coull et al., 2005; Vázquez-Villoldo et al., 2014). Other studies also describe a significant upregulation of BDNF in the dorsal horn of the spinal cord in EAE (Zhu et al., 2012; Bernardes et al., 2013; Khan et al., 2015). At the same

disease time point, we find that there is a decrease in KCC2 levels in the dorsal horn. We postulate that the reduced levels of KCC2 in EAE is mediated via the significant increase in microglial activation in this region.

NKCC1 upregulation in the DRG has been noted in various models of peripheral neuropathy (Chen et al., 2014a; Modol et al., 2014). We too, have observed an upregulation of NKCC1 protein expression but no change in NKCC1 mRNA levels at the level of the DRG.

Immunostaining methods are largely hindered by poor antibodies for NKCC1 (Price et al., 2009) albeit immunoblotting for NKCC1 is more reliable (Price et al., 2006b, 2009). Furthermore, satellite glial cells in the DRG have been known to possess NKCC1 mRNA and express NKCC1 protein (Price et al., 2006b). Since satellite glial cells are tightly wrapped around DRG neurons, NKCC1 expression in these glial cells give a “membrane-associated” immunoreactivity pattern that may be misinterpreted as originating from DRG neurons (Price et al., 2006b, 2009). NKCC1 in DRG neurons has previously been implicated in increasing GABAergic conductance (Cervero et al., 2003) and regeneration of sensory axons (Modol et al., 2015). The role of NKCC1 expression in satellite glial cells however, remains elusive.

Bumetanide is an inhibitor of NKCC1 and NKCC2 and is commonly used as a diuretic. Since the nervous system exclusively expresses NKCC1 (Price et al., 2006b), many studies of peripheral nerve injury use bumetanide treatment to assess the role of NKCC1 in the nervous system (Valencia-de Ita et al., 2006; Pitcher et al., 2007; Cramer et al., 2008; Hasbargen et al., 2010; Pitcher and Cervero, 2010; Modol et al., 2014, 2015). In order to counter the increased levels of NKCC1 in the DRG at disease onset in mice with EAE, we administered bumetanide intraperitoneally daily from day 7 post immunization (the presymptomatic stage of EAE). Mice were tested for changes in mechanical threshold at onset along with their CFA control

counterparts. We did not however, observe any change in Von Frey thresholds in bumetanide treated mice. Our biochemical analysis revealed that bumetanide treated mice had reduced levels of NKCC1 in the DRG and increased NKCC1 in the dSC suggesting that bumetanide was functioning at the molecular level. Furthermore, mice treated with bumetanide exhibited polyuria which was another indicator that the drug was circulating in the body (Asbury and Gatenby, 1972).

There have been reports that there exists a relationship between NKCC1 levels in the PNS and KCC2 levels in the CNS (Modol et al., 2014). In a model of peripheral nerve injury, administration of bumetanide reduced the phosphorylation of NKCC1 and thereby prevented a downregulation of KCC2 in the CNS (Modol et al., 2014). Administration of bumetanide in our study also reversed the downregulation of monomeric KCC2, however, it failed to normalize the oligomeric form of KCC2. Oligomerization of KCC2 in non-rafts is known to enhance chloride extrusion capabilities of the transporter (Hartmann and Nothwang, 2014). As the oligomeric form of KCC2 represents a more 'functional' chloride co-transporter, this suggests that a loss of active KCC2 is an important aspect for the tactile hypersensitivity in EAE. Currently, two novel drugs, CLP257 and CLP290, are under investigation as potential KCC2 activators that enhance oligomerization and phosphorylation of KCC2 in order to mitigate hyperalgesia (Blaesse et al., 2006).

NKCC1 and KCC2 are chloride symporters that use the electrochemical gradient of sodium and potassium ions to actively pump chloride ions into or out of the cells. In the CNS, KCC2 expression dominates and it is primarily responsible for chloride-mediated hyperpolarizing currents (Price and Prescott, 2015). KCC2 activity can be enhanced by (de)phosphorylation (Kahle et al., 2013) of specific residues and by oligomerization of KCC2 into a homo-oligomeric

organization (Blaesse et al., 2006). We noticed a significant down-regulation of the oligomeric form of KCC2 along with its monomeric form at the onset of clinical sign in EAE. This indicates that KCC2 is being functionally depressed along with being transcriptionally reduced in EAE. Future studies targeting the activation of KCC2 may uncover the role of phosphorylation and oligomerization of KCC2 for regulating pain behaviours in the disease. Furthermore, a limitation of our study was the lack of electrophysiological data. Future electrophysiological studies are required to elucidate the role of these chloride co-transporters in hyperexcitability of peripheral and central neurons.

This study is the first of its kind to assess the role of chloride cotransporters in mediating pain in EAE. As a model of T-cell mediated global inflammation, EAE is phenotypically different from other more widely used pain models. Discrepancies between EAE and other focal lesions or injury models may be inherent in the model itself. As an example, NKCC1 levels in the DRG were reduced in a model of arthritis and NKCC1 and KCC2 mRNA and protein levels were elevated in superficial dorsal horn (Morales-Aza et al., 2004). This is in contrast to our study as well as a plethora of peripheral neuropathy studies (Coull et al., 2003; Pitcher et al., 2007; Cramer et al., 2008; Miletic and Miletic, 2008; Hasbargen et al., 2010; Beggs and Salter, 2013; Modol et al., 2014). Also, bumetanide treatment in peripheral nerve injury models of neuropathic pain is typically effective at resolving mechanical hyperalgesia (Valencia-de Ita et al., 2006; Pitcher et al., 2007; Cramer et al., 2008; Hasbargen et al., 2010; Pitcher and Cervero, 2010; Modol et al., 2014, 2015). However, it failed to do so in our study. This may be due to a persistent immune-mediated inflammation in the CNS of EAE animals which is largely absent in peripheral nerve injury models (Khan and Smith, 2014).

Tables:

Table 2.1. Primers used in qRT-PCR reactions.

Gene	GenBank Accession	PrimerBank ID	FWD/REV	Primer (5' - 3')	Calculated Efficiency (%)
PPIA	NM_008907.1	6679439a1	FWD	GAGCTGTTTGCAGACAAAGTTC	99
			REV	CCCTGGCACATGAATCCTGG	
NKCC1	NM_009194.3	N/A	FWD	TCAGTCAGCCATACCCAAAGG	96
			REV	GAACAACACACGAACCCACAG	
KCC2	NM_020333.2	28972652a1	FWD	GGGCAGAGAGTACGATGGC	96
			REV	TGGGGTAGGTTGGTGTAGTTG	

Figures:

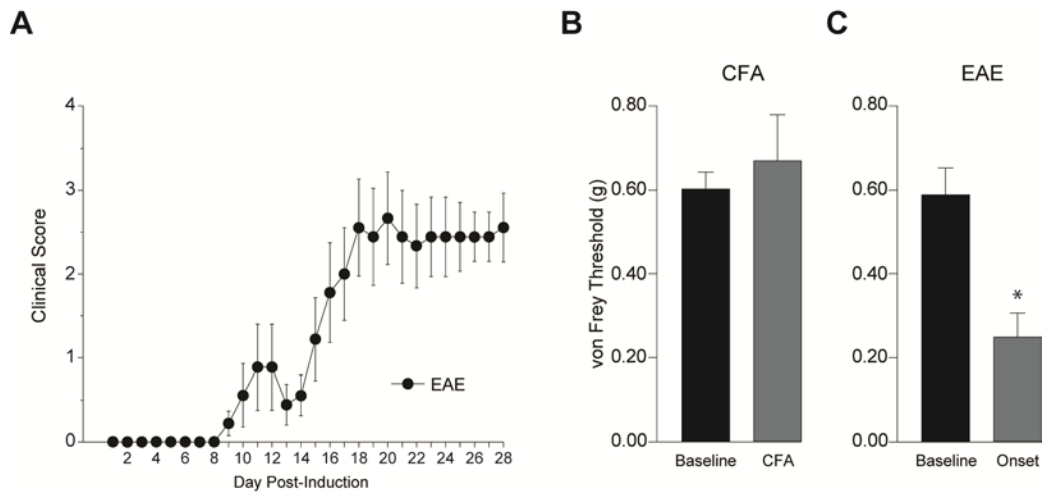


Figure 2.1. Mice with EAE show evidence of mechanical allodynia.

(A) EAE disease course depicts the severity of EAE with day post-induction of MOG₃₅₋₅₅. On average, mice induced with EAE show onset of symptoms at day 15. (B, C) Von Frey threshold of CFA control mice did not differ significantly from their baseline whereas EAE mice showed a significant reduction in their von Frey thresholds at disease onset. CFA mice were tested at the same time point as their EAE littermates at the time of disease onset. CFA (n=10), Onset (n=6).

* Paired samples t-test, $t(5) = 6.158, p=0.002$.

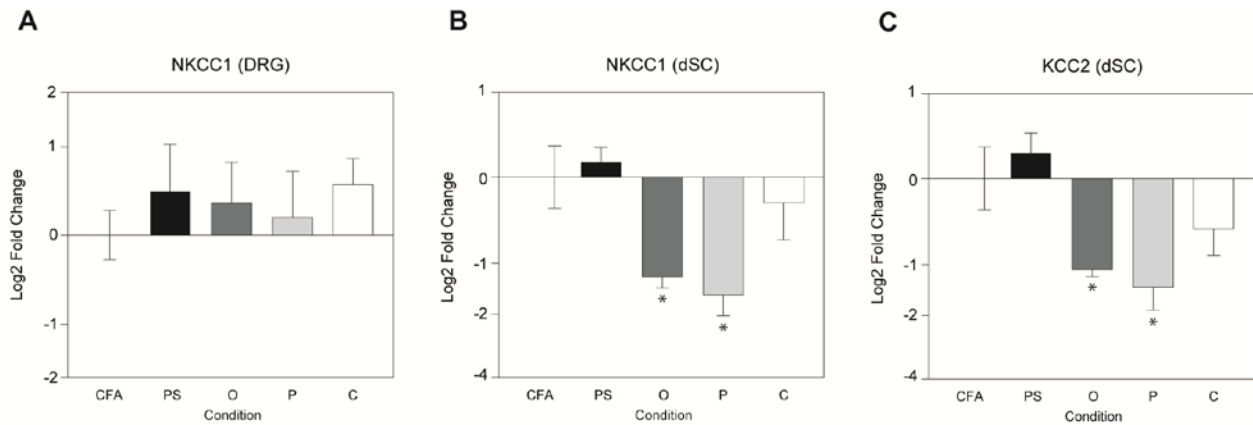


Figure 2.2. NKCC1 and KCC2 mRNA expression in the DRG and dSC.

(A) NKCC1 mRNA expression in the DRG remains relatively consistent throughout the EAE disease course. (B,C) There is a significant decrease in NKCC1 and KCC2 mRNA levels in the dSC at EAE onset and peak. CFA (n=5), PS (Presymptomatic; n=6), O (Onset; n=5), P (Peak; n=4), C (Chronic; n=5). All analyses were performed using the PffafI method and REST2009 (Qiagen) software. *p<0.05. Exact statistics are reported in the text.

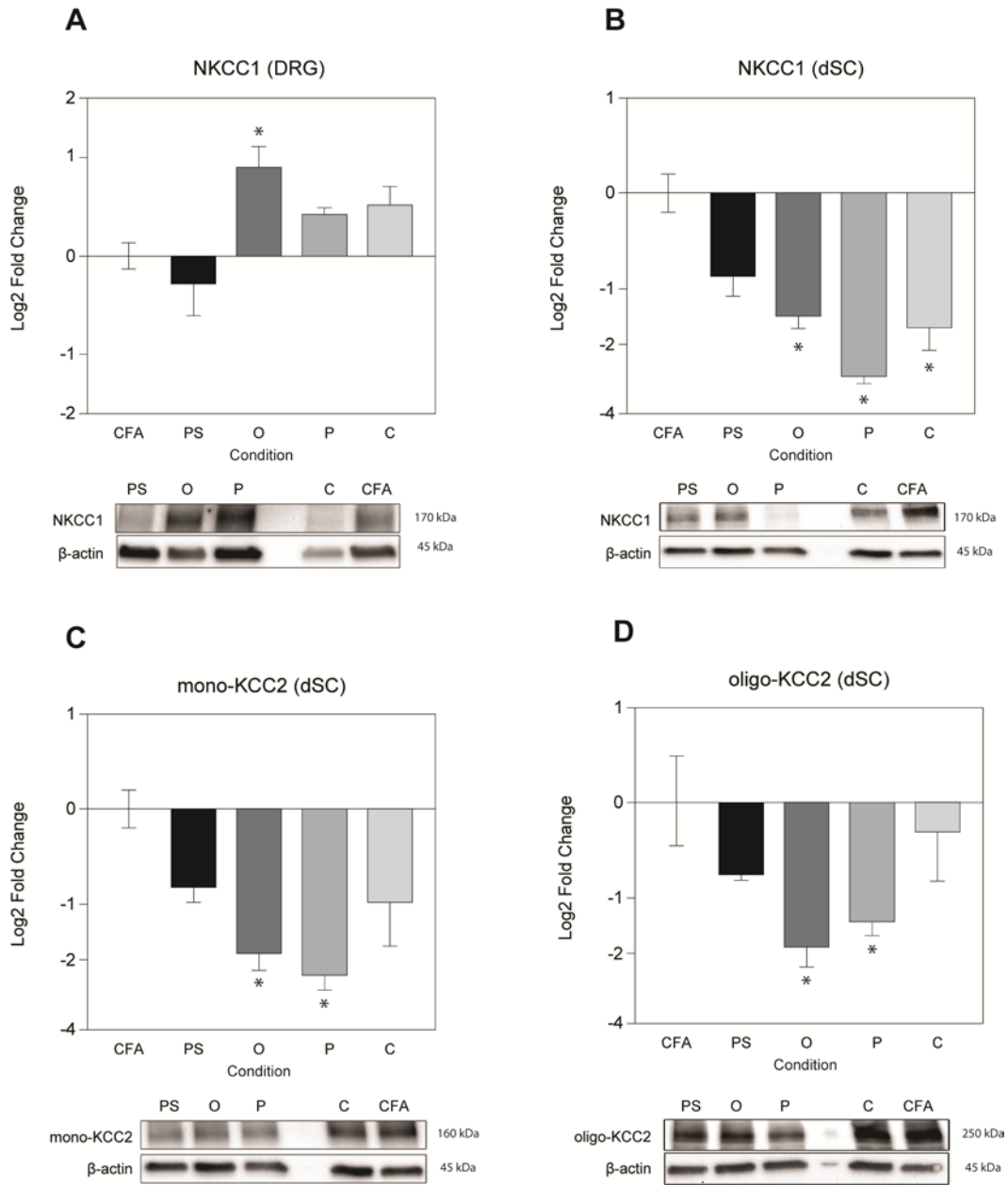


Figure 2.3. Western blot analysis reveals a dysregulation of NKCC1 and KCC2 in the DRG and the dSC.

(A) NKCC1 expression is significantly elevated with disease onset in the DRG only to normalize as the disease progresses. (B) In the dSC, however, there is a consistent decrease in NKCC1 expression beginning at the onset of symptoms until the chronic time-point. (C) Similarly, a

downregulation of monomeric KCC2 was observed at disease onset and peak. At the chronic stage, however, monomeric KCC2 was trending towards a decrease, albeit, insignificantly. (D) The oligomeric form of KCC2 also showed a significant reduction in expression at disease onset and peak with full recuperation at the chronic stage. CFA (n=5), PS (Presymptomatic; n=5), O (Onset; n=4), P (Peak; n=4), C (Chronic; n=4). Data was subjected to one-way ANOVA followed by Dunnett's t-test post-hoc comparison vs CFA. * $p < 0.05$. Exact statistics are reported in the text.

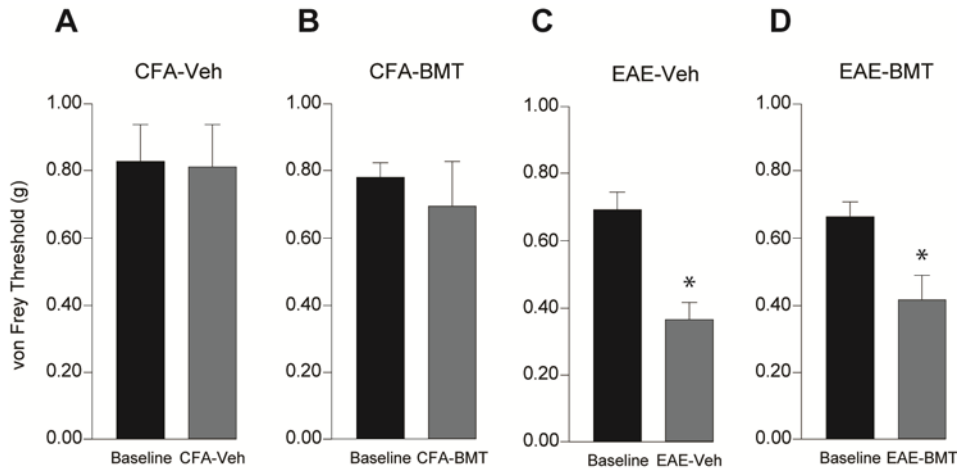


Figure 2.4. Bumetanide treatment does not alleviate mechanical allodynia.

(A, B) Vehicle treated and bumetanide (BMT) treated mice did not show any change in their von Frey thresholds. (C) Vehicle treated EAE mice at onset had a significantly lower von Frey threshold. (D) However, treatment of EAE mice with bumetanide failed to reverse mechanical allodynia and as a result these mice remained hypersensitive. CFA-Veh (n=9), CFA-BMT (n=10), EAE-Veh (n=10), EAE-BMT (n=7). Each animal was compared to its own baseline using paired samples t-test. *p<0.05. Exact statistics are reported in the text.

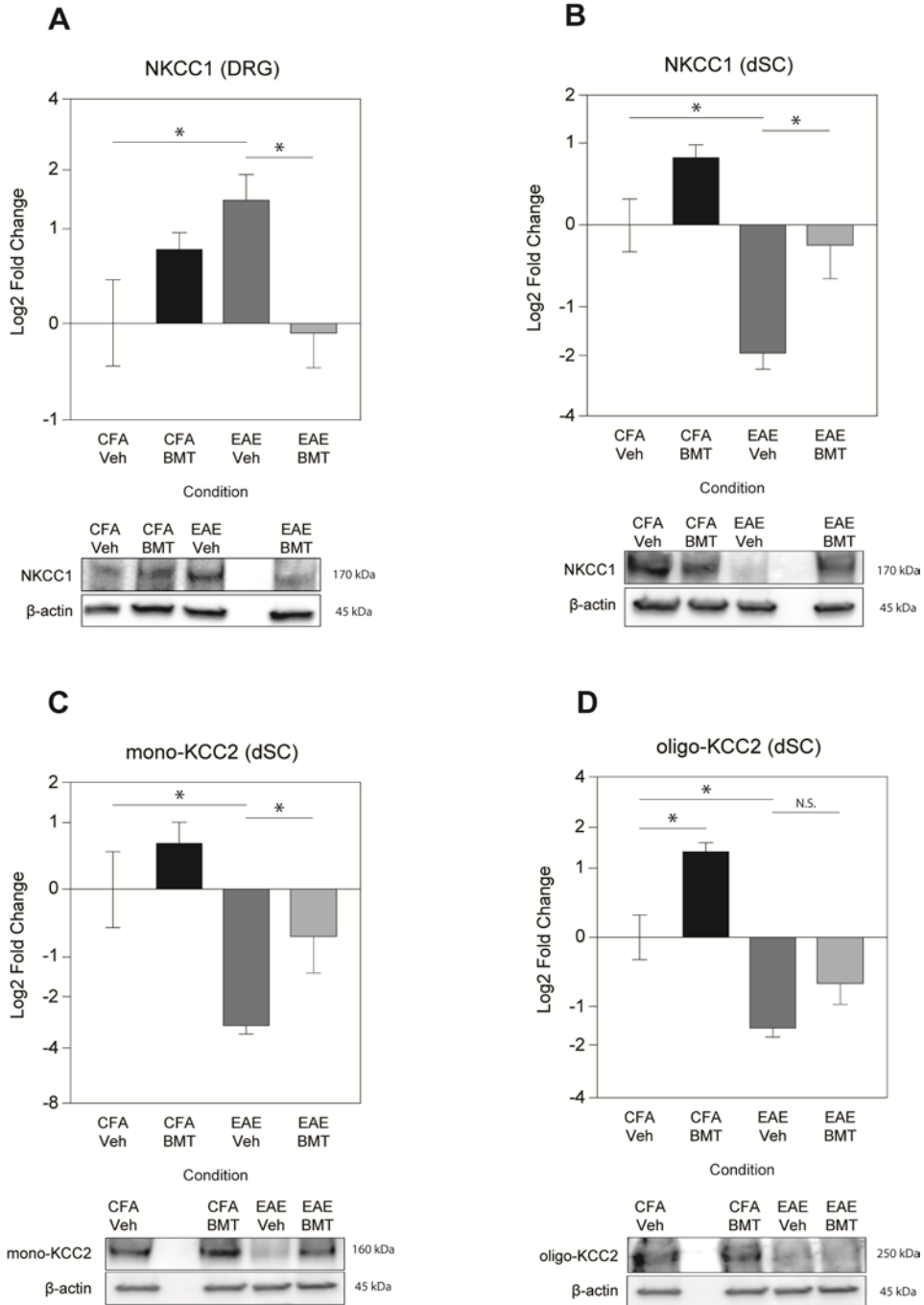


Figure 2.5. Bumetanide treatment modifies the expression of chloride cotransporters in the DRG and the dSC.

(A) NKCC1 expression is significantly elevated in the DRG of vehicle treated EAE mice. (B, C) NKCC1 and monomeric KCC2 protein levels in the dSC decrease significantly at disease onset in vehicle treated mice. Bumetanide treatment was able to normalize NKCC1 and monomeric

KCC2 expression in the DRG as well as the dSC. (D) Vehicle treatment in EAE mice at onset showed a significant down-regulation in oligomeric KCC2 as compared to vehicle treated CFA animals. Bumetanide treatment significantly upregulated oligo-KCC2 in CFA mice but failed to normalized oligo-KCC2 levels in the EAE mice. CFA-Veh (n=5), CFA-BMT (n=6), EAE-Veh (n=5), EAE-BMT (n=5). Data was subjected to one-way ANOVA followed by Dunnett's t-test post-hoc comparison versus CFA-Veh and EAE-Veh. * $p < 0.05$. Exact statistics are reported in the text.

Chapter 3 : Endoplasmic reticulum stress in the periphery contributes to pain in a model of multiple sclerosis

Introduction

Multiple sclerosis (MS) is a chronic, neurodegenerative disorder characterized by immune activation and loss of myelin in the central nervous system (CNS). Among the many sensory abnormalities associated with MS, pain is common and often debilitating. Pain is experienced by one third to a half of the population with MS at some point during their disease course and a significant percentage are diagnosed with neuropathic pain (Drulovic et al., 2015; Solaro et al., 2018). Current pharmacological approaches to alleviate this pain in have been largely ineffective with low patient confidence in prevailing treatment approaches (Hadjimichael et al., 2007). To investigate the pathophysiology of pain in MS, we employed a commonly used experimental autoimmune encephalomyelitis (EAE) mouse model.

Neuropathic pain is thought to arise from increased excitability of neurons along the pain axis, comprising sensory neurons in the peripheral dorsal root ganglion (DRG), and the trigeminal ganglion and the integrative central processes of the spinal cord and the brain (Chung and Chung, 2002; Latremoliere and Woolf, 2009; Waxman and Zamponi, 2014). The role of the CNS as a modulator of pain in MS/EAE has been widely studied (Khan and Smith, 2014). However, only a handful of studies to date has investigated the contribution of the peripheral branch of the somatosensory nervous system to pain pathophysiology in EAE and MS (Lu et al., 2012; Duffy et al., 2016; Frezel et al., 2016; Thorburn et al., 2016; Yousuf et al., 2017; Mifflin et al., 2019).

In response to MS/EAE, the central projections of the DRG neuronal somata may sustain indirect injury through chronic neuroinflammatory processes occurring in the CNS. These

injuries at the spinal terminal may evoke a retrograde stress response in the cell bodies of the DRG. When cells are subject to chronic stressors, such as prolonged inflammation and cytoskeletal disruption, they may undergo endoplasmic reticulum (ER) stress. The ER is an important organelle required for lipid biosynthesis, calcium ion (Ca^{2+}) storage and protein folding and processing (Stone and Lin, 2015). Stress can impair protein folding thus triggering a cascade of events that are collectively known as the unfolded protein response (UPR) (Sano and Reed, 2013; Hetz and Mollereau, 2014).

The ER-based signalling mechanism initially functions to mitigate cellular damage. Activation of the UPR is mediated by three ER stress sensor proteins, IRE1, PERK, and ATF6 (Stone and Lin, 2015). Signaling initiated through these three independent pathways promotes cell survival by ultimately reducing misfolded protein levels both via reducing mRNA translation and via enhancing the ER's folding capacity. If the stressor is particularly severe or prolonged however, the UPR can drive the cell into an apoptotic program of regulated cell death (Sano and Reed, 2013; Stone and Lin, 2015). Emerging evidence is now demonstrating that ER stress may also be a significant factor for developing pain hypersensitivity in various animal models across a variety of cell types (Inceoglu et al., 2015; Khoutorsky et al., 2016; Gavini et al., 2018; Yamaguchi et al., 2018; Chen et al., 2019; Chopra et al., 2019; Kong et al., 2019; Pan et al., 2019). In this study, we investigated whether ER stress in DRG neurons contributes to the well characterised pain hypersensitivity that occurs in the EAE model and by extension in MS (Benson and Kerr, 2014; Khan and Smith, 2014).

Materials and Methods

Human Tissue

Human tissue was obtained from the Netherlands Brain Bank (NBB; <http://www.brainbank.nl>). Subjects or their next of kin provided written informed consent for the use of their tissue and clinical information for research purposes to the NBB. All MS individuals (n=9) experienced the progressive phase of the disease and presented evidence of chronic pain such as trigeminal neuralgia, migraine, extremity pain, and back pain. The average disease duration was 21.0 ± 4.61 years. Average age at death was 78.6 ± 4.32 years for the non-demented controls (n=7) and 59.7 ± 4.04 years for individuals with MS. The majority of the donors elected to be euthanized with a combination of barbiturates (thiopental, pentobarbital) and muscle relaxant (Rocuronium bromide). Only female human tissue was examined. Patient demographics are further summarized in **Table 1**.

Snap frozen human DRGs were sectioned onto superfrost plus glass slides (VWR International, Leuven, Belgium) at $10\mu\text{m}$ thickness. Ten $10\mu\text{m}$ thick sections were harvested for RNA and protein analysis. Tissue was lysed in $600\mu\text{l}$ of Buffer RLT (Qiagen, 79216) with β -mercaptoethanol (Sigma, M3148, $10\mu\text{l/ml}$ of Buffer RLT) using a 2 ml Potter-Elvehjem homogenizer. The homogenate was then centrifuged at full speed for 2 min in QIAshredder column (Qiagen, 79656). RNA was extracted from the flow-through using the RNeasy Mini Kit (Qiagen, 74104) according to manufacturer's instructions. RNA was quantified using a Nanodrop 2000. Reverse transcription and PCR analysis was performed as described later.

The flow-through after RNeasy spin column centrifugation step was stored at 4°C for protein extraction. The protein was precipitated using ice-cold acetone ($500\mu\text{l}$ sample + $1500\mu\text{l}$ acetone). The acetone laden sample was store at -20°C for 2 hours and then centrifuged at

15,000g for 10 min at 4°C. The supernatant was discarded and the pellet was redissolved in 100µl of 5% SDS. Protein was quantified using the DC Protein Assay (BioRad, 5000112). Western blots using 10µg of protein were performed as described below.

Immunohistochemical analysis of human DRG sections were performed similar to previously described (Schenk et al., 2013; Yousuf et al., 2019). In brief, slides were fixed in acetone for 10 min, followed by three 5-min gentle PBS washes, after which the slides were air dried in a fumehood for 30 min. The sections were blocked at room temperature with 10% NGS in PBS. Primary antibody dissolved in antibody solution (1% BSA and 0.2% NGS in PBS) was placed over the DRG sections overnight. The slides were then washed in PBS (3x–5min each) followed by 1 hour incubation in secondary antibody (1:200) dissolved in antibody solution. Another set of washes in PBS (3x–5 min each) were performed and then the slides were mounted using Vectashield with DAPI (Vector Labs, H-1200).

The use of tissue and access to medical records was approved from the Ethics Committee of the VU University Medical Center, Amsterdam, The Netherlands.

EAE induction and scoring

As previously described (Yousuf et al., 2017), experimental autoimmune encephalomyelitis (EAE) was induced in female C57BL/6 mice (8-10 weeks old; Charles River) by subcutaneously injecting 50µg myelin oligodendrocyte glycoprotein (MOG₃₅₋₅₅; Hooke Laboratories) emulsified in complete Freund's adjuvant (CFA; 1.5mg/ml) followed by inoculations with 300ng of pertussis toxin, *Bordatella pertussis*, (List Biological Labs) on the day of induction and 48 hours later. Animals were quarantined for 72 hours after induction. Mice were monitored daily for clinical signs of EAE and scored accordingly: Grade 0, no signs; Grade

1, flaccid tail; Grade 2, mild hindlimb weakness; Grade 3, severe hindlimb weakness; Grade 4, complete hindlimb paralysis; Grade 5, moribund. Presentation of initial clinical signs of EAE (Grade 1) was considered “onset” and 21-days after induction was considered the “chronic” time point. At study endpoints, mice were euthanized by intraperitoneal injection of pentobarbital (Euthansol, 0.1ml of 340mg/ml) followed by a cardiac perfusion with ice cold 0.9% saline.

All animal experiments were performed according to Canadian Council on Animal Care’s Guidelines and Policies with approval from University of Alberta Health Sciences Animal Care and Use Committee.

Behavioural assessments

Mechanical hypersensitivity, facial sensitivity, and gross locomotor ability were assessed as previously described (Olechowski et al., 2013; Thorburn et al., 2016; Yousuf et al., 2017). Data was compared to the baseline threshold of individual mice in order to control for individual differences.

4-PBA administration in vivo

4-PBA (200mg/kg; Tocris, 2682) was completely dissolved in 1X sterile PBS and injected intraperitoneally (n=6) daily, beginning at disease onset until day 7-10 post-onset. PBS was administered as a vehicle control (n=5). Von Frey testing was performed one-hour after injection on the day of disease onset. Facial sensitivity was assessed using the air puff assay one-hour after the final injection 7-10 days post onset.

Immunohistochemistry

The mouse tissue was fixed with 4% paraformaldehyde (PFA) in 0.1M phosphate buffer (PB) overnight at 4°C followed by two 30% sucrose washes, each overnight at 4°C. After removing excess sucrose, the tissue was embedded in Tissue-Tek OCT (Sakura Finetek, 4583). DRGs were cryosectioned with 10µm thickness while the spinal cords were sectioned at 20µm onto glass slides. The remaining staining protocol was identical to a previously established protocol (Yousuf et al., 2019).

Western blotting

Protein lysates were diluted in RIPA (25mM Tris, 150mM NaCl, 0.1% SDS, 0.5% Na deoxycholate, 1% NP-40) with protease (cOmplete EDTA-free, Roche, 04693159001) and phosphatase inhibitors (PhosSTOP, Roche, 04906837001) and 5X sample buffer was added. Directly before loading onto 10% SDS-PAGE gels, samples were boiled at 100°C for 10 min. Gels were run at 150 V for 60 min and transferred onto nitrocellulose membranes with 400 mA over 120 min.

Membranes were stained with REVERT Total Protein Stain (Licor) according to manufacturer's instructions and then blocked in 2% BSA in 1X DPBS for 1 hour at room temperature followed by overnight incubation at 4°C with a primary antibody dissolved in blocking solution. Membranes were then washed 3 times (3 minutes each) in TBS-T and incubated in 2% milk in TBS-T with Alexa Fluor coupled secondary antibodies for 1 h at room temperature. After another wash step, membranes were scanned using an Odyssey infrared imager (Licor).

Western blots using human tissue were performed as previously described (Yousuf et al., 2019). Stain free gels (BioRad, 456-8093, 4-20%) were transferred onto low-fluorescence PVDF blots (BioRad, 1704274) using the Trans-Blot Turbo transfer system (BioRad). Total protein was quantified using Stain-Free technology (BioRad) according to manufacturer's instructions. Blots were imaged with BioRad ChemiDoc XRS+ system and quantified using Image Lab 6.0 (BioRad) with total protein as loading control. Antibodies are summarized in **Table 2**.

Quantitative real-time PCR

Reverse transcription and PCR analyses were performed as previously described (Yousuf et al., 2019). Reverse transcription on human samples was performed using 160ng of total RNA. PCRs were performed on StepOne Plus thermocycler using *Rpl5* (mouse) or *RPLP0* (human) as housekeeping genes. Primers used in this study were obtained from Qiagen: *Rpl5* (PPM25102A), *Xbp1* (PPM05627A), *Ddit3* (PPM03736A), *Hspa5* (PPM03586B), *Kcnmb1* (PPM04055A), *RPLP0* (PPH21138F), *C3AR1* (PPH02514A), *C5AR1* (PPH06063F), *CD3E* (PPH01486B), *CD4* (PPH01629C), *XBPI* (PPH02850A).

Dissociated DRG cultures

Dissociated DRG cultures for calcium imaging were prepared from freshly excised DRGs according to our previously published protocol (see “Dissociated dorsal root ganglia cultures”, Mifflin et al., 2019) with STEMzyme I (2mg/ml; Worthington, LS004106) replacing collagenase IV. For electrophysiology experiments, DRG neurons were dissociated with a mix of STEMzyme I (1mg/ml) and trypsin (0.5mg/ml; HyClone, SV3003101).

In vitro application of 4-PBA was prepared as a stock solution of 100mM in Hank's balanced salt solution (HBSS) (Hyclone, SH30030.02). Stock solution of AMG44 (Tocris, 5517, 3mM) was prepared in sterile 60% dimethyl sulfoxide (DMSO; Sigma, D2650). Dissociated cells received diluted 4-PBA (final concentration: 10mM) and AMG44 (final concentration: 5 μ M) treatment one-hour after plating in cell media (DMEM/F12 [Gibco, 10565018], 1% N₂ [Gibco, 17502048], 1% penicillin/streptomycin [Gibco, 1570063]). Vehicle treatment in each experiment consisted of equal volume of either HBSS or DMSO (final concentration: 0.1%). Cells were incubated in their respective treatment conditions for 20-24 hours prior to Ca²⁺ imaging and electrophysiology.

Gene knockdown experiments were performed with HiPerfect transfection system (Qiagen, 301705) using Flexitube siRNA (Qiagen; XBP1: GS22433, Ddit3: GS13198, AllStars Negative Control siRNA: 1027284). The Flexitube siRNA contains a cocktail of multiple siRNA targeting multiple regions of the mRNA. The siRNA cocktail was prepared according to manufacturer's instructions. The final total siRNA concentration was 0.04 μ M (4 individual siRNAs, each at 0.01 μ M). 100 μ l of siRNA mixture was added to cells (100 μ l droplet) one hour after plating them onto glass coverslips. The cells were incubated for 10 min at 37°C and then topped up to 1 ml in cell media followed by incubation for 20-24 hours prior to Ca²⁺ imaging.

Live cell Ca²⁺ imaging in DRG neurons

Confocal imaging of cytosolic Ca²⁺ transients was performed as previously described (see "Ca²⁺ imaging of dorsal root ganglia cultures", Mifflin et al., 2019) with the addition of caffeine (Sigma, C0750) dissolved in superfusate (in mM) (120 NaCl, 3 KCl, 1 CaCl₂, 2 MgSO₄, 20 glucose). After 5 min of equilibration in the optical recording chamber with superfusate,

administered with a peristaltic pump at 4 ml/min) the imaging paradigm was as follows: 30s superfusate perfusion (baseline), 30s caffeine (20mM), 4 min superfusate perfusion, 5 min washout period, 30s superfusate perfusion (baseline), 30s KCl (30mM), 4 min superfusate perfusion. The imaging data were analyzed using Olympus FV10-ASW software with the first 30s as baseline for each caffeine and KCl application. The remaining recording was divided by the baseline to obtain a ratio of change in fluorescence (Fluo-4 F/F). These data were further normalized to an internal control of the particular experiment (e.g. Ca^{2+} transients were normalized to CFA in the AMG44 experiment, EAE vehicle in the 4-PBA and siRNA experiments). Once the imaging was completed, the 15 mm diameter coverslips were placed in 12 well plate with 600 μ l of Buffer RLT (Qiagen). These plates were stored at -80 °C until RNA extraction. Total RNA was extracted from individual coverslips using RNeasy Micro Kit (Qiagen, 74004) according to manufacturer's instructions.

Perforated patch whole-cell recordings

Solutions: The extracellular bath solution contained (in mM): 135 NMDG, 5 KCl, 2.8 NaCH₃CO₂, 1CaCl₂, 1MgCl₂, 10 HEPES and was adjusted to pH 7.4 with HCl. The intracellular (pipette) solution contained (in mM): 135 KCl, 5 EGTA, 10 HEPES and was adjusted to pH 7.2 with KOH. Amphotericin B was used to perforate the patch and solutions were made fresh before use. 6 mg amphotericin powder (Sigma) was added to 100 μ l of DMSO and solubilized in a 1.5 ml centrifuge tube. From the 60 mg/ml stock solution, 20 μ l was added to 5 ml of pipette solution for a final concentration of 240 μ g/ml. Paxilline (Tocris), used to inhibit BK channels, was dissolved in EtOH at a stock concentration of 1mM. Paxilline was added to 40 ml of bath solution for a desired working concentration of 1 μ M and perfused into the chamber when appropriate.

Data acquisition and analysis: Prior to experiments, 5 μ l of Alexa488-conjugated IB4-antibody (Invitrogen, 1 mg/ml) was added for 10 minutes then removed, to differentiate between IB4+ and IB4- DRG neurons. Glass coverslips containing cells were removed from the incubator (37°C) and placed in a superfusion chamber containing the bath solution at ambient temperature (22-23°C). IB4+ neurons were observed with epifluorescence illumination. Patch pipettes were manufactured from soda lime glass (Fisher), using a Sutter P-97 puller (Sutter Instrument). When filled with internal solution, patch pipettes had a tip resistance of 2-4 M Ω . After formation of a gigaohm seal between pipette tip and cell, currents were recorded through amphotericin B-induced pores. Whole-cell perforated patch clamp recordings were acquired and analyzed using a Digidata 1440 digitizer, an Axopatch 200B amplifier and Clampex 10 software (Molecular Devices). Recordings were sampled at 10 kHz and filtered at 5 kHz, with manual capacitance compensation and series resistance compensation at (80%). In voltage-clamp mode, total IK was measured by stepping between -130 and 200 mV (100 ms in 10 mV increments) from a -100 mV holding potential followed by a 100 ms tail current voltage at -30 mV. Bath solution containing 1 μ M paxilline was perfused in the chamber for 2 minutes to inhibit BK channels. During perfusion, IK was recorded with a +60 mV depolarizing pulse for 150 ms with 5 s interpulses from a -80 mV holding voltage to observe paxilline-induced current reduction. To isolate BK currents, currents were subtracted immediately before and after application of 1 μ M Paxilline from paxilline-sensitive (IB4+) DRG neurons. BK channel conductance-voltage (G/V) relationships were generated by analyzing the tail current amplitudes and fit with a Boltzmann function. BK channel current density was measured by dividing the current amplitude (pA) at +60 mV by cell capacitance (pF). Resting membrane potentials were recorded using current clamp mode from IB4+ DRG neurons using perforated-patch clamp. Vehicle treatment with HBSS (vehicle for 4-

PBA) and 0.01% DMSO (vehicle for AMG44) resulted in identical recordings and hence, two vehicle treatments were collapsed into a single group. DRG neurons from EAE animals were obtained at disease onset and the chronic time point (7-10 days post onset).

Experimental Design and Statistical Analysis

Statistical analyses were performed using GraphPad Prism 6 with appropriate statistical tests. Detailed statistical analyses have been mentioned in the Results section. Animals were assigned to each experimental group randomly. Western blot and PCR data were log-transformed prior to statistical testing in order to ensure the data fit the homogeneity of variance assumptions for each statistical test. The data presented in the figures is back-transformed onto a linear scale for the ease of the reader. Statistical annotations represent output of tests performed on log-transformed data. Significance was set at $p < 0.05$.

Data availability

The data that support the findings of this study are available from the corresponding author, upon reasonable request.

Results

Inflammation and ER stress in the post-mortem MS DRG

Although MS is classically identified as a CNS targeted disease, we sought to investigate whether sensory neurons residing in the DRG of the PNS would also be subject to increased inflammation. We first examined post mortem DRG tissue from people with MS using molecular analysis to examine innate and adaptive immune responses. At the transcript level, the complement component 3a receptor 1, C3aR1, and complement component 5a receptor 1, C5aR1, were upregulated in MS tissue in comparison to non-demented controls ($t_{C3aR1}(10)=2.019$, $p=0.0711$; $t_{C5aR1}(11)=3.928$, $p=0.0024$, unpaired t-test) (Fig. 1A, B). We also noted a significant increase in the T-cell marker transcripts, CD3 and CD4, further suggesting that the adaptive immune response was engaged in the DRG during the disease ($t_{CD3E}(11)=4.358$, $p=0.0011$; $t_{CD4}(11)=3.466$, $p=0.0053$, unpaired t-test) (Fig. 1C, D). Similar activation at the level of the DRG in the EAE animal model has been previously described by our group (Yousuf et al., 2019). Western blots and PCRs revealed a significant increase in total XBP1 mRNA and spliced XBP1 protein in MS tissue suggesting that MS DRGs underwent ER stress (PCR: $t_{XBP1}(9.119)=3.482$, $p=0.0068$, unpaired t-test with Welch's correction; WB: $t_{XBP1}(13)=2.525$, $p=0.0253$, unpaired t-test) (Fig. 1E-G). To localize and identify the cells with increased molecular markers of inflammation and ER stress, we performed immunofluorescence experiments. C5aR1 (CD88), and CD3 immunopositive immune cells were increased in MS samples as compared to non-demented controls (Fig. 1H). Furthermore, BiP expression was observed to be increased in MS DRGs and largely localized to sensory neurons (Fig. 1H). This data indicates that peripheral sensory neurons in the DRG of MS patients are subjected to active inflammation and ER stress in people with MS.

EAE mice develop pain hypersensitivity

We next generated EAE in female C57BL/6 mice using myelin oligodendrocyte glycoprotein (MOG₃₅₋₅₅). The median day for the onset of EAE clinical signs was day 10 post immunization (Fig. 2A, B). Behavioural testing (i.e. von Frey filament test and the rotarod test) was carried out at this time-point. In our model of EAE, mice exhibit a characteristic mechanical hypersensitivity at disease onset that is reflected by a reduced threshold to von Frey hair stimulation as expressed as a percentage of their own baseline threshold ($F_{\text{interaction}(1,11)}=28.43$, $p=0.0002$, $F_{\text{timepoint}(1,11)}=29.40$, $p=0.0002$, $F_{\text{disease}(1,11)}=7.932$, $p=0.0168$, $F_{\text{subjects}(11,11)}=3.584$, $p=0.0224$, RM two-way ANOVA) (Fig. 2C). At this time point, we do not observe any significant change in locomotor abilities (time spent on the rotarod) ($F_{\text{interaction}(1,8)}=1.090$, $p=0.3269$, $F_{\text{timepoint}(1,8)}=0.7348$, $p=0.4163$, $F_{\text{disease}(1,8)}=0.6992$, $p=0.4273$, $F_{\text{subjects}(8,8)}=1.035$, $p=0.4811$, RM two-way ANOVA) (Fig. 2D). Hence, mechanical hypersensitivity observed in EAE mice at disease onset was not confounded by paralysis or lack of motor coordination.

ER stress in the DRG of EAE mice

We next assessed ER proteins important in mediating and mitigating ER stress at the level of the DRG in mice with EAE over the course of the disease. Western blot analysis revealed that protein levels of a transmembrane chaperone, calnexin (CNX), remained relatively stable throughout the disease course as is typical for a UPR induction ($F_{\text{CNX}(2,10)}=0.4604$, $p=0.6438$) (Fig. 2E). The levels of BiP (GRP78), a luminal chaperone, were elevated in the DRG at the chronic stage of the disease ($F_{\text{BiP}(2, 10)}=4.552$, $p=0.0393$, One-way ANOVA) (Fig. 2F). Levels of phosphorylated eIF2 α (p-eIF2 α) were significantly upregulated at the chronic time point whereas total eIF2 α (eIF2 α) levels only trended toward an increase with the progression of disease ($F_{\text{p-eIF2}\alpha}(2,9)}=6.011$, $p=0.0220$; $F_{\text{eIF2}\alpha}(2,9)}=3.348$, $p=0.0818$, One-way ANOVA) (Fig.

2G, H). Interestingly, levels of the UPR transcription factors XBP1 and CHOP were upregulated at disease onset and remained elevated into the chronic phase of the disease ($F_{\text{XBP1}}(2,9)=10.21$, $p=0.0049$; $F_{\text{CHOP}}(2,10)=5.871$, $p=0.0206$, One-way ANOVA) (Fig. 2I, J).

In response to UPR, IRE1 α splices XBP1 mRNA to generate a spliced isoform of XBP1 which acts as a potent transcription factor unlike its non-spliced isoform (Vidal and Hetz, 2013; Hetz and Mollereau, 2014). To further elucidate the cellular origin of XBP1, we performed an IHC experiment and discovered that the proportion of neurons with nuclear staining of XBP1 (nXBP1) was increased significantly in the DRG of mice with EAE ($F_{\text{total cells}}(2,12)=9.910$, $p=0.0029$, One-way ANOVA) (Fig. 2L, M). On closer inspection, smaller (<30 μm) diameter neurons demonstrated a significant increase in nXBP1 expression with EAE while larger ($\geq 30\mu\text{m}$) diameter cells showed minimal change in nXBP1 levels. ($F_{<30\mu\text{m}}(2,12)=12.12$, $p=0.0013$; $F_{\geq 30\mu\text{m}}(2,12)=0.3210$, $p=0.7314$, One-way ANOVA) (Fig. 2N, O). These results suggest that the ER stress-pertinent spliced isoform of XBP1 is upregulated in small but not large diameter neurons in the DRG.

4-PBA treatment alleviates mechanical and facial hypersensitivity

Recently, the chemical chaperone, 4-phenylbutyric acid (4-PBA), has been shown to ameliorate diabetes and vasculitis-induced neuropathic pain by reducing ER stress and associated chaperones (Ayala et al., 2012; Inceoglu et al., 2015; Chen et al., 2019). We wanted to investigate if daily systemic treatment with 4-PBA (200 mg/kg) starting at the onset of disease (Fig. 3A) would alter EAE disease course and relieve mechanical and orofacial hypersensitivity in mice with EAE. DRGs were harvested after 7-10 days of treatment with either 4-PBA or vehicle (1x PBS). We did not observe any changes in disease course following 4-PBA treatment ($F(10,183)=0.2834$, $p=0.9842$) (Fig. 3B). Mice were tested for mechanical hypersensitivity in the

hindpaw using von Frey filaments before and one-hour after 4-PBA injection on the day of disease onset ($F_{\text{Vehicle}}(1.304,13.04)=71.29$, $p<0.0001$; $F_{4\text{-PBA}}(1.696,16.96)=13.32$, $p=0.0005$, RM one-way ANOVA) (Fig. 3C, D). At the onset of clinical signs and before 4-PBA administration, we observed the characteristic reduction in von Frey thresholds in mice with EAE. One-hour after 4-PBA injection, the von Frey threshold recovered to baseline levels. Vehicle administration did not have any behavioural effects (Fig. 3C, D). Due to the ensuing paralysis of the hind limbs at later stages in the disease, we could not assess hindpaw mechanical hypersensitivity 7-10 days post onset at the time of tissue harvest. Instead, we analysed orofacial pain behaviours (headshakes, single swipe, and continuous swipes) using an air puff assay (Thorburn et al., 2016). As compared to vehicle treated animals, daily 4-PBA treatment dampened total facial pain behaviours by 50%, headshakes by 66%, single swipe by 50%, and continuous swipes by 33% (Fig. 3E).

4-PBA treatment does not alter inflammation and ER stress in the spinal dorsal horn

CNS inflammation has classically been linked to pain hypersensitivity in EAE mice (Benson and Kerr, 2014). To assess whether the antinociceptive effects of 4-PBA were mediated by altered inflammatory responses in the superficial dorsal horn, we quantified the levels of Iba1+ microglia/macrophages and CD4+ T-cells in this region (Fig. 4A, B). The levels of Iba1 and CD4 immunoreactivity were elevated in the superficial dorsal horn of the spinal cord of both vehicle and 4-PBA treated animals and were not significantly different between treatments ($F_{\text{Iba1}}(2,11)=17.38$, $p=0.0004$; $F_{\text{CD4}}(2,11)=32.88$, $p<0.0001$, one-way ANOVA). Interestingly, XBP1 immunoreactivity was also increased in the superficial dorsal horn with disease but its expression was not affected with 4-PBA treatment ($F_{\text{XBP1}}(2,11)=7.845$, $p=0.0076$, one-way ANOVA) (Fig. 4C). cFOS, a commonly used marker of cellular activity, was elevated in the

superficial dorsal horn of EAE animals as shown previously (Olechowski et al., 2010). cFOS expression in the superficial dorsal horn of 4-PBA administered animals was however, normalized ($F_{\text{cFOS}(2,12)}=3.998$, $p=0.0467$, one-way ANOVA) (Fig. 4D). Collectively, these results suggest that 4-PBA's antinociceptive effects were not due to a change in immune activation or infiltration in the superficial dorsal horn nor can it be accounted for by a reduction in ER stress in this region. Instead, the normalized levels of cFOS with 4-PBA treatment suggest a possible reduction in peripheral afferent drive into the spinal dorsal horn.

4-PBA treatment reduces ER stress in the DRG

To further investigate the mechanism of 4-PBA's beneficial effects on pain behaviours in EAE, levels of UPR-related proteins in the DRG were assessed after 4-PBA treatment (Fig. 5). The levels of the ER stress proteins, CNX, BiP, and p-eIF2 α , were all reduced with 4-PBA treatment however these changes did not reach statistical significance ($t_{\text{CNX}(9)}=1.592$, $p=0.0729$; $t_{\text{BiP}(9)}=1.191$, $p=0.1321$; $t_{\text{p-eIF2}\alpha(9)}=0.7515$, $p=0.2358$; unpaired one-tailed t-test) (Fig. 5A, B, D). We did however, find significant reductions in eIF2 α , XBP1, and CHOP levels in DRG samples of mice treated with 4-PBA as compared to vehicle administration ($t_{\text{eIF2}\alpha(9)}=2.013$, $p=0.0375$; $t_{\text{XBP1}(9)}=1.949$, $p=0.0415$; $t_{\text{CHOP}(9)}=2.624$, $p=0.0276$; unpaired one-tailed t-test) (Fig. 5C, E, F). Taken together, these findings suggest that 4-PBA's antinociceptive effects were due to its ability to dampen ER stress in the DRG, particularly the levels of eIF2 α , XBP1, and CHOP, each of which represent different pathways of ER stress induced UPR.

4-PBA dampens Ca²⁺ responses in small diameter neurons

4-PBA, or its salt sodium 4-phenylbutyrate, can alleviate ER stress primarily as a chemical chaperone (Mimori et al., 2013; Kaur et al., 2018) (Fig. 6A). To further investigate the impact of 4-PBA on neuronal function, we imaged cytosolic Ca²⁺ transients in dissociated DRG neurons

from EAE animals upon caffeine (20mM) and potassium chloride (KCl; 30mM) stimulation (Fig. 6B). Caffeine is known to sensitize ryanodine receptors to cytosolic Ca^{2+} leading to a Ca^{2+} -induced calcium release (CICR) from the ER. Consistent with a reduction of ER stress-mediated hyperactivation of Ca^{2+} signaling, 4-PBA treatment reduced the amplitude of caffeine and KCl-mediated Ca^{2+} rises in small (<30 μ m), diameter cells ($t_{Caffeine}(149)=3.236$, $p=0.0015$; $t_{KCl}(185)=2.238$, $p=0.0264$, unpaired t-test) (Fig. 6C-F). 4-PBA reduced mRNA levels of *Ddit3*, *Xbp1*, and *Hspa5* indicating a reduction in ER stress ($t_{Ddit3}(6)=2.165$, $p=0.0735$; $t_{Xbp1}(6)=3.511$, $p=0.0127$, $t_{Hspa5}(6)=3.511$, $p=0.0155$, unpaired t-test) (Fig. 6G-I). These results suggest that 4-PBA reduces CICR and KCl mediated excitability in small diameter cells of the DRG from EAE mice by dampening ER stress.

Knockdown of Ddit3 and Xbp1 mRNA does not alter evoked Ca^{2+} rises

Earlier, we observed a reduction in CHOP and XBP1 *in vivo* after treatment with 4-PBA. To ascertain the contribution of these transcription factors to enhanced Ca^{2+} signalling observed in EAE cells (Fig. 6; Mifflin *et al.*, 2019), we silenced gene expression of CHOP (encoded by *Ddit3*) and *Xbp1* in dissociated DRG neurons from EAE animals (Fig. 7A). Neither XBP1 nor CHOP siRNA treatment changed cytosolic Ca^{2+} rises upon caffeine and KCl stimulation ($F_{Caffeine}(2,221)=0.5593$, $p=0.5724$, $F_{KCl}(2,268)=1.119$, $p=0.3282$, one-way ANOVA) (Fig. 7B-F). As confirmation of the siRNA efficacy, XBP1 and CHOP siRNA reduced the expression of their respective genes, *Xbp1* and *Ddit3*, as well as *Hspa5* (BiP) which may be induced by both XBP1 and CHOP ($F_{Xbp1}(2,12)=32.13$, $p<0.0001$, $F_{Ddit3}(2,12)=25.67$, $p<0.0001$, $F_{Hspa5}(2,12)=5.020$, $p=0.0260$, one-way ANOVA) (Fig. 7G-I). Moreover, in order to further assess the efficacy of the transfection system, we transfected dissociated neurons with Alexa Fluor 488-conjugated nonsilencing siRNA which has no known homology to any mammalian

gene (Fig. 7J). The presence of this siRNA in our neurons suggested that our experimental siRNAs were indeed being delivered into the neurons. Altogether, these data indicate that a selective reduction in either CHOP or XBP1 is not sufficient to reduce CICR or KCl excitability in dissociated DRG neurons from EAE animals.

The PERK inhibitor, AMG44, reduces Ca²⁺ signalling in small diameter neurons

To investigate the contribution of ER stress-mediated and PERK induced eIF2 α activation, we treated DRG cells from EAE animals with a novel PERK inhibitor, AMG PERK 44 (AMG44) (Smith et al., 2015) (Fig. 8A). CICR amplitude, as measured by caffeine stimulation, and KCl depolarization is enhanced in vehicle (0.1% DMSO) treated EAE cells as compared to DRG neurons obtained from CFA mice. AMG44 treatment normalizes both caffeine and KCl induced Ca²⁺ rises in small (<30 μ m) diameter neurons ($F_{\text{Caffeine}(2,171)}=3.391$, $p=0.0360$, $F_{\text{KCl}(2,209)}=4.146$, $p=0.0171$, one-way ANOVA) (Fig. 8B-F). PCR analysis of dissociated DRG cells revealed that *Ddit3* transcripts were reduced with AMG44 treatment as compared to vehicle treated EAE cells ($t(8)=7.013$, $p=0.0001$, unpaired t-test). Furthermore, AMG44 treatment increased the expression of *Xbp1* and *Hspa5* transcripts ($t_{\text{Xbp1}(8)}=2.865$, $p=0.0210$; $t_{\text{Hspa5}(8)}=2.738$, $p=0.0255$, unpaired t-test) (Supplementary Fig. 1) suggesting that blocking the PERK arm of UPR allows for a shift towards a more protective IRE1-XBP1-BiP branch of UPR.

BK channel current is rescued by 4-PBA and AMG44 treatment

In a previous study (Yousuf et al., 2019), we noted a reduction in the afterhyperpolarization amplitude of small diameter, putative nociceptive neurons from mice with EAE. Ca²⁺ is known to alter the function of Ca²⁺-sensitive K⁺ channels and hence, we asked whether BK channel properties are modified with EAE disease. In order to prevent dialysing intracellular calcium, we performed amphotericin B perforated patch clamp recordings. We found paxilline-sensitive BK

channel current in almost exclusively in small diameter IB4⁺ neurons similar to previous reports (Fig. 9A, D) (Zhang et al., 2010). We also found that the conductance-voltage (GV) curve was right-shifted in IB4⁺ EAE neurons as compared to neurons from CFA animals suggesting that BK channel activity was modified in EAE (Fig. 9B, E). 4-PBA and AMG44 treatment normalized the GV relationship of the BK channels (Fig. 9C, F). EAE responses (red) are the same in Fig. 9B and C. In effect, 0 mV test voltage (red trace) minimally activated paxilline-sensitive BK currents in EAE neurons compared to other conditions illustrating the strong shift in voltage-dependent gating of BK channels in EAE neurons (red trace; Fig. 9E, F). The conductance-voltage relationship was quantified as the voltage required for half the maximum conductance (i.e. $V_{1/2}$) across the cell membrane (Fig. 9G) ($F(3,34)=6.631$, $p=0.0012$, one-way ANOVA). The current density was not significantly altered (Fig. 9H) ($F(3,18)=1.525$, $p=0.2421$, one-way ANOVA). However, the resting membrane potential was more depolarized in IB4⁺ neurons from EAE animals as compared to IB4⁺ control neurons and this effect was rescued by 4-PBA and AMG44 treatment *in vitro* (Fig. 9I) ($F(3,19)=11.11$, $p=0.0002$, one-way ANOVA). In order to investigate the molecular underpinnings of this phenomenon, we assessed the expression of the $\beta 1$ subunit of the BK channel (*Kcnmb1*). We found that at the onset of EAE symptoms and chronically but not at the presymptomatic time point, the *Kcnmb1* mRNA was significantly reduced, coinciding with increased pain hypersensitivity observed in the model ($F(3,11)=9.583$, $p=0.0021$, one-way ANOVA) (Fig. 9J). Furthermore, 4-PBA and AMG44 administration *in vitro* was able to reverse this effect and increase *Kcnmb1* mRNA expression ($t_{4\text{-PBA}}(6)=2.479$, $p=0.0479$; $t_{\text{AMG44}}(8)=2.574$, $p=0.0329$, unpaired t-test) (Fig. 9K, L). These data suggest that EAE-induced ER stress alters BK channel functioning via the $\beta 1$ subunit in IB4⁺, non-peptidergic nociceptors.

Discussion

Multiple sclerosis (MS) is an immune-mediated disease of the nervous system characterized by inflammation, demyelination, and degeneration. Despite a century of research on the disease, the cause of MS is still unknown (Thompson et al., 2018). Research to date has largely been focused on the most prominent pathology in the CNS. However, our results show for the first time that post-mortem DRGs from MS patients show evidence of inflammation and immune activation as well as increased expression of ER stress markers. These observations demonstrate that MS pathology extends beyond the CNS into the PNS.

To further study the PNS contribution to pain in MS, we used the EAE model to demonstrate that DRGs of mice also undergo ER stress (Fig. 3). Treatment with 4-PBA resolves this stress and ameliorates pain hypersensitivity without altering the EAE disease course (Fig. 4). *In vitro* Ca^{2+} imaging of EAE sensory neurons revealed that 4-PBA and AMG44, a potent PERK inhibitor, dampens CICR and KCl-evoked excitability increases of small diameter, putative nociceptive neurons (Fig. 6, 8). Gene knock-down of the specific ER stress transcription factors, CHOP and XBP1, did not have any functional effect on cellular Ca^{2+} homeostasis. This further suggests that the activation of PERK and phosphorylation of eIF2 α , independent of CHOP, leads to aberrant hyperexcitability in small diameter sensory neurons of EAE mice (Fig. 7). Our perforated patch clamp experiments further showed that small diameter, IB4⁺ (non-peptidergic) nociceptors from mice with EAE were the most affected with the disease having reduced BK channel current and a more depolarized resting membrane potential (Fig. 9). These effects could be remedied with 4-PBA and AMG44 treatment *in vitro*. Taken together, our results demonstrate that IB4⁺ sensory neurons respond to ER stress in EAE by altering their Ca^{2+} dynamics and BK channel properties, presumably driving pain in the disease.

Several recent reports have implicated ER stress in mediating pain hypersensitivity in various models of neuropathy, including diabetic neuropathy (Inceoglu et al., 2015; Barragán-Iglesias et al., 2019; Kong et al., 2019), spinal nerve ligation (Zhang et al., 2015; Yamaguchi et al., 2018), vasculitic peripheral neuropathy (Chen et al., 2019) and CFA-induced orofacial neuropathy (Yang et al., 2014). Although MS, like many other neurodegenerative disorders, has previously been associated with ER stress (Hetz and Mollereau, 2014; Stone and Lin, 2015; Andhavarapu et al., 2019), prior reports have largely focused on studying ER stress and the integrated stress response in oligodendrocytes in EAE in the context of CNS demyelination (Lin et al., 2013; Stone et al., 2018; Yue et al., 2019). In contrast, our study highlights a novel role of ER stress in sensory neurons of the PNS for mediating pain in MS/EAE.

ER stress and the integrated stress response may be modulated by a variety of compounds and small molecules (Hetz et al., 2019). In particular, 4-PBA is known to act as an ammonia scavenger and a histone deacetylase inhibitor (HDACi) (Cuadrado-Tejedor et al., 2013; Mimori et al., 2013; Kolb et al., 2015). However, a recent proteomics study concluded that 4-PBA does not directly alter the expression profile of proteins but rather functions as an authentic chemical chaperone by minimizing the toxic effects of tunicamycin, an N-glycosylation inhibitor and a known ER stress inducer (Kaur et al., 2018). Application of 4-PBA has been shown to improve metabolic syndromes, congenital and genetic protein misfolding disorders, inflammation, and neurological disorders such as Parkinson's disease and ischemic brain injury (Kolb et al., 2015). Daily administration of 4-PBA in our study ameliorated acute mechanical hypersensitivity as well as chronic facial pain behaviours without altering the clinical signs of the disease (Fig. 3). The only previous study, to our knowledge, using 4-PBA in EAE, used the drug in an MBP-primed T-cell adoptive transfer model and noticed that treatment with 4-PBA (400 mg/kg/day) at

the time of induction prevented disease development and reduced clinical signs (Dasgupta et al., 2003). In addition to using a different EAE model based on the MOG peptide, we designed our study with 4-PBA administration beginning after the onset of EAE to limit the effects of reduced disease severity and its impact on the measurement of pain behaviours. We were interested in investigating the role of ER stress on pain hypersensitivity in EAE rather than the effect of 4-PBA on the disease itself. Evidently, once EAE has been initiated, 4-PBA administration does not affect EAE disease course or immune activation in the dorsal spinal cord (Fig. 3, 4). In the DRG however, 4-PBA broadly reduced levels of ER stress related proteins (Fig. 5).

The ISR has previously been implicated in pain pathophysiology (Khoutorsky et al., 2016; Barragán-Iglesias et al., 2019) as well as EAE (Lin et al., 2007b; Hussien et al., 2014). The ISR pathway involves the phosphorylation of eIF2 α by an assortment of kinases – PERK, protein kinase R (PKR), heme-regulated eIF2 α kinase (HRI), and general control nonderepressible 2 kinase (GCN2) – each of which is initiated by a variety of stress responses (reviewed in Pakos-Zebrucka et al., 2016; Khoutorsky and Price, 2018). Phosphorylation of eIF2 α allows the cell to rapidly respond to a stressor by reducing translation of certain genes and increasing translation of others, especially genes with upstream open reading frame (uORF) including, but not limited to, ATF4 and CHOP. Selective translation of genes that may enhance excitability of sensory neurons, particularly IB4⁺ nociceptors, has recently been alluded to (Barragán-Iglesias et al., 2019). Integrated stress response inhibitor (ISRIB) is a commonly used compound to suppress the effects of p-eIF2 α without altering its levels (Hetz et al., 2019) however the initiating stressors (e.g. UPR, viral infection, amino acid deprivation etc.) remain ambiguous. In this study, we hoped to isolate the functional effects of UPR mediated eIF2 α signalling using a recently developed inhibitor of PERK phosphorylation, AMG44 (Smith et al.,

2015). We found that AMG44 *in vitro* could suppress caffeine stimulated CICR and KCl mediated Ca^{2+} excitability in small diameter cells while gene knock-down of CHOP and XBP1 had no effect on Ca^{2+} responses of sensory neurons (Fig. 8). AMG44 also normalized BK channel physiology in dissociated DRGs from EAE mice as well as mRNA levels of *Kcnmb1*, gene encoding the $\beta 1$ auxiliary subunit of BK channels (Fig. 9). Taken together, these results suggest that EAE mediated activation of PERK and concomitant phosphorylation of eIF2 α in IB4⁺ sensory neurons alter ER and cytosolic Ca^{2+} dynamics as well as BK channel physiology resulting in a hyperexcitable state and a painful phenotype.

Ca^{2+} is a key ion required for many neuronal processes ranging from neurotransmitter release to intracellular signalling (Verkhratsky, 2005). The ER stores the majority of cellular Ca^{2+} and tightly regulates the cytosolic Ca^{2+} concentrations through transporters namely sarco/endoplasmic reticulum Ca^{2+} -ATPase (SERCA), inositol triphosphate receptors (IP3R), and ryanodine receptors (RyR). Caffeine is known to sensitize RyRs to very low concentrations of cytosolic Ca^{2+} which in turn open the channel allowing ER Ca^{2+} to enter the cytosol (CICR) (Verkhratsky, 2005). Caffeine also prevents IP3-induced Ca^{2+} release suggesting that caffeine's effect on ER Ca^{2+} is primarily due to the opening of RyRs (Verkhratsky, 2005). Furthermore, since caffeine stimulation depletes ER Ca^{2+} stores, we used caffeine-induced Ca^{2+} transients to examine the levels of luminal Ca^{2+} in the ER. Ultimately, the effect of increased ER luminal Ca^{2+} on neuronal function is multifaceted primarily because Ca^{2+} plays such a varied role inside the cell (Verkhratsky, 2005). Small diameter sensory neurons in EAE were found to have increased CICR and KCl mediated cytosolic Ca^{2+} transients. *In vitro* application of 4-PBA and AMG44 on dissociated DRG neurons from EAE animals reduced the sensitivity to caffeine and KCl

stimulation suggesting that these drugs alter ER Ca^{2+} dynamics as well as the excitability of small diameter sensory neurons.

We investigated the role of BK channels since they act as “coincidence detectors” consolidating both cytosolic Ca^{2+} concentration and membrane depolarization, both of which are important factors in initiating and maintaining sensitization (Contet et al., 2016). To this effect, reduction in BK channel current in the DRG is also associated with nerve injury (Chen et al., 2009; Cao et al., 2012) and inflammation-induced (Zhang et al., 2012; Berta et al., 2014) pain. In this study, we found paxilline-sensitive BK channel currents almost exclusively in IB4⁺ sensory neurons similar to what has previously been reported (Fig. 9; Zhang *et al.*, 2010). BK channels are known to be spatially coupled to voltage-gated Ca^{2+} channels and ryanodine receptors allowing increased Ca^{2+} in the cytosol to immediately influence the excitability of the cell (Wang et al., 2016; Irie and Trussell, 2017). Moreover, reduced or delayed BK channel activation, as observed in this study, has been implicated in increased neurotransmitter release (Contet et al., 2016; Griguoli et al., 2016) and hyperexcitability (Zhang et al., 2010). This may further explain the increased spinal cFOS expression we observe in the superficial dorsal horn of mice with EAE (Fig. 4). Taken together these observations suggest that alleviating ER stress at the level of the DRG can reduce the afferent drive and dampen resulting cellular activity in the spinal cord.

The effect of BK channels on neuronal activity can be excitatory or inhibitory depending on the timing of activation of the BK channel (Contet et al., 2016). In this regard, the presence of β and γ subunits of BK channels further modulate Ca^{2+} and voltage sensitivity that ultimately contributes to spike repolarization and/or afterhyperpolarization of the cell (Contet et al., 2016; Wang et al., 2016). A single-cell RNA-sequencing database of mouse DRGs indicated that the *Kcnmb1* gene (β 1 subunit) was almost exclusively expressed in non-peptidergic cells (Usoskin et

al., 2015). The $\beta 1$ subunit of BK channels is known to increase the apparent Ca^{2+} sensitivity of the K^+ channel by 10 times at 0 mV, and significantly hyperpolarize the $V_{1/2}$ of the BK channel (Cox and Aldrich, 2000; Castillo et al., 2015). As such, we observed a loss of $\beta 1$ mRNA expression at the onset of EAE, corresponding to a depolarizing shift in the $V_{1/2}$ of BK channels in IB4⁺ neurons and the onset of pain hypersensitivity in our model. Interestingly, we observed no change in *Kcnmb1* expression in presymptomatic mice (i.e. mice obtained 7 days after EAE induction that did not present any motor impairment characteristic of EAE disease). *In vitro*, 4-PBA and AMG44 treatment on EAE neurons increased the expression of *Kcnmb1* and normalized BK channel properties. Similarly, treatment with GSK inhibitors of PERK rescued $\beta 1$ expression and consequent BK current in a model of vascular dysfunction (Sun et al., 2017b). Of note, AMG44 is a more specific and more potent inhibitor of PERK activity than GSK inhibitors (GSK2606414 and GSK2656157), both of which are also receptor-interacting serine/threonine-protein kinase 1 (RIPK1) inhibitors (Rojas-Rivera et al., 2017). Ultimately, these results suggest that ER stress, particularly the PERK-eIF2 α arm, modulates BK channel properties via the expression of the $\beta 1$ subunits.

Current approaches to treat pain in MS generally involves NSAIDs, opioids, antidepressants, and antiepileptics. However, these treatment avenues offer minimal relief and accompany a host of undesired side-effects (Hadjimichael et al., 2007; Urits et al., 2019). Since BK channels are ubiquitously expressed in a variety of tissues, including the heart and the circulatory system, pharmacologically targeting BK channels directly may also result in unforeseen side-effects (Kshatri et al., 2018). In contrast, as a chemical chaperone, 4-PBA can alleviate ER stress at the source and does not target a specific molecule thus limiting the chances

for adverse side-effects. Here, we propose that ER stress modulators, like 4-PBA and AMG44, may be beneficial for treating pain in MS.

Tables:

Table 3.1. Demographics of MS patients and non-demented controls.

Patient ID	Sex	Age	Post-mortem delay (hh:mm)	Disease subtype	Chronic pain	Spinal lesion	MS duration	Cause of death
GS02	F	85	6:25	NDC	Y	N	-	Euthanasia*
GS05	F	78	7:10	NDC	Y	N	-	Euthanasia
GS07	F	60	8:10	NDC	Y	N	-	Cancer [§]
GS11 ^{&}	F	95	7:05	NDC	N	N	-	Sepsis
GS15 ^{&}	F	75	9:10	NDC	Y	N	-	Euthanasia
GS19	F	88	6:20	NDC	N	N	-	Euthanasia
GS20 [§]	F	60	5:30	NDC	Y	N	-	Euthanasia
GS01	F	65	10:45	SPMS	Y	Y	16	CVA
GS04 ^{&}	F	56	10:30	SPMS	N	Y	21	Euthanasia
GS06	F	35	10:20	SPMS	N	N	10	Euthanasia
GS08	F	61	10:00	SPMS	Y	Y	2	Euthanasia
GS09	F	74	7:50	SPMS	Y	Y	50	Euthanasia
GS10	F	57	10:40	SPMS	Y	Y	25	Euthanasia
GS13	F	50	9:05	SPMS	Y	Y	12	Euthanasia
GS17	F	66	9:45	PPMS	Y	Y	23	Pneumonia
GS18	F	73	7:05	PPMS	Y	N/A	30	Euthanasia

*Euthanasia was typically performed with barbiturate (thiopental, pentobarbital) overdose coupled with a muscle relaxant (rocuronium bromide). [§]Metastasized mammary carcinoma. Some samples were selectively used for [&]western blots and [§]PCRs depending on the quality and yield of extracted protein and RNA. CVA: Cardiovascular accident, SPMS: Secondary progressive MS, PPMS: Primary progressive MS, NDC: Non-demented control

Table 3.2. Antibodies used in this study.

Antibody	Host	Source	Dilution Factor
CNX	Rb	(Lynes et al., 2012)	1:2,500
BiP	Ms	BD Biosciences, 610979	1:1,000 (WB)
BiP	Rb	Novus, NBP1-06274	1:2,000 (WB) 1:200 (IHC)
CHOP	Ms	Enzo Life Sciences, ALX-804-551-C100	1:1,000
XBP1	Rb	Abcam, ab37152	1:1,000 (WB), 1:200 (IHC)
eIF2 α	Rb	Cell Signaling, 9722	1:1,000
p-eIF2 α (Ser51)	Rb	Cell Signaling, 3597	1:1,000
Iba1	Rb	Wako, 019-19741	1:500
CD4	Rt	BioRad, MCA2691	1:200
cFOS	Rb	Cell Signalling, 2250	1:1,000
CD88 (or C5aR1)	Rt	BioRad, MCA2456	1:200
CD3	Rt	BioRad, MCA1477	1:200
NFH	Ck	ThermoFisher, PA1-10002	1:5,000
IB4–AF488	-	ThermoFisher, I21411	1:100
Goat anti-Mouse IgG, AF750	Gt	Abcam, ab175733	1:10,000
Goat anti-Rabbit IgG, AF680	Gt	ThermoFisher, A21057	1:10,000
Goat anti-Chicken IgG AF594	Gt	ThermoFisher, A11042	1:200
Goat anti-Rabbit IgG AF488	Gt	ThermoFisher, A11008	1:200

Goat anti-Rat IgG AF594	Gt	ThermoFisher, A11007	1:200
Goat anti-Rabbit IgG HRP	Gt	Jackson Laboratories, 111-035-144	1:10,000

Figures:

Figure 1

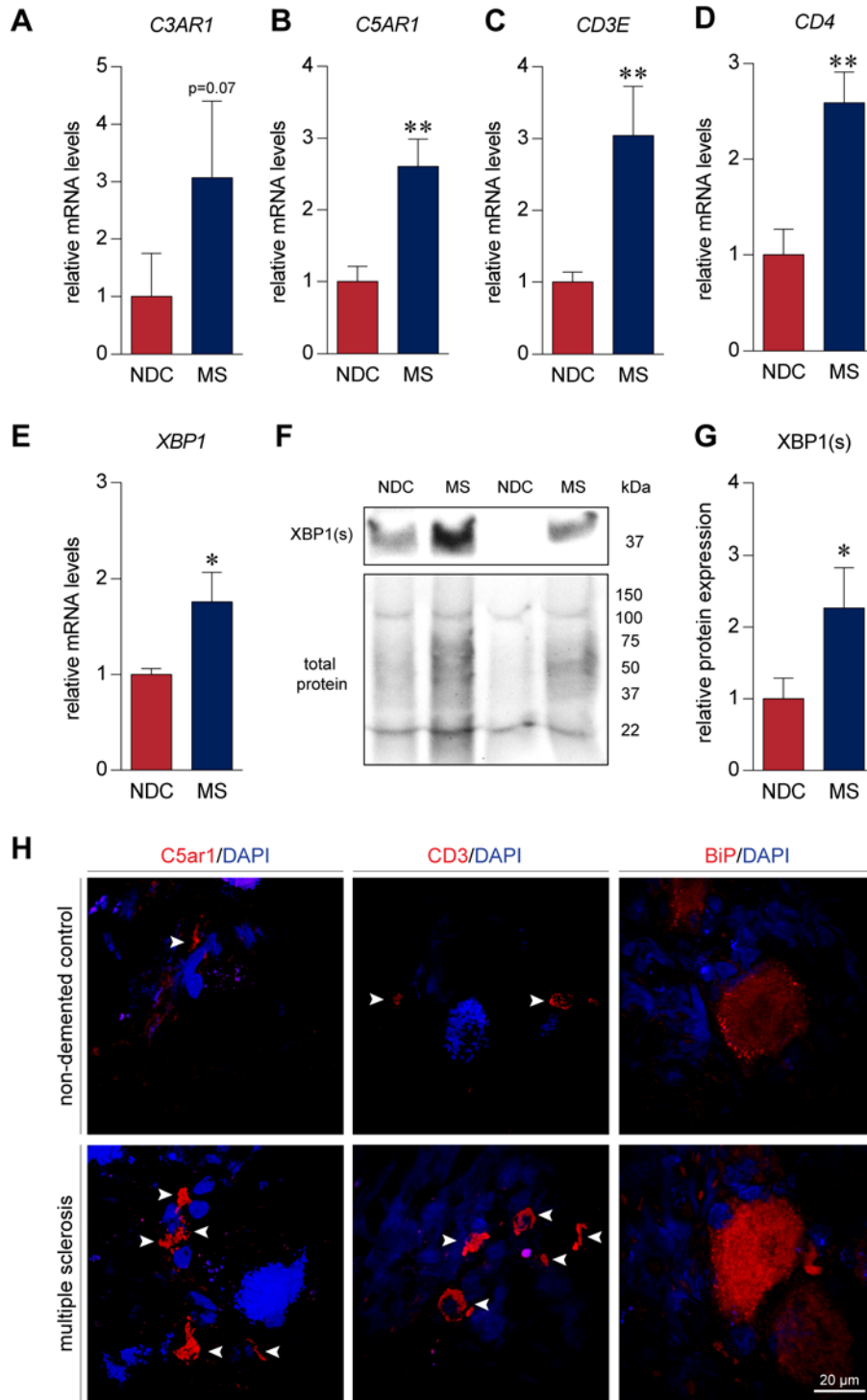


Figure 3.1. Human DRGs undergo inflammation, immune activation, and ER stress in MS.

(A-B) PCR analysis of post-mortem human DRGs revealed that the complement component C3a receptor 1, C3AR1, and component C5a receptor 1, C5AR1, genes are upregulated in chronic MS tissue (n=8) as compared to DRGs obtained from non-demented controls (NDC; n=5). (C, D) Similarly, we observed an increase in CD3E and CD4 mRNA expression in MS tissue as compared to NDC. (E-F) mRNA transcripts and protein levels of X-box binding protein (XBP1) and its spliced isoform (XBP1(s)), was also found to be elevated in MS DRG tissue (n=9) with respect to levels in NDC samples (n=6). (H) Immunofluorescence experiments localized expression of C5ar1 and CD3 in immune cells however binding immunoglobulin protein, BiP, expression was primarily found to be elevated in neurons. Bars indicate mean \pm standard error of mean (SEM). * $p < 0.05$, ** $p < 0.01$, unpaired t-test.

Figure 2

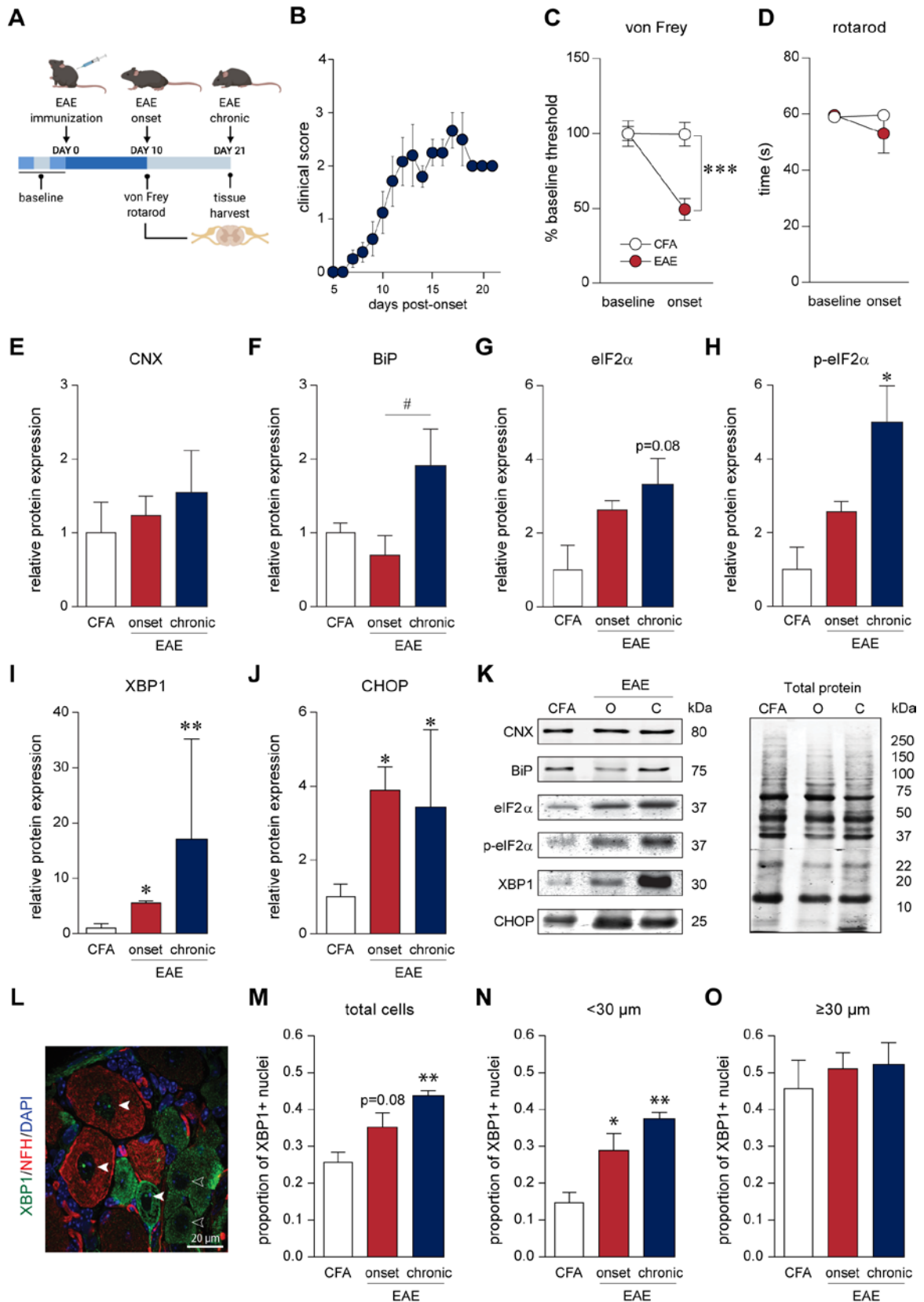


Figure 3.2. ER stress-associated proteins are dysregulated in the DRG of EAE mice.

(A, B) 8-10 week old female mice were immunized against myelin oligodendrocyte glycoprotein (MOG35-55) to induce EAE. Behavioural analyses were performed at the onset of EAE signs. Mice developed initial clinical symptoms (clinical score of 1) on median at day 10 post-immunization. Mice were followed for 21 days after immunization. Baseline behaviour was assessed on three separate days before EAE induction. (C) EAE mice present mechanical hypersensitivity as indicated by a reduction in their von Frey thresholds. (D) In contrast, EAE mice at onset do not show a significant reduction in the time spent on the rotarod suggesting no or limited signs of hindpaw paralysis and lack of motor coordination. *** $p < 0.001$, paired t-test. (E) CNX protein levels remain relatively stable throughout EAE disease course. (F) Another ER chaperone, BiP, protein levels are elevated chronically in the disease. (G-H) Total eIF2 α protein levels trend towards an increase with EAE disease course while its phosphorylated isoform (p-eIF2 α) significantly increases at the chronic time point. (I-J) XBP1 and CHOP proteins are upregulated with disease onset and remain elevated chronically in the DRGs of EAE mice. (CFA: n=5, onset: n=4, chronic: n=4). (L-O) Further IHC analysis of XBP1 demonstrates a global increase in the transcriptionally-active spliced XBP1 as nuclear staining within neurons. Further analysis revealed that small DRG neurons (<30 μ m in diameter) presented the greatest increased XBP1-positive nuclei. (L) Filled arrow-heads indicate XBP1-positive nuclei in DRG neurons whereas, empty arrowheads indicate XBP1-negative nuclei. (CFA: n=5, onset: n=5, chronic: n=5). Bars indicate mean \pm standard error of mean (SEM). EAE = experimental autoimmune encephalomyelitis, CFA = complete Freund's adjuvant. *, # $p < 0.05$, ** $p < 0.01$, one-way ANOVAs with Tukey's post-hoc analysis.

Figure 3

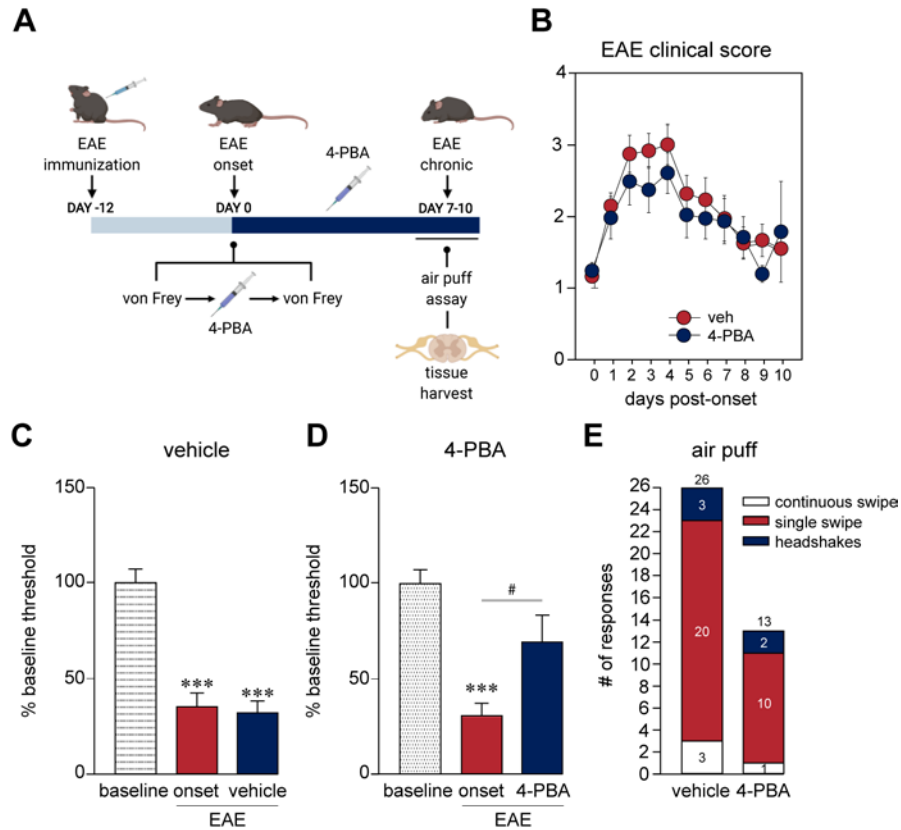


Figure 3.3. Daily 4-PBA treatment alleviates EAE-induced mechanical hypersensitivity.

(A) Mice that were immunized with MOG35-55 developed EAE symptoms on median 12 days after induction. At disease onset (day 0), mice were subjected to von Frey filaments test followed by treatment with 4-PBA (i.p., 200 mg/kg, n=12) or vehicle (PBS, n=12). An hour later, another von Frey filaments test was conducted. On subsequent days, mice were administered 4-PBA (200 mg/kg) daily. Mice underwent the air puff assay an hour after the final drug administration 7-10 days post onset after which they were euthanized. (B) 4-PBA treatment did not significantly alter EAE disease course. (C-D) As expected, von Frey thresholds were diminished in EAE animals as compared to baseline only to recover in the 4-PBA treated animals. (E) 4-PBA treated

animals also showed a 50% reduction in overall nociceptive behaviours (continuous swipe, single swipe, headshakes) in response to the air puff assay. # $p < 0.05$, *** $p < 0.001$, one-way ANOVAs with Tukey's post-hoc analysis.

animals. (D) EAE enhanced cFOS expression in the dorsal horn of EAE mice. 4-PBA administration was able to rescue some of the disease-mediated increase in cFOS+ cells. * $p < 0.05$, ** $p < 0.01$, *** $p < 0.001$, one-way ANOVAs with Tukey's post-hoc analysis.

Figure 5

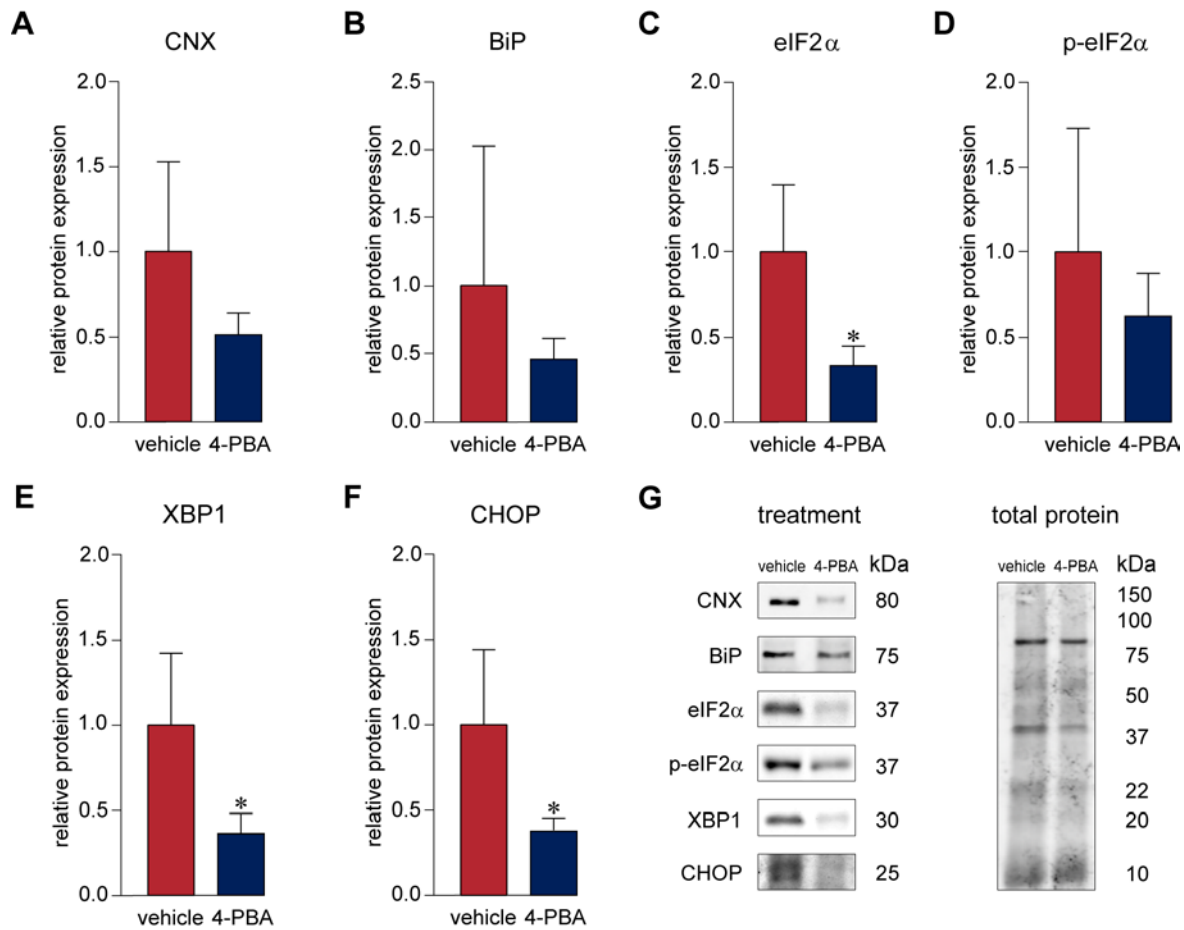


Figure 3.5. 4-PBA treatment reduces the expression of UPR-associated proteins in the DRG.

(A-G) Western blot analysis of DRG samples from 4-PBA treated mice demonstrate a reduction in the levels of UPR-associated proteins. In particular, eIF2 α , XBP1 and CHOP levels were significantly downregulated in the DRGs of 4-PBA treated EAE mice. (CFA: n=5, onset: n=6)

*p < 0.05, unpaired t-test.

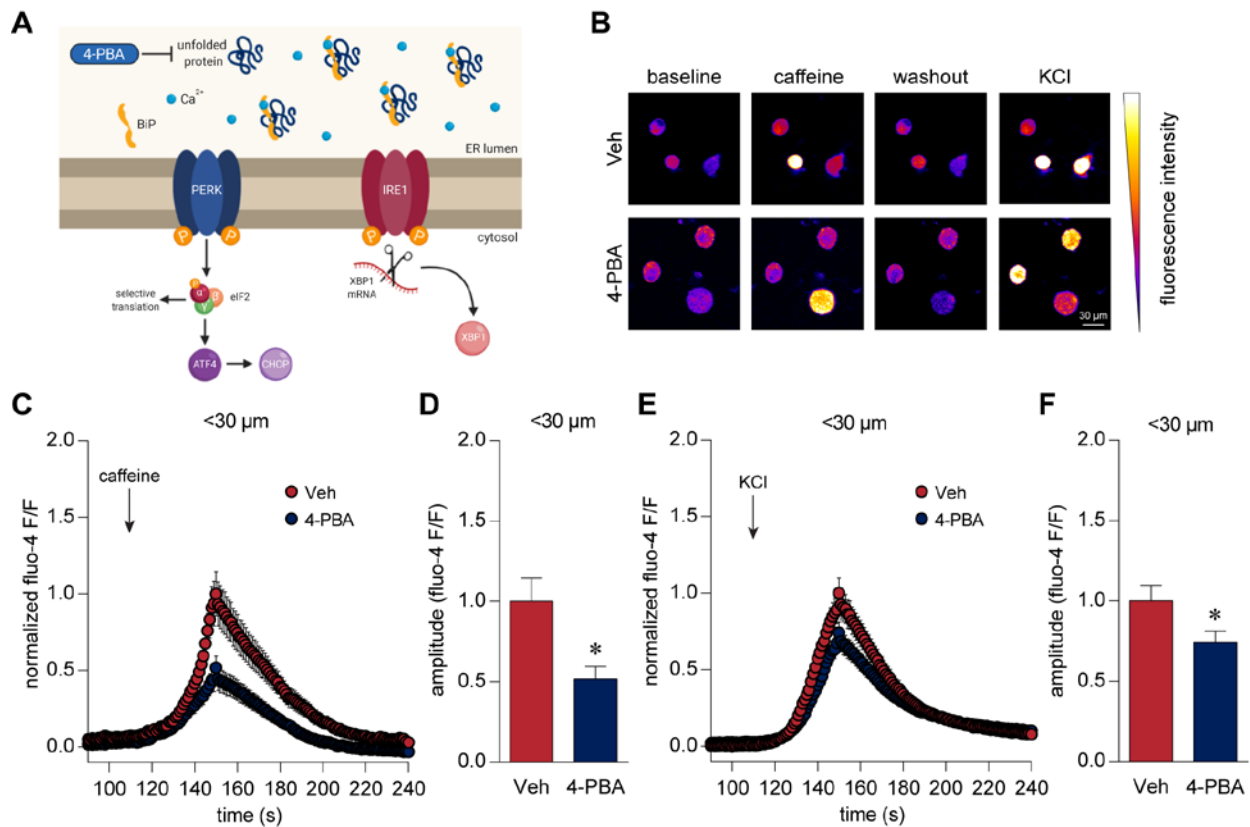


Figure 3.6. 4-PBA diminishes cellular Ca^{2+} responses in small-diameter DRG neurons.

(A) As a chemical chaperone, 4-PBA aims to reduce unfolded protein response at the source by aiding in protein folding and dampening the accumulation of unfolded/misfolded proteins. (B-F) Ca^{2+} imaging of small (<30 μ m) dissociated neurons at onset show reduced Ca^{2+} rises in 4-PBA treated neurons (n=113) upon caffeine (20 mM) and KCl (30 mM) stimulation. Responses were normalized to the Ca^{2+} responses in the vehicle (HBSS) treated group (n=74). Data were analysed as a ratio of baseline fluorescence. * $p < 0.05$, unpaired t-test.

Figure 7

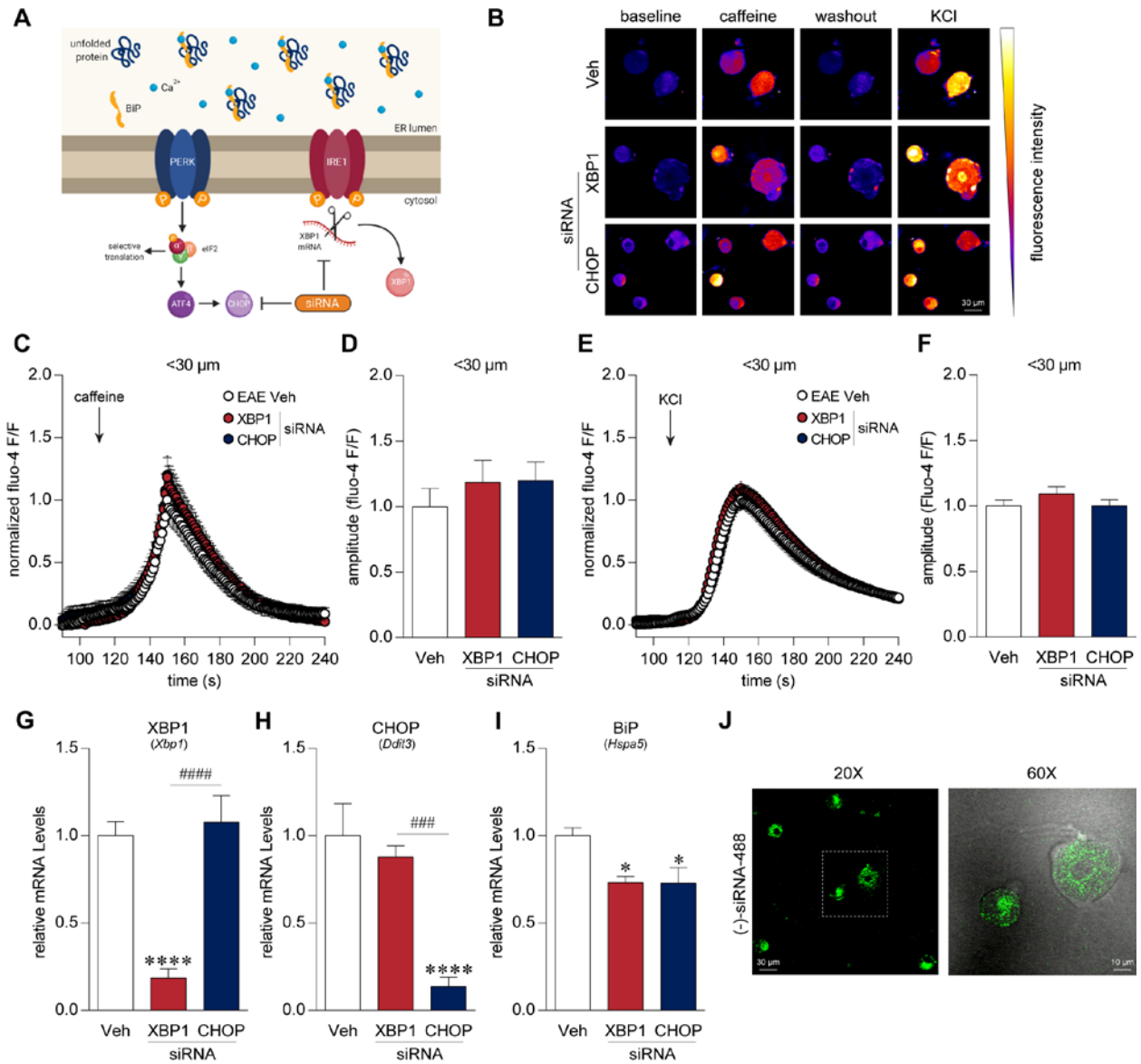


Figure 3.7. Gene knockdown of XBP1 and CHOP did not alter Ca²⁺ transients in small-diameter DRG neurons.

(A) siRNA transfection knocked down expression of CHOP and XBP1 mRNA. (B-E) Dissociated EAE cells were transfected with XBP1 (n=77) and CHOP (n=100) siRNA 20-24 hours prior to Ca²⁺ imaging. We observed no change in the Ca²⁺ transients of EAE DRG

neurons during stimulation with caffeine (20 mM) or KCl (30 mM) after siRNA knockdown of XBP1 and CHOP as compared to vehicle (transfection reagent HiPerfect) treated EAE neurons (n=94). (G, H) As confirmation, PCR analysis of transfected DRG neurons demonstrated a drastic reduction in their respective gene. XBP1 transcript expression was dampened in XBP1 siRNA treated cells (n=5) and similarly, CHOP mRNA levels were diminished upon CHOP siRNA treatment (n=5) as compared to vehicle-treated cells (n=5). (I) We observed that BiP (Hspa5) expression was also reduced upon knockdown of XBP1 and CHOP mRNA. (J) To further validate our siRNA delivery system, we transfected cells with a negative siRNA tagged with Alexa Fluor 488. We found that dissociated neurons were transfected with (-)-siRNA using our delivery system further suggesting that XBP1 and CHOP siRNA were successfully delivered in our primary neurons. ### p < 0.001; ***,##### p < 0.0001, one-way ANOVAs with Tukey's post-hoc analysis.

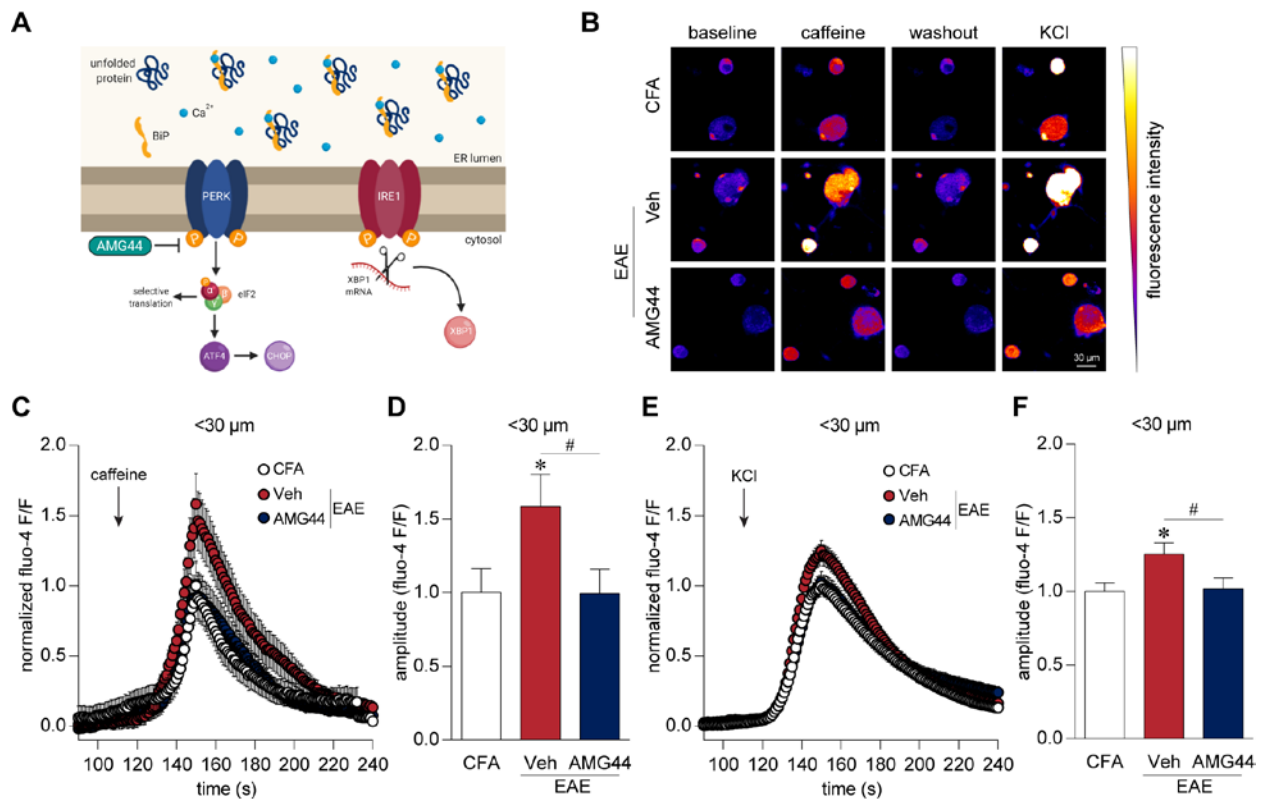


Figure 3.8. AMG44 treatment dampens cytosolic Ca^{2+} responses in small-diameter DRG neurons.

(A) AMG44, a recently identified PERK inhibitor, aims to prevent PERK phosphorylation and thereby block the PERK-eIF2 α signalling in response to ER stress. (B-F). Vehicle treated (0.01% DMSO) EAE neurons (n=74) demonstrate enhanced Ca^{2+} responses upon caffeine (20 mM) and KCl (30 mM) administration as compared to vehicle-treated dissociated neurons obtained from CFA-control animals (n=70). These transients are normalized with AMG44 treatment (n=68) suggesting that the PERK-eIF2 α arm mediates Ca^{2+} -induced Ca^{2+} release from the ER as well as cytosolic Ca^{2+} dynamics *, # p<0.05, one-way ANOVAs with Tukey's post-hoc analysis.

Figure 9

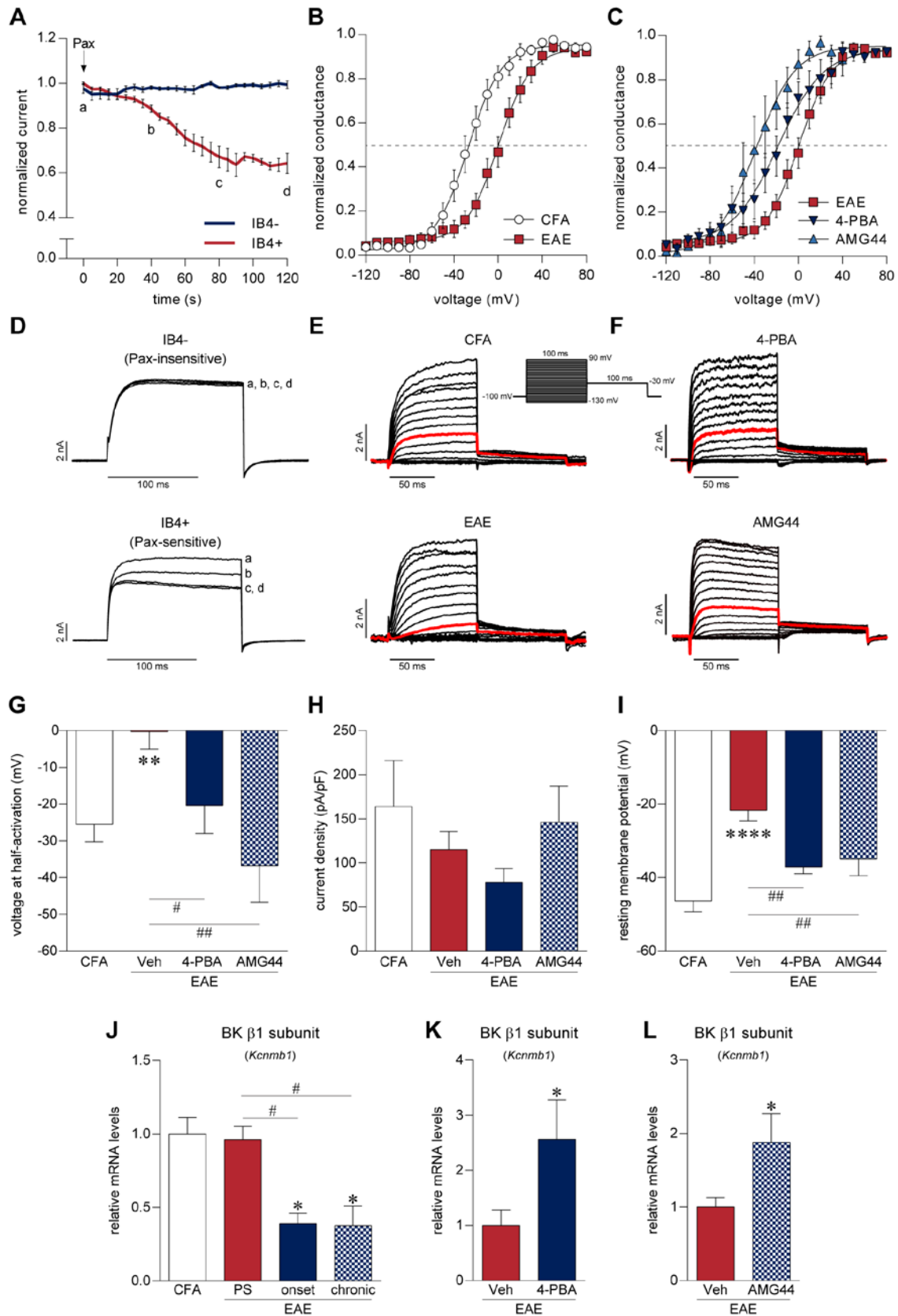
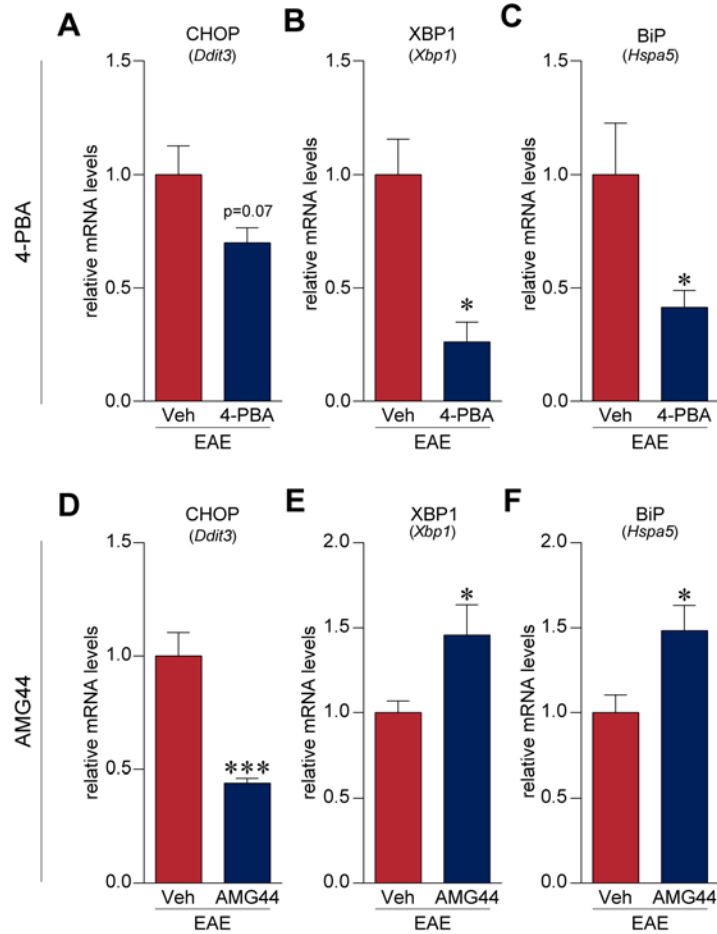


Figure 3.9. ER stress modulators rescues EAE-mediated changes in Ca²⁺-sensitive BK channel properties.

(A, D) Perforated patch-clamp recordings of DRG neurons from naïve animals revealed that paxilline-sensitive BK current was almost exclusively present in IB4⁺ non-peptidergic neurons. (D) Exemplar BK currents of IB4⁻ and IB4⁺ neurons in response to paxilline application at 0 (a), 40 (b), 80 (c), 120 (d) seconds. (B, C) Conductance-voltage (G-V) relationship among paxilline-sensitive IB4⁺ DRG neurons extracted from (B) CFA and EAE mice, and (C) EAE neurons treated with 4-PBA and AMG44. Solid lines represent Boltzmann fit of the G-V relationship. Intersection of the Boltzmann curve and the dotted line represents voltage at half conduction (E, F) Representative traces of IB4⁺ neurons from CFA and EAE animals as well as EAE neurons treated with 4-PBA and AMG44. Red trace indicates BK channel conductance at 0 mV. (G) Conductance-voltage relationship was quantified as voltage at half-activation ($V_{1/2}$) of BK channels. Vehicle treated EAE neurons (n=15) demonstrated a more positive $V_{1/2}$ in comparison to CFA neurons (n=12). This effect was reversed with 4-PBA (n=7) and AMG44 (n=4) treatment. (H) BK current density in IB4⁺ neurons was not found to be significantly altered. CFA: n=5, Veh: n=6, 4-PBA: n=7, AMG44: n=4. (I) Resting membrane potential was found to be more depolarized in the vehicle treated EAE neurons (n=9) as compared to CFA control neurons (n=5). This was reversed with treatment with ER stress modulators, 4-PBA (n=4) and AMG44 (n=5). # p<0.05, ** p<0.01, *** p<0.001, **** p<0.0001, one-way ANOVAs with Holm-Sidak multiple comparison test. (J) PCR analysis of DRGs extracted from EAE animals revealed that the BK $\beta 1$ subunit (*Kcnmb1*) mRNA expression was reduced beginning at the onset (n=4) of EAE into the chronic (n=3) phase coinciding with pain behaviours in these animals.

Presymptomatic (PS) DRGs (n=4) did not show any reduction in *Kcnmb1* expression as compared to DRGs from CFA control (n=4) animals. (K, L) In vitro application of 4-PBA (n=4) and AMG44 (n=5) enhanced the expression *Kcnmb1* transcripts correlating with the normalization of BK current in diseased neurons. *, # p<0.05, one-way ANOVAs with Tukey's post-hoc analysis.

Supplementary Figure 1



Supplementary Figure 3.1. 4-PBA and AMG44 treatment, in vitro, alters gene expression of UPR-associated transcripts.

(A, B, C) 4-PBA treatment (n=4) in EAE cells reduced expression of XBP1, and BiP mRNA expression as compared to vehicle (HBSS) treated EAE neurons (n=4). CHOP expression trended towards a reduction with 4-PBA treatment. (D, E, F) AMG44 (n=5) significantly dampened the mRNA levels of CHOP, as intended, in dissociated DRG neurons from EAE animals. However, AMG44 treatment elevated XBP1 and BiP transcripts as compared to vehicle (0.01% DMSO) treated EAE neurons (n=5). * p<0.05, *** p<0.001, unpaired t-test.

Conclusions:

Multiple sclerosis (MS) is an autoimmune inflammatory disorder of the central nervous system characterised by motor and sensory impairments, including neuropathic pain (Thompson et al., 2018). To study the pathophysiology of pain in MS, we employed a model of T-cell mediated inflammation, known as experimental autoimmune encephalomyelitis (EAE), which reliably recapitulates various pathological features of MS and resulting motor and sensory dysfunction (Iannitti et al., 2014; Khan and Smith, 2014). Very little research has been done to date elucidating the peripheral mechanisms of pain in EAE. Since EAE and other systemic inflammation models are not focal and traumatic, many treatments from peripheral neuropathy models are not effective in EAE and MS (Hadjimichael et al., 2007; Khan and Smith, 2014). The central theme of my PhD dissertation was to identify the role of sensory neurons in mediating pain in EAE.

EAE is associated with muscle weakness ascending rostrally from the tail (Olechowski et al., 2009). At the onset of EAE signs, mice also experience mechanical hypersensitivity, facial and cold allodynia (Olechowski et al., 2009; Thorburn et al., 2016; Catunescu et al., 2019). The dorsal root ganglia (DRG) from the EAE mice undergo activation of the complement system and the NLRP3 inflammasome (Chapter 1). Furthermore, a transient increase in activated T-cells and macrophages is observed. Along with others, our group has also noted an increase in pro-inflammatory cytokines, such as TNF α , IL1 β , and IL18, in the DRG of EAE animals (Melanson et al., 2009). Electrophysiological experiments of dissociated DRG neurons found diseased neurons to be hyperexcitable with altered spike parameters, such as afterhyperpolarization and rise and decay slopes.

Since the turn of the century, there has been great emphasis on chloride homeostasis in pain pathophysiology. NKCC1 and KCC2 are two of the main chloride transporters in neurons that maintain the inhibitory tone of GABA (Gagnon et al., 2013; Price and Prescott, 2015). In painful conditions, activation of spinal microglia by purinergic receptors enhances BDNF release which, when bound to TrkB receptors, reduces neuronal KCC2 expression (Trang et al., 2009). Hence, the intracellular chloride gradient is reduced such that GABAergic stimulation leads to a loss of chloride from the cell further depolarizing it. This reduced inhibitory effect of GABA (i.e. disinhibition) on the projection neurons of the spinal cord is thought to mediate the opening of the “pain gate” (Price and Prescott, 2015). Furthermore, increased NKCC1 expression on sensory neurons is linked to primary afferent depolarization which further enhances pain transmission in the spinal cord (Pitcher and Cervero, 2010). Similar to other pain pathologies, we found increased NKCC1 in the DRG of EAE mice as well as dampened expression of KCC2 in the dorsal horn of the spinal cord at the onset of disease. Treatment with bumetanide, an NKCC1 inhibitor, did not reverse pain behaviours in EAE mice although it normalized levels of NKCC1 in the DRG and monomeric KCC2 in the spinal cord. However, bumetanide treatment did not reverse the spinal loss of oligomeric KCC2, the more active form of the channel (Hartmann and Nothwang, 2014). These results suggest that increased NKCC1 levels in the periphery does not contribute to pain in EAE.

Considering active inflammation and altered electrophysiological properties, it is clear that the peripheral nervous system is altered as a result of EAE. We next investigated the role of endoplasmic reticulum stress, a phenomenon previously linked to inflammation (Hetz and Mollereau, 2014), in mediating pain hypersensitivity in EAE mice. We found increased levels of ER stress transducer proteins including XBP1, CHOP, and eIF2 α at the onset of disease and

corresponding to mechanical hypersensitivity. Treatment with a chemical chaperone, 4-PBA, alleviated ER stress and reversed mechanical and facial hypersensitivity. To further identify how ER stress alters electrophysiological properties of neurons, we treated dissociated DRG neurons from EAE mice with 4-PBA and AMG44, a potent PERK inhibitor, as well as siRNA against CHOP (encoded by Ddit3) and XBP1. Gene knockdown of CHOP and XBP1 had no effect on Ca^{2+} transients in EAE neurons. On the contrary, 4-PBA and AMG44 treatment were able to normalize disease-mediated enhanced Ca^{2+} excitability. Furthermore, perforated patch-clamp recordings identified dysregulated BK channel currents in almost exclusively in IB4+ sensory neurons. Particularly, the $\beta 1$ subunit of BK channels was found to be reduced with EAE and in vitro treatment with ER stress modulators, 4-PBA and AMG44, was able to rescue levels of the $\beta 1$ subunit. These results further suggest that ER stress in EAE affects BK channel physiology in IB4+ neurons.

Majority of studies examining neuropathic pain have been performed in male animals (Mogil, 2009). In contrast, my research studies covered in this dissertation focused only on pathological processes in female mice. The reason for this was two-fold. Primarily, studying responses in female EAE mice allows for a greater translational capacity since MS, like other autoimmune disorders, affects three-times as many females as males (Orton et al., 2006). Secondly, another study from our lab noted enhanced Ca^{2+} responses in female but not male dissociated DRG neurons from EAE mice (Mifflin et al., 2019). Furthermore, our unpublished next generation sequencing data of DRGs from male and female EAE mice revealed over 3500 differentially expressed genes and 29 microRNAs in female DRGs as compared to only 189 differentially expressed genes and 3 microRNAs in males. In the dorsal horn of the spinal cord, male and female mice experience similar levels of T-cell infiltration and microglia/macrophage

activation (Catuneanu et al., 2019). However, male spinal cords have increased astrogliosis and experience greater axonal damage with increased dendritic arborisation suggesting that pathogenesis of pain in EAE in males may be more centrally mediated than in females (Catuneanu et al., 2019). For the first time, we demonstrate inflammation and ER stress in the post-mortem DRG tissue of female MS patients. This finding provides further confidence to our results in the EAE model. Taken together, these studies suggest that female DRGs are uniquely affected by the disease and therapies targeting the PNS, at least in females, may provide better resolution of pain than current treatment options.

References

- Abdulla FA, Smith PA (2001a) Axotomy- and autotomy-induced changes in the excitability of rat dorsal root ganglion neurons. *J Neurophysiol* 85:630–643.
- Abdulla FA, Smith PA (2001b) Axotomy- and autotomy-induced changes in Ca²⁺ and K⁺ channel currents of rat dorsal root ganglion neurons. *J Neurophysiol* 85:644–658.
- Alessi DR, Zhang J, Khanna A, Hochdorfer T, Shang Y, Kahle KT (2014) The WNK-SPAK/OSR1 pathway: master regulator of cation-chloride cotransporters. *Sci Signal* 7:re3.
- Alles SRA, Smith PA (2018) Etiology and Pharmacology of Neuropathic Pain. *Pharmacol Rev* 70:315–347.
- Andhavarapu S, Mubariz F, Arvas M, Bever C, Makar TK (2019) Interplay between ER stress and autophagy: A possible mechanism in multiple sclerosis pathology. *Exp Mol Pathol* 108:183–190.
- Ankathatti Munegowda M, Deng Y, Chibbar R, Xu Q, Freywald A, Mulligan SJ, van Drunen Littel-van den Hurk S, Sun D, Xiong S, Xiang J (2011) A distinct role of CD4⁺ Th17- and Th17-stimulated CD8⁺ CTL in the pathogenesis of type 1 diabetes and experimental autoimmune encephalomyelitis. *J Clin Immunol* 31:811–826.
- Arbore G et al. (2016) T helper 1 immunity requires complement-driven NLRP3 inflammasome activity in CD4⁺ T cells. *Science* (80-) 352:aad1210-1210.
- Asbury M, Gatenby P (1972) Bumetanide: potent new “loop” diuretic. *Br Med J* 1:211–213.
- Ascherio A, Munger KL, Simon KC (2010) Vitamin D and multiple sclerosis. *Lancet Neurol* 9:599–612.
- Ayala P, Montenegro J, Vivar R, Letelier A, Urroz PA, Copaja M, Pivet D, Humeres C, Troncoso R, Vicencio JM, Lavandero S, Díaz-Araya G (2012) Attenuation of endoplasmic reticulum stress using the chemical chaperone 4-phenylbutyric acid prevents cardiac fibrosis induced by isoproterenol. *Exp Mol Pathol* 92:97–104.
- Backonja M-M, Stacey B (2004) Neuropathic pain symptoms relative to overall pain rating. *J Pain* 5:491–497.
- Baron R, Hans G, Dickenson AH (2013) Peripheral input and its importance for central sensitization. *Ann Neurol* 74:630–636.
- Barragán-Iglesias P, Kuhn J, Vidal-Cantú GC, Salinas-Abarca AB, Granados-Soto V, Dussor GO, Campbell ZT, Price TJ (2019) Activation of the integrated stress response in nociceptors drives methylglyoxal-induced pain. *Pain* 160:160–171.
- Basbaum AI, Bautista DM, Scherrer G, Julius D (2009) Cellular and molecular mechanisms of pain. *Cell* 139:267–284.
- Beggs S, Salter MW (2013) The known knowns of microglia-neuronal signalling in neuropathic pain. *Neurosci Lett* 557 Pt A:37–42.

- Begum F, Zhu W, Cortes C, MacNeil B, Namaka M (2013) Elevation of tumor necrosis factor α in dorsal root ganglia and spinal cord is associated with neuroimmune modulation of pain in an animal model of multiple sclerosis. *J Neuroimmune Pharmacol* 8:677–690.
- Benson C, Paylor JW, Tenorio G, Winship I, Baker G, Kerr BJ (2015) Voluntary wheel running delays disease onset and reduces pain hypersensitivity in early experimental autoimmune encephalomyelitis (EAE). *Exp Neurol* 271:279–290.
- Benson CA, Kerr BJ (2014) Pain and Cognition in Multiple Sclerosis. *Curr Top Behav Neurosci* 20:201–215.
- Benson CA, Wong G, Tenorio G, Baker GB, Kerr BJ (2013) The MAO inhibitor phenelzine can improve functional outcomes in mice with established clinical signs in experimental autoimmune encephalomyelitis (EAE). *Behav Brain Res* 252:302–311.
- Berard JL, Wolak K, Fournier S, David S (2010) Characterization of relapsing-remitting and chronic forms of experimental autoimmune encephalomyelitis in C57BL/6 mice. *Glia* 58:434–445.
- Bernardes D, Oliveira-Lima OC, Silva TV da, Faraco CCF, Leite HR, Juliano MA, Santos DM dos, Bethea JR, Brambilla R, Orian JM, Arantes RME, Carvalho-Tavares J (2013) Differential brain and spinal cord cytokine and BDNF levels in experimental autoimmune encephalomyelitis are modulated by prior and regular exercise. *J Neuroimmunol* 264:24–34.
- Berta T, Park C-K, Xu Z-Z, Xie R-G, Liu T, Lü N, Liu Y-C, Ji R-R (2014) Extracellular caspase-6 drives murine inflammatory pain via microglial TNF- α secretion. *J Clin Invest* 124:1173–1186.
- Bezprozvanny I, Watras J, Ehrlich BE (1991) Bell-shaped calcium-response curves of Ins(1,4,5)P₃- and calcium-gated channels from endoplasmic reticulum of cerebellum. *Nature* 351:751–754.
- Binshtok AM, Wang H, Zimmermann K, Amaya F, Vardeh D, Shi L, Brenner GJ, Ji R-R, Bean BP, Woolf CJ, Samad TA (2008) Nociceptors are interleukin-1beta sensors. *J Neurosci* 28:14062–14073.
- Blaesse P, Guillemain I, Schindler J, Schweizer M, Delpire E, Khiroug L, Friauf E, Nothwang HG (2006) Oligomerization of KCC2 correlates with development of inhibitory neurotransmission. *J Neurosci* 26:10407–10419.
- Boiko T, Rasband MN, Levinson SR, Caldwell JH, Mandel G, Trimmer JS, Matthews G (2001) Compact myelin dictates the differential targeting of two sodium channel isoforms in the same axon. *Neuron* 30:91–104.
- Brambilla R (2019) The contribution of astrocytes to the neuroinflammatory response in multiple sclerosis and experimental autoimmune encephalomyelitis. *Acta Neuropathol* 137:757–783.
- Caldwell JH, Schaller KL, Lasher RS, Peles E, Levinson SR (2000) Sodium channel Na(v)1.6 is localized at nodes of ranvier, dendrites, and synapses. *Proc Natl Acad Sci U S A* 97:5616–5620.
- Calfon M, Zeng H, Urano F, Till JH, Hubbard SR, Harding HP, Clark SG, Ron D (2002) IRE1

- couples endoplasmic reticulum load to secretory capacity by processing the XBP-1 mRNA. *Nature* 415:92–96.
- Calvo M, Bennett DLH (2012) The mechanisms of microgliosis and pain following peripheral nerve injury. *Exp Neurol* 234:271–282.
- Cao X-H, Chen S-R, Li L, Pan H-L (2012) Nerve injury increases brain-derived neurotrophic factor levels to suppress BK channel activity in primary sensory neurons. *J Neurochem* 121:944–953.
- Cao Y, Goods BA, Raddassi K, Nepom GT, Kwok WW, Love JC, Hafler DA (2015) Functional inflammatory profiles distinguish myelin-reactive T cells from patients with multiple sclerosis. *Sci Transl Med* 7:287ra74.
- Carrara M, Prischi F, Nowak PR, Ali MM (2015) Crystal structures reveal transient PERK luminal domain tetramerization in endoplasmic reticulum stress signaling. *EMBO J* 34:1589–1600.
- Castillo K, Contreras GF, Pupo A, Torres YP, Neely A, González C, Latorre R (2015) Molecular mechanism underlying β 1 regulation in voltage- and calcium-activated potassium (BK) channels. *Proc Natl Acad Sci U S A*.
- Castro CA, Hogan JB, Benson KA, Shehata CW, Landauer MR (1995) Behavioral effects of vehicles: DMSO, ethanol, Tween-20, Tween-80, and emulphor-620. *Pharmacol Biochem Behav* 50:521–526.
- Catuneanu A, Paylor JW, Winship I, Colbourne F, Kerr BJ (2019) Sex differences in central nervous system plasticity and pain in experimental autoimmune encephalomyelitis. *Pain*.
- Cervero F, Laird JM (1996) Mechanisms of touch-evoked pain (allodynia): a new model. *Pain* 68:13–23.
- Cervero F, Laird JMA, García-Nicas E (2003) Secondary hyperalgesia and presynaptic inhibition: an update. *Eur J Pain* 7:345–351.
- Chen C-H, Shih P-C, Lin H-Y, Wang P-K, Pan P-T, Chuang C-W, Kao M-C (2019) 4-Phenylbutyric acid protects against vasculitic peripheral neuropathy induced by ischaemia-reperfusion through attenuating endoplasmic reticulum stress. *Inflammopharmacology* 27:713–722.
- Chen JT, Guo D, Campanelli D, Frattini F, Mayer F, Zhou L, Kuner R, Heppenstall PA, Knipper M, Hu J (2014a) Presynaptic GABAergic inhibition regulated by BDNF contributes to neuropathic pain induction. *Nat Commun* 5:5331.
- Chen L, Huang LY (1992) Protein kinase C reduces Mg^{2+} block of NMDA-receptor channels as a mechanism of modulation. *Nature* 356:521–523.
- Chen S-R, Cai Y-Q, Pan H-L (2009) Plasticity and emerging role of BKCa channels in nociceptive control in neuropathic pain. *J Neurochem* 110:352–362.
- Chen SR, Li X, Ebisawa K, Zhang L (1997) Functional characterization of the recombinant type 3 Ca^{2+} release channel (ryanodine receptor) expressed in HEK293 cells. *J Biol Chem*

272:24234–24246.

- Chen SR, Zhu L, Chen H, Wen L, Laumet G, Pan HL (2014b) Increased Spinal Cord NKCC1 Activity Contributes to Impairment of Synaptic Inhibition in Paclitaxel-induced Neuropathic Pain. *J Biol Chem* 289:31111–31120.
- Chen W, Koop A, Liu Y, Guo W, Wei J, Wang R, MacLennan DH, Dirksen RT, Chen SRW (2017) Reduced threshold for store overload-induced Ca²⁺ release is a common defect of RyR1 mutations associated with malignant hyperthermia and central core disease. *Biochem J* 474:2749–2761.
- Chen X, Shen J, Prywes R (2002) The luminal domain of ATF6 senses endoplasmic reticulum (ER) stress and causes translocation of ATF6 from the ER to the Golgi. *J Biol Chem* 277:13045–13052.
- Chopra S et al. (2019) IRE1 α -XBP1 signaling in leukocytes controls prostaglandin biosynthesis and pain. *Science* 365.
- Chu F, Shi M, Zheng C, Shen D, Zhu J, Zheng X, Cui L (2018) The roles of macrophages and microglia in multiple sclerosis and experimental autoimmune encephalomyelitis. *J Neuroimmunol* 318:1–7.
- Chung JM, Chung K (2002) Importance of Hyperexcitability of DRG Neurons in Neuropathic Pain. *Pain Pract* 2:87–97.
- Compston A, Coles A (2008) Multiple sclerosis. *Lancet (London, England)* 372:1502–1517.
- Contet C, Goulding SP, Kuljis DA, Barth AL (2016) BK Channels in the Central Nervous System. In: *International Review of Neurobiology*.
- Coull J a M, Beggs S, Boudreau D, Boivin D, Tsuda M, Inoue K, Gravel C, Salter MW, De Koninck Y (2005) BDNF from microglia causes the shift in neuronal anion gradient underlying neuropathic pain. *Nature* 438:1017–1021.
- Coull JAM, Boudreau D, Bachand K, Prescott SA, Nault F, S k A, De Koninck P, De Koninck Y (2003) Trans-synaptic shift in anion gradient in spinal lamina I neurons as a mechanism of neuropathic pain. *Nature* 424:938–942.
- Cox DH, Aldrich RW (2000) Role of the β 1 subunit in large-conductance Ca²⁺-activated K⁺ channel gating energetics: Mechanisms of enhanced Ca²⁺ sensitivity. *J Gen Physiol*.
- Cox JS, Shamu CE, Walter P (1993) Transcriptional induction of genes encoding endoplasmic reticulum resident proteins requires a transmembrane protein kinase. *Cell* 73:1197–1206.
- Cramer SW, Baggott C, Cain J, Tilghman J, Allcock B, Miranpuri G, Rajpal S, Sun D, Resnick D (2008) The role of cation-dependent chloride transporters in neuropathic pain following spinal cord injury. *Mol Pain* 4.
- Craner MJ, Newcombe J, Black JA, Hartle C, Cuzner ML, Waxman SG (2004) Molecular changes in neurons in multiple sclerosis: Altered axonal expression of Nav1.2 and Nav1.6 sodium channels and Na⁺/Ca²⁺ exchanger. *Proc Natl Acad Sci U S A*.
- Cuadrado-Tejedor M, Ricobaraza AL, Torrijo R, Franco R, Garcia-Osta A (2013)

- Phenylbutyrate is a multifaceted drug that exerts neuroprotective effects and reverses the Alzheimer's disease-like phenotype of a commonly used mouse model. *Curr Pharm Des* 19:5076–5084.
- Czeschik JC, Hagenacker T, Schäfers M, Büsselberg D (2008) TNF-alpha differentially modulates ion channels of nociceptive neurons. *Neurosci Lett* 434:293–298.
- Dasgupta S, Zhou Y, Jana M, Banik NL, Pahan K (2003) Sodium phenylacetate inhibits adoptive transfer of experimental allergic encephalomyelitis in SJL/J mice at multiple steps. *J Immunol* 170:3874–3882.
- Davis KD, Meyer RA, Campbell JN (1993) Chemosensitivity and sensitization of nociceptive afferents that innervate the hairy skin of monkey. *J Neurophysiol* 69:1071–1081.
- Debono DJ, Hoeksema LJ, Hobbs RD (2013) Caring for patients with chronic pain: pearls and pitfalls. *J Am Osteopath Assoc* 113:620–627.
- Del Prete D, Checler F, Chami M (2014) Ryanodine receptors: physiological function and deregulation in Alzheimer disease. *Mol Neurodegener* 9:21.
- Dendrou CA, Fugger L (2017) Immunomodulation in multiple sclerosis: promises and pitfalls. *Curr Opin Immunol* 49:37–43.
- Dharmshaktu P, Tayal V, Kalra BS (2012) Efficacy of antidepressants as analgesics: a review. *J Clin Pharmacol* 52:6–17.
- Diehl JA, McQuiston A (2017) Recent insights into PERK-dependent signaling from the stressed endoplasmic reticulum. *F1000Research*.
- Drulovic J, Basic-Kes V, Grgic S, Vojinovic S, Dincic E, Toncev G, Kezic MG, Kusic-Tepavcevic D, Dujmovic I, Mesaros S, Miletic-Drakulic S, Pekmezovic T (2015) The Prevalence of Pain in Adults with Multiple Sclerosis: A Multicenter Cross-Sectional Survey. *Pain Med* 16:1597–1602.
- Duffy SS, Keating BA, Perera CJ, Lees JG, Tonkin RS, Makker PGS, Carrive P, Butovsky O, Moalem-Taylor G (2019) Regulatory T cells and their derived cytokine, interleukin-35, reduce pain in experimental autoimmune encephalomyelitis. *J Neurosci*.
- Duffy SS, Perera CJ, Makker PGS, Lees JG, Carrive P, Moalem-Taylor G (2016) Peripheral and Central Neuroinflammatory Changes and Pain Behaviors in an Animal Model of Multiple Sclerosis. *Front Immunol* 7:369.
- Emery EC, Luiz AP, Sikandar S, Magnúsdóttir R, Dong X, Wood JN (2016) In vivo characterization of distinct modality-specific subsets of somatosensory neurons using GCaMP. *Sci Adv* 2:e1600990.
- Estornes Y, Aguilera MA, Dubuisson C, De Keyser J, Goossens V, Kersse K, Samali A, Vandenabeele P, Bertrand MJM (2015) RIPK1 promotes death receptor-independent caspase-8-mediated apoptosis under unresolved ER stress conditions. *Cell Death Dis* 6:e1798.
- Faissner S, Plemel JR, Gold R, Yong VW (2019) Progressive multiple sclerosis: from

- pathophysiology to therapeutic strategies. *Nat Rev Drug Discov*.
- Falcão AM, van Bruggen D, Marques S, Meijer M, Jäkel S, Agirre E, Samudyata, Floriddia EM, Vanichkina DP, French-Constant C, Williams A, Guerreiro-Cacais AO, Castelo-Branco G (2018) Disease-specific oligodendrocyte lineage cells arise in multiple sclerosis. *Nat Med*.
- Falcon M, Guendelman D, Stolberg A (1996) Development of thermal nociception in rats. *Pain* 67:203–208.
- Fitzgerald M, Gibson S (1984) The postnatal physiological and neurochemical development of peripheral sensory C fibres. *Neuroscience* 13:933–944.
- Fleetwood-Walker SM, Hope PJ, Mitchell R (1988) Antinociceptive actions of descending dopaminergic tracts on cat and rat dorsal horn somatosensory neurones. *J Physiol* 399:335–348.
- Foley PL, Vesterinen HM, Laird BJ, Sena ES, Colvin LA, Chandran S, MacLeod MR, Fallon MT (2013) Prevalence and natural history of pain in adults with multiple sclerosis: systematic review and meta-analysis. *Pain* 154:632–642.
- Frezel NN, Sohet F, Daneman R, Basbaum AI, Braz JM (2016) Peripheral and central neuronal ATF3 precedes CD4+ T-cell infiltration in EAE. *Exp Neurol* 283:224–234.
- Fujimori T, Suno R, Iemura S-I, Natsume T, Wada I, Hosokawa N (2017) Endoplasmic reticulum proteins SDF2 and SDF2L1 act as components of the BiP chaperone cycle to prevent protein aggregation. *Genes Cells* 22:684–698.
- Gagnon M, Bergeron MJ, Lavertu G, Castonguay A, Tripathy S, Bonin RP, Perez-Sanchez J, Boudreau D, Wang B, Dumas L, Valade I, Bachand K, Jacob-Wagner M, Tardif C, Kianicka I, Isenring P, Attardo G, Coull J a M, De Koninck Y (2013) Chloride extrusion enhancers as novel therapeutics for neurological diseases. *Nat Med* 19:1524–1528.
- Garcia-Nicas E, Laird JM, Cervero F (2001) Vasodilatation in hyperalgesic rat skin evoked by stimulation of afferent A beta-fibers: further evidence for a role of dorsal root reflexes in allodynia. *Pain* 94:283–291.
- Garrison SR, Weyer AD, Barabas ME, Beutler BA, Stucky CL (2014) A gain-of-function voltage-gated sodium channel 1.8 mutation drives intense hyperexcitability of A- and C-fiber neurons. *Pain* 155:896–905.
- Gaskin DJ, Richard P (2012) The economic costs of pain in the United States. *J Pain* 13:715–724.
- Gavini CK, Bookout AL, Bonomo R, Gautron L, Lee S, Mansuy-Aubert V (2018) Liver X Receptors Protect Dorsal Root Ganglia from Obesity-Induced Endoplasmic Reticulum Stress and Mechanical Allodynia. *Cell Rep* 25:271-277.e4.
- Gillespie D, Chen H, Fill M (2012) Is ryanodine receptor a calcium or magnesium channel? Roles of K⁺ and Mg²⁺ during Ca²⁺ release. *Cell Calcium* 51:427–433.
- Griffin RS, Costigan M, Brenner GJ, Ma CHE, Scholz J, Moss A, Allchorne AJ, Stahl GL, Woolf CJ (2007) Complement induction in spinal cord microglia results in anaphylatoxin

- C5a-mediated pain hypersensitivity. *J Neurosci* 27:8699–8708.
- Griguoli M, Sgritta M, Cherubini E (2016) Presynaptic BK channels control transmitter release: physiological relevance and potential therapeutic implications. *J Physiol* 594:3489–3500.
- Hadjimichael O, Kerns RD, Rizzo MA, Cutter G, Vollmer T (2007) Persistent pain and uncomfortable sensations in persons with multiple sclerosis. *Pain* 127:35–41.
- Hagar RE, Burgstahler AD, Nathanson MH, Ehrlich BE (1998) Type III InsP3 receptor channel stays open in the presence of increased calcium. *Nature* 396:81–84.
- Haines JD, Inglese M, Casaccia P (2011) Axonal damage in multiple sclerosis. *Mt Sinai J Med* 78:231–243.
- Haines JL, Terwedow HA, Burgess K, Pericak-Vance MA, Rimmler JB, Martin ER, Oksenberg JR, Lincoln R, Zhang DY, Banatao DR, Gatto N, Goodkin DE, Hauser SL (1998) Linkage of the MHC to familial multiple sclerosis suggests genetic heterogeneity. The Multiple Sclerosis Genetics Group. *Hum Mol Genet* 7:1229–1234.
- Han J, Back SH, Hur J, Lin YH, Gildersleeve R, Shan J, Yuan CL, Krokowski D, Wang S, Hatzoglou M, Kilberg MS, Sartor MA, Kaufman RJ (2013) ER-stress-induced transcriptional regulation increases protein synthesis leading to cell death. *Nat Cell Biol*.
- Hanani M, Blum E, Liu S, Peng L, Liang S (2014) Satellite glial cells in dorsal root ganglia are activated in streptozotocin-treated rodents. *J Cell Mol Med*.
- Hannaert P, Alvarez-Guerra M, Pirot D, Nazaret C, Garay R (2002) Rat NKCC2/NKCC1 cotransporter selectivity for loop diuretic drugs. *Naunyn Schmiedebergs Arch Pharmacol* 365:193–199.
- Harding HP, Novoa I, Zhang Y, Zeng H, Wek R, Schapira M, Ron D (2000) Regulated translation initiation controls stress-induced gene expression in mammalian cells. *Mol Cell* 6:1099–1108.
- Häring M, Zeisel A, Hochgerner H, Rinwa P, Jakobsson JET, Lönnerberg P, La Manno G, Sharma N, Borgius L, Kiehn O, Lagerström MC, Linnarsson S, Ernfors P (2018) Neuronal atlas of the dorsal horn defines its architecture and links sensory input to transcriptional cell types. *Nat Neurosci* 21:869–880.
- Harp CT, Lovett-Racke AE, Racke MK, Frohman EM, Monson NL (2008) Impact of myelin-specific antigen presenting B cells on T cell activation in multiple sclerosis. *Clin Immunol* 128:382–391.
- Hartmann A-M, Nothwang HG (2014) Molecular and evolutionary insights into the structural organization of cation chloride cotransporters. *Front Cell Neurosci* 8:470.
- Hasbargen T, Ahmed MM, Miranpuri G, Li L, Kahle KT, Resnick D, Sun D (2010) Role of NKCC1 and KCC2 in the development of chronic neuropathic pain following spinal cord injury. *Ann N Y Acad Sci* 1198:168–172.
- Hauser SL, Bhan AK, Gilles F, Kemp M, Kerr C, Weiner HL (1986) Immunohistochemical analysis of the cellular infiltrate in multiple sclerosis lesions. *Ann Neurol* 19:578–587.

- Hemmer B, Kerschensteiner M, Korn T (2015) Role of the innate and adaptive immune responses in the course of multiple sclerosis. *Lancet Neurol* 14:406–419.
- Henderson APD, Barnett MH, Parratt JDE, Prineas JW (2009) Multiple sclerosis: distribution of inflammatory cells in newly forming lesions. *Ann Neurol* 66:739–753.
- Herder V, Iskandar CD, Kegler K, Hansmann F, Elmarabet SA, Khan MA, Kalkuhl A, Deschl U, Baumgärtner W, Ulrich R, Beineke A (2015) Dynamic Changes of Microglia/Macrophage M1 and M2 Polarization in Theiler's Murine Encephalomyelitis. *Brain Pathol* 25:712–723.
- Hetz C, Axten JM, Patterson JB (2019) Pharmacological targeting of the unfolded protein response for disease intervention. *Nat Chem Biol* 15:764–775.
- Hetz C, Mollereau B (2014) Disturbance of endoplasmic reticulum proteostasis in neurodegenerative diseases. *Nat Rev Neurosci* 15:233–249.
- Hillary RF, FitzGerald U (2018) A lifetime of stress: ATF6 in development and homeostasis. *J Biomed Sci* 25:48.
- Ho J, Clark JD, Li X, Yorek MS, Usachev YM, Brennan TJ (2010) Nociceptive sensitization by complement C5a and C3a in mouse. *Pain* 148:343–352.
- Hofstetter HH, Shive CL, Forsthuber TG (2002) Pertussis toxin modulates the immune response to neuroantigens injected in incomplete Freund's adjuvant: induction of Th1 cells and experimental autoimmune encephalomyelitis in the presence of high frequencies of Th2 cells. *J Immunol* 169:117–125.
- Hollien J, Lin JH, Li H, Stevens N, Walter P, Weissman JS (2009) Regulated Ire1-dependent decay of messenger RNAs in mammalian cells. *J Cell Biol* 186:323–331.
- Hoshino H, Obata H, Nakajima K, Mieda R, Saito S (2014) The antihyperalgesic effects of intrathecal bupropion, a dopamine and noradrenaline reuptake inhibitor, in a rat model of neuropathic pain. *Anesth Analg* XXX:1–7.
- Howard J, Trevick S, Younger DS (2016) Epidemiology of Multiple Sclerosis. *Neurol Clin*.
- Hu P, Han Z, Couvillon AD, Kaufman RJ, Exton JH (2006) Autocrine tumor necrosis factor alpha links endoplasmic reticulum stress to the membrane death receptor pathway through IRE1alpha-mediated NF-kappaB activation and down-regulation of TRAF2 expression. *Mol Cell Biol* 26:3071–3084.
- Hu X, Huang F, Wang ZJ (2018) CaMKII α Mediates the Effect of IL-17 To Promote Ongoing Spontaneous and Evoked Pain in Multiple Sclerosis. *J Neurosci* 38:232–244.
- Huang T-Y, Belzer V, Hanani M (2010) Gap junctions in dorsal root ganglia: possible contribution to visceral pain. *Eur J Pain*.
- Huber M et al. (2013) IL-17A secretion by CD8⁺ T cells supports Th17-mediated autoimmune encephalomyelitis. *J Clin Invest* 123:247–260.
- Hunt D, Raivich G, Anderson PN (2012) Activating Transcription Factor 3 and the Nervous System. *Front Mol Neurosci* 5.

- Hussien Y, Cavener DR, Popko B (2014) Genetic inactivation of PERK signaling in mouse oligodendrocytes: normal developmental myelination with increased susceptibility to inflammatory demyelination. *Glia* 62:680–691.
- Iannitti T, Kerr BJ, Taylor BK (2014) Mechanisms and pharmacology of neuropathic pain in multiple sclerosis. *Curr Top Behav Neurosci*.
- Ifergan I, Kebir H, Alvarez JI, Marceau G, Bernard M, Bourbonnière L, Poirier J, Duquette P, Talbot PJ, Arbour N, Prat A (2011) Central nervous system recruitment of effector memory CD8⁺ T lymphocytes during neuroinflammation is dependent on $\alpha 4$ integrin. *Brain* 134:3560–3577.
- Inceoglu B, Bettaieb A, Trindade da Silva CA, Lee KSS, Haj FG, Hammock BD (2015) Endoplasmic reticulum stress in the peripheral nervous system is a significant driver of neuropathic pain. *Proc Natl Acad Sci U S A* 112:9082–9087.
- Inui M, Saito A, Fleischer S (1987) Purification of the ryanodine receptor and identity with feet structures of junctional terminal cisternae of sarcoplasmic reticulum from fast skeletal muscle. *J Biol Chem* 262:1740–1747.
- Irie T, Trussell LO (2017) Double-Nanodomain Coupling of Calcium Channels, Ryanodine Receptors, and BK Channels Controls the Generation of Burst Firing. *Neuron* 96:856–870.e4.
- Jacquemyn J, Cascalho A, Goodchild RE (2017) The ins and outs of endoplasmic reticulum-controlled lipid biosynthesis. *EMBO Rep* 18:1905–1921.
- Jäkel S, Agirre E, Mendanha Falcão A, van Bruggen D, Lee KW, Knuesel I, Malhotra D, French-Constant C, Williams A, Castelo-Branco G (2019) Altered human oligodendrocyte heterogeneity in multiple sclerosis. *Nature*.
- Jann MW, Slade JH (2007) Antidepressant agents for the treatment of chronic pain and depression. *Pharmacotherapy* 27:1571–1587.
- Ji R-R, Gereau RW, Malcangio M, Strichartz GR (2009) MAP kinase and pain. *Brain Res Rev* 60:135–148.
- Jiang MC, Gebhart GF (1998) Development of mustard oil-induced hyperalgesia in rats. *Pain* 77:305–313.
- John LM, Lechleiter JD, Camacho P (1998) Differential modulation of SERCA2 isoforms by calreticulin. *J Cell Biol* 142:963–973.
- Junjappa RP, Patil P, Bhattarai KR, Kim HR, Chae HJ (2018) IRE1 α implications in endoplasmic reticulum stress-mediated development and pathogenesis of autoimmune diseases. *Front Immunol*.
- Kahle KT, Deeb TZ, Puskarjov M, Silayeva L, Liang B, Kaila K, Moss SJ (2013) Modulation of neuronal activity by phosphorylation of the K-Cl cotransporter KCC2. *Trends Neurosci* 36:726–737.
- Kaneko M, Niinuma Y, Nomura Y (2003) Activation signal of nuclear factor-kappa B in

- response to endoplasmic reticulum stress is transduced via IRE1 and tumor necrosis factor receptor-associated factor 2. *Biol Pharm Bull* 26:931–935.
- Karagöz GE, Acosta-Alvear D, Nguyen HT, Lee CP, Chu F, Walter P (2017) An unfolded protein-induced conformational switch activates mammalian IRE1. *Elife* 6.
- Kaur B, Bhat A, Chakraborty R, Adlakha K, Sengupta S, Roy S, Chakraborty K (2018) Proteomic profile of 4-PBA treated human neuronal cells during ER stress. *Mol Omi* 14:53–63.
- Khan N, Gordon R, Woodruff TM, Smith MT (2015) Antiallodynic effects of alpha lipoic acid in an optimized RR-EAE mouse model of MS-neuropathic pain are accompanied by attenuation of upregulated BDNF-TrkB-ERK signaling in the dorsal horn of the spinal cord. *Pharmacol Res Perspect* 3:e00137.
- Khan N, Smith MT (2014) Multiple sclerosis-induced neuropathic pain: pharmacological management and pathophysiological insights from rodent EAE models. *Inflammopharmacology* 22:1–22.
- Khoutorsky A, Price TJ (2018) Translational Control Mechanisms in Persistent Pain. *Trends Neurosci*.
- Khoutorsky A, Sorge RE, Prager-Khoutorsky M, Pawlowski SA, Longo G, Jafarnejad SM, Tahmasebi S, Martin LJ, Pitcher MH, Gkogkas CG, Sharif-Naeini R, Ribeiro-da-Silva A, Bourque CW, Cervero F, Mogil JS, Sonenberg N (2016) eIF2 α phosphorylation controls thermal nociception. *Proc Natl Acad Sci U S A* 113:11949–11954.
- Kim J-Y V., Tillu D V., Quinn TL, Mejia GL, Shy A, Asiedu MNK, Murad E, Schumann AP, Totsch SK, Sorge RE, Mantyh PW, Dussor G, Price TJ (2015) Spinal dopaminergic projections control the transition to pathological pain plasticity via a D1/D5-mediated mechanism. *J Neurosci* 35:6307–6317.
- Kipp M, Nyamoya S, Hochstrasser T, Amor S (2017) Multiple sclerosis animal models: a clinical and histopathological perspective. *Brain Pathol*.
- Kirby L, Jin J, Cardona JG, Smith MD, Martin KA, Wang J, Strasburger H, Herbst L, Alexis M, Karnell J, Davidson T, Dutta R, Goverman J, Bergles D, Calabresi PA (2019) Oligodendrocyte precursor cells present antigen and are cytotoxic targets in inflammatory demyelination. *Nat Commun*.
- Kirkcaldie MTK, Collins JM (2016) The axon as a physical structure in health and acute trauma. *J Chem Neuroanat* 76:9–18.
- Koch SC, Acton D, Goulding M (2018) Spinal Circuits for Touch, Pain, and Itch. *Annu Rev Physiol* 80:189–217.
- Kocur M, Schneider R, Pulm A-K, Bauer J, Kropp S, Gliem M, Ingwersen J, Goebels N, Alferink J, Prozorovski T, Aktas O, Scheu S (2015) IFN β secreted by microglia mediates clearance of myelin debris in CNS autoimmunity. *Acta Neuropathol Commun* 3:20.
- Kolb PS, Ayaub EA, Zhou W, Yum V, Dickhout JG, Ask K (2015) The therapeutic effects of 4-phenylbutyric acid in maintaining proteostasis. *Int J Biochem Cell Biol* 61:45–52.

- Kong D, Guo Z, Yang W, Wang Q, Yu Y, Zhang L (2019) Tanshinone II A Affects Diabetic Peripheral Neuropathic Pain via Spinal Dorsal Horn Neuronal Circuitry by Modulating Endoplasmic Reticulum Stress Pathways. *Exp Clin Endocrinol Diabetes*.
- Kong W, Hooper KM, Ganea D (2016) The natural dual cyclooxygenase and 5-lipoxygenase inhibitor flavocoxid is protective in EAE through effects on Th1/Th17 differentiation and macrophage/microglia activation. *Brain Behav Immun* 53:59–71.
- Korennykh A V, Egea PF, Korostelev AA, Finer-Moore J, Zhang C, Shokat KM, Stroud RM, Walter P (2009) The unfolded protein response signals through high-order assembly of Ire1. *Nature* 457:687–693.
- Kramer JLK, Minhas NK, Jutzeler CR, Erskine ELKS, Liu LJW, Ramer MS (2017) Neuropathic pain following traumatic spinal cord injury: Models, measurement, and mechanisms. *J Neurosci Res* 95:1295–1306.
- Krebs J, Agellon LB, Michalak M (2015) Ca²⁺ homeostasis and endoplasmic reticulum (ER) stress: An integrated view of calcium signaling. *Biochem Biophys Res Commun* 460:114–121.
- Kshatri AS, Gonzalez-Hernandez A, Giraldez T (2018) Physiological Roles and Therapeutic Potential of Ca²⁺ Activated Potassium Channels in the Nervous System. *Front Mol Neurosci*.
- Kutzelnigg A, Lucchinetti CF, Stadelmann C, Brück W, Rauschka H, Bergmann M, Schmidbauer M, Parisi JE, Lassmann H (2005) Cortical demyelination and diffuse white matter injury in multiple sclerosis. *Brain* 128:2705–2712.
- Langford DJ, Bailey AL, Chanda ML, Clarke SE, Drummond TE, Echols S, Glick S, Ingrao J, Klassen-Ross T, Lacroix-Fralish ML, Matsumiya L, Sorge RE, Sotocinal SG, Tabaka JM, Wong D, Van Den Maagdenberg AMJM, Ferrari MD, Craig KD, Mogil JS (2010) Coding of facial expressions of pain in the laboratory mouse. *Nat Methods* 7:447–449.
- Lassmann H (2010) Axonal and neuronal pathology in multiple sclerosis: what have we learnt from animal models. *Exp Neurol* 225:2–8.
- Latremliere A, Woolf CJ (2009) Central sensitization: a generator of pain hypersensitivity by central neural plasticity. *J Pain* 10:895–926.
- Leadley RM, Armstrong N, Reid KJ, Allen A, Misso K V, Kleijnen J (2014) Healthy aging in relation to chronic pain and quality of life in Europe. *Pain Pract* 14:547–558.
- Lee A-H, Iwakoshi NN, Glimcher LH (2003) XBP-1 regulates a subset of endoplasmic reticulum resident chaperone genes in the unfolded protein response. *Mol Cell Biol* 23:7448–7459.
- Lee K, Tirasophon W, Shen X, Michalak M, Prywes R, Okada T, Yoshida H, Mori K, Kaufman RJ (2002) IRE1-mediated unconventional mRNA splicing and S2P-mediated ATF6 cleavage merge to regulate XBP1 in signaling the unfolded protein response. *Genes Dev* 16:452–466.
- Lee Y, Morrison BM, Li Y, Lengacher S, Farah MH, Hoffman PN, Liu Y, Tsingalia A, Jin L, Zhang P-WW, Pellerin L, Magistretti PJ, Rothstein JD (2012) Oligodendroglia

- metabolically support axons and contribute to neurodegeneration. *Nature* 487:443–448.
- Lehmann HC, Compston A, Hartung H-P (2018) 150th anniversary of clinical description of multiple sclerosis: Leopold Ordenstein's legacy. *Neurology* 90:1011–1016.
- Lencer WI, DeLuca H, Grey MJ, Cho JA (2015) Innate immunity at mucosal surfaces: the IRE1-RIDD-RIG-I pathway. *Trends Immunol* 36:401–409.
- Leung L, Cahill CM (2010) TNF-alpha and neuropathic pain--a review. *J Neuroinflammation* 7:27.
- Levin LI, Munger KL, Rubertone M V, Peck CA, Lennette ET, Spiegelman D, Ascherio A (2005) Temporal relationship between elevation of epstein-barr virus antibody titers and initial onset of neurological symptoms in multiple sclerosis. *JAMA* 293:2496–2500.
- Li Y, Camacho P (2004) Ca²⁺-dependent redox modulation of SERCA 2b by ERp57. *J Cell Biol* 164:35–46.
- Liang DY, Li X, Shi X, Sun Y, Sahbaie P, Li WW, Clark JD (2012) The complement component C5a receptor mediates pain and inflammation in a postsurgical pain model. *Pain* 153:366–372.
- Liddel SA, Barres BA (2017) Reactive Astrocytes: Production, Function, and Therapeutic Potential. *Immunity* 46:957–967.
- Lin Q, Li D, Xu X, Zou X, Fang L (2007a) Roles of TRPV1 and neuropeptidergic receptors in dorsal root reflex-mediated neurogenic inflammation induced by intradermal injection of capsaicin. *Mol Pain* 3:30.
- Lin Q, Wu J, Willis WD (1999) Dorsal root reflexes and cutaneous neurogenic inflammation after intradermal injection of capsaicin in rats. *J Neurophysiol* 82:2602–2611.
- Lin W, Bailey SL, Ho H, Harding HP, Ron D, Miller SD, Popko B (2007b) The integrated stress response prevents demyelination by protecting oligodendrocytes against immune-mediated damage. *J Clin Invest* 117:448–456.
- Lin W, Lin Y, Li J, Fenstermaker AG, Way SW, Clayton B, Jamison S, Harding HP, Ron D, Popko B (2013) Oligodendrocyte-specific activation of PERK signaling protects mice against experimental autoimmune encephalomyelitis. *J Neurosci* 33:5980–5991.
- Loeser JD, Treede RD (2008) The Kyoto protocol of IASP Basic Pain Terminology. *Pain* 137:473–477.
- Lozano-Ondoua AN, Symons-Liguori AM, Vanderah TW (2013) Cancer-induced bone pain: Mechanisms and models. *Neurosci Lett* 557 Pt A:52–59.
- Lu J, Kurejova M, Wirotanseng LN, Linker RA, Kuner R, Tappe-Theodor A (2012) Pain in experimental autoimmune encephalitis: a comparative study between different mouse models. *J Neuroinflammation* 9:233.
- Lynes EM, Bui M, Yap MC, Benson MD, Schneider B, Ellgaard L, Berthiaume LG, Simmen T (2012) Palmitoylated TMX and calnexin target to the mitochondria-associated membrane. *EMBO J* 31:457–470.

- Ma C, Shu Y, Zheng Z, Chen Y, Yao H, Greenquist KW, White FA, LaMotte RH (2003) Similar electrophysiological changes in axotomized and neighboring intact dorsal root ganglion neurons. *J Neurophysiol* 89:1588–1602.
- Ma K, Vattem KM, Wek RC (2002) Dimerization and release of molecular chaperone inhibition facilitate activation of eukaryotic initiation factor-2 kinase in response to endoplasmic reticulum stress. *J Biol Chem* 277:18728–18735.
- Man SM, Karki R, Kanneganti T-D (2017) Molecular mechanisms and functions of pyroptosis, inflammatory caspases and inflammasomes in infectious diseases. *Immunol Rev* 277:61–75.
- Manotheepan R, Danielsen TK, Sadredini M, Anderson ME, Carlson CR, Lehnart SE, Sjaastad I, Stokke MK (2016) Exercise training prevents ventricular tachycardia in CPVT1 due to reduced CaMKII-dependent arrhythmogenic Ca²⁺ release. *Cardiovasc Res* 111:295–306.
- Marsh D, Dickenson A, Hatch D, Fitzgerald M (1999) Epidural opioid analgesia in infant rats I: mechanical and heat responses. *Pain* 82:23–32.
- Martínez G, Khatiwada S, Costa-Mattioli M, Hetz C (2018) ER Proteostasis Control of Neuronal Physiology and Synaptic Function. *Trends Neurosci*.
- Mathern DR, Heeger PS (2015) Molecules Great and Small: The Complement System. *Clin J Am Soc Nephrol* 10:1636–1650.
- Matsushita T, Horikawa M, Iwata Y, Tedder TF (2010) Regulatory B cells (B10 cells) and regulatory T cells have independent roles in controlling experimental autoimmune encephalomyelitis initiation and late-phase immunopathogenesis. *J Immunol* 185:2240–2252.
- Matsushita T, Yanaba K, Bouaziz J-D, Fujimoto M, Tedder TF (2008) Regulatory B cells inhibit EAE initiation in mice while other B cells promote disease progression. *J Clin Invest* 118:3420–3430.
- Mayo L, Trauger SA, Blain M, Nadeau M, Patel B, Alvarez JI, Mascanfroni ID, Yeste A, Kivisäkk P, Kallas K, Ellezam B, Bakshi R, Prat A, Antel JP, Weiner HL, Quintana FJ (2014) Regulation of astrocyte activation by glycolipids drives chronic CNS inflammation. *Nat Med* 20:1147–1156.
- McPherson RC, Cambrook HE, O'Connor RA, Anderton SM (2014) Induction of passive EAE using myelin-reactive CD4⁺ T cells. *Methods Mol Biol* 1193:187–198.
- Megat S, Ray PR, Tavares-Ferreira D, Moy JK, Sankaranarayanan I, Wangzhou A, Fang Lou T, Barragan-Iglesias P, Campbell ZT, Dussor G, Price TJ (2019) Differences between Dorsal Root and Trigeminal Ganglion Nociceptors in Mice Revealed by Translational Profiling. *J Neurosci* 39:6829–6847.
- Megat S, Shiers S, Moy JK, Barragan-Iglesias P, Pradhan G, Seal RP, Dussor G, Price TJ (2018) A critical role for dopamine D5 receptors in pain chronicity in male mice. *J Neurosci* 38:379–397.
- Melanson M, Miao P, Eisenstat D, Gong Y, Gu X, Au K, Zhu W, Begum F, Frost EE, Namaka M (2009) Experimental autoimmune encephalomyelitis-induced upregulation of tumor

- necrosis factor-alpha in the dorsal root ganglia. *Mult Scler* 15:1135–1145.
- Melzack R, Wall PD (1965) Pain mechanisms: a new theory. *Science* (80-) 150:971–979.
- Mendell LM, Wall PD (1965) Responses of single dorsal cord cells to peripheral cutaneous unmyelinated fibres [23]. *Nature*.
- Michel L, Touil H, Pikor NB, Gommerman JL, Prat A, Bar-Or A (2015) B Cells in the Multiple Sclerosis Central Nervous System: Trafficking and Contribution to CNS-Compartmentalized Inflammation. *Front Immunol* 6:636.
- Mifflin KA, Yousuf MS, Thorburn KC, Huang J, Pérez-Muñoz ME, Tenorio G, Walter J, Ballanyi K, Drohomysky PC, Dunn SE, Kerr BJ (2019) Voluntary wheel running reveals sex-specific nociceptive factors in murine experimental autoimmune encephalomyelitis. *Pain*.
- Miletic G, Miletic V (2008) Loose ligation of the sciatic nerve is associated with TrkB receptor-dependent decreases in KCC2 protein levels in the ipsilateral spinal dorsal horn. *Pain* 137:532–539.
- Mimori S, Ohtaka H, Koshikawa Y, Kawada K, Kaneko M, Okuma Y, Nomura Y, Murakami Y, Hamana H (2013) 4-Phenylbutyric acid protects against neuronal cell death by primarily acting as a chemical chaperone rather than histone deacetylase inhibitor. *Bioorg Med Chem Lett* 23:6015–6018.
- Modol L, Cobiañchi S, Navarro X (2014) Prevention of NKCC1 phosphorylation avoids downregulation of KCC2 in central sensory pathways and reduces neuropathic pain after peripheral nerve injury. *Pain* 155:1577–1590.
- Modol L, Santos D, Cobiañchi S, Gonzalez-Perez F, Lopez-Alvarez V, Navarro X (2015) NKCC1 Activation Is Required for Myelinated Sensory Neurons Regeneration through JNK-Dependent Pathway. *J Neurosci* 35:7414–7427.
- Moehring F, Halder P, Seal RP, Stucky CL (2018) Uncovering the Cells and Circuits of Touch in Normal and Pathological Settings. *Neuron*.
- Mogil JS et al. (2005) Variable sensitivity to noxious heat is mediated by differential expression of the CGRP gene. *Proc Natl Acad Sci U S A*.
- Mogil JS (2009) Animal models of pain: Progress and challenges. *Nat Rev Neurosci*.
- Mogil JS, Bailey AL (2010) Sex and gender differences in pain and analgesia. In: *Progress in Brain Research*.
- Morales-Aza BM, Chillingworth NL, Payne JA, Donaldson LF (2004) Inflammation alters cation chloride cotransporter expression in sensory neurons. *Neurobiol Dis* 17:62–69.
- Moy JK, Khoutorsky A, Asiedu MN, Black BJ, Kuhn JL, Barragán-Iglesias P, Megat S, Burton MD, Burgos-Vega CC, Melemedjian OK, Boitano S, Vagner J, Gkogkas CG, Pancrazio JJ, Mogil JS, Dussor G, Sonenberg N, Price TJ (2017) The MNK-eIF4E Signaling Axis Contributes to Injury-Induced Nociceptive Plasticity and the Development of Chronic Pain. *J Neurosci* 37:7481–7499.

- Mule NK, Singh JN, Shah KU, Gulati A, Sharma SS (2017) Endothelin-1 Decreases Excitability of the Dorsal Root Ganglion Neurons via ETB Receptor. *Mol Neurobiol*.
- Murayama T, Ogawa Y (1996) Properties of Ryr3 ryanodine receptor isoform in mammalian brain. *J Biol Chem* 271:5079–5084.
- Murayama T, Ogawa Y (1997) Characterization of type 3 ryanodine receptor (RyR3) of sarcoplasmic reticulum from rabbit skeletal muscles. *J Biol Chem* 272:24030–24037.
- Murphy KL, Fischer R, Swanson KA, Bhatt IJ, Oakley L, Smeyne R, Bracchi-Ricard V, Bethea JR (2019) Synaptic alterations and immune response are sexually dimorphic in a non-pertussis toxin model of experimental autoimmune encephalomyelitis. *Exp Neurol*:113061.
- Nakajima K, Obata H, Iriuchijima N, Saito S (2012) An increase in spinal cord noradrenaline is a major contributor to the antihyperalgesic effect of antidepressants after peripheral nerve injury in the rat. *Pain* 153:990–997.
- Nave K-A, Werner HB (2014) Myelination of the Nervous System: Mechanisms and Functions. *Annu Rev Cell Dev Biol* 30:503–533.
- Nemmani KVS, Grisel JE, Stowe JR, Smith-Carliss R, Mogil JS (2004) Modulation of morphine analgesia by site-specific N-methyl-D-aspartate receptor antagonists: Dependence on sex, site of antagonism, morphine dose, and time. *Pain*.
- Nikawa J -I, Yamashita S (1992) IRE1 encodes a putative protein kinase containing a membrane-spanning domain and is required for inositol phototrophy in *Saccharomyces cerevisiae*. *Mol Microbiol*.
- Ning B, Zhang Q, Wang N, Deng M, Fang Y (2019) β -Asarone Regulates ER Stress and Autophagy Via Inhibition of the PERK/CHOP/Bcl-2/Beclin-1 Pathway in 6-OHDA-Induced Parkinsonian Rats. *Neurochem Res* 44:1159–1166.
- Nomura H, Sakai A, Nagano M, Umino M, Suzuki H (2006) Expression changes of cation chloride cotransporters in the rat spinal cord following intraplantar formalin. *Neurosci Res* 56:435–440.
- O'Connor RA, Anderton SM (2008) Foxp3+ regulatory T cells in the control of experimental CNS autoimmune disease. *J Neuroimmunol* 193:1–11.
- Ohl K, Tenbrock K, Kipp M (2016) Oxidative stress in multiple sclerosis: Central and peripheral mode of action. *Exp Neurol* 277:58–67.
- Okamura K, Kimata Y, Higashio H, Tsuru A, Kohno K (2000) Dissociation of Kar2p/BiP from an ER sensory molecule, Ire1p, triggers the unfolded protein response in yeast. *Biochem Biophys Res Commun*.
- Olechowski CJ, Parmar A, Miller B, Stephan J, Tenorio G, Tran K, Leighton J, Kerr BJ (2010) A diminished response to formalin stimulation reveals a role for the glutamate transporters in the altered pain sensitivity of mice with experimental autoimmune encephalomyelitis (EAE). *Pain* 149:565–572.
- Olechowski CJ, Tenorio G, Sauve Y, Kerr BJ (2013) Changes in nociceptive sensitivity and

- object recognition in experimental autoimmune encephalomyelitis (EAE). *Exp Neurol* 241:113–121.
- Olechowski CJ, Truong JJ, Kerr BJ (2009) Neuropathic pain behaviours in a chronic-relapsing model of experimental autoimmune encephalomyelitis (EAE). *Pain* 141:156–164.
- Ortega SB, Kashi VP, Tyler AF, Cunnusamy K, Mendoza JP, Karandikar NJ (2013) The disease-ameliorating function of autoregulatory CD8 T cells is mediated by targeting of encephalitogenic CD4 T cells in experimental autoimmune encephalomyelitis. *J Immunol* 191:117–126.
- Orton S-MM, Herrera BM, Yee IM, Valdar W, Ramagopalan S V., Sadovnick AD, Ebers GC (2006) Sex ratio of multiple sclerosis in Canada: a longitudinal study. *Lancet Neurol* 5.
- Ossipov MH, Morimura K, Porreca F (2014) Descending pain modulation and chronification of pain. *Curr Opin Support Palliat Care* 8:143–151.
- Osterberg A, Boivie J, Thuomas K-A (2005) Central pain in multiple sclerosis--prevalence and clinical characteristics. *Eur J Pain* 9:531–542.
- Pagany M, Jagodic M, Schubart A, Pham-Dinh D, Bachelin C, Baron van Evercooren A, Lachapelle F, Olsson T, Linington C (2003) Myelin oligodendrocyte glycoprotein is expressed in the peripheral nervous system of rodents and primates. *Neurosci Lett* 350:165–168.
- Pakos-Zebrucka K, Koryga I, Mnich K, Ljujic M, Samali A, Gorman AM (2016) The integrated stress response. *EMBO Rep* 17:1374–1395.
- Pan P-T, Lin H-Y, Chuang C-W, Wang P-K, Wan H-C, Lee M-C, Kao M-C (2019) Resveratrol alleviates nuclear factor- κ B-mediated neuroinflammation in vasculitic peripheral neuropathy induced by ischaemia-reperfusion via suppressing endoplasmic reticulum stress. *Clin Exp Pharmacol Physiol* 46:770–779.
- Park C, Ponath G, Levine-Ritterman M, Bull E, Swanson EC, De Jager PL, Segal BM, Pitt D (2019) The landscape of myeloid and astrocyte phenotypes in acute multiple sclerosis lesions. *Acta Neuropathol Commun*.
- Pender MP (1986) Ascending impairment of nociception in rats with experimental allergic encephalomyelitis. *J Neurol Sci* 75:317–328.
- Pender MP, Sears TA (1982) Conduction block in the peripheral nervous system in experimental allergic encephalomyelitis. *Nature* 296:860–862.
- Pender MP, Sears TA (1986) Involvement of the dorsal root ganglion in acute experimental allergic encephalomyelitis in the Lewis rat. A histological and electrophysiological study. *J Neurol Sci* 72:231–242.
- Pfaffl MW (2001) A new mathematical model for relative quantification in real-time RT-PCR. *Nucleic Acids Res* 29:e45.
- Pfaffl MW, Horgan GW, Dempfle L (2002) Relative expression software tool (REST) for group-wise comparison and statistical analysis of relative expression results in real-time PCR.

Nucleic Acids Res 30:e36.

- Pitcher MH, Cervero F (2010) Role of the NKCC1 co-transporter in sensitization of spinal nociceptive neurons. *Pain* 151:756–762.
- Pitcher MH, Price TJ, Entrena JM, Cervero F (2007) Spinal NKCC1 blockade inhibits TRPV1-dependent referred allodynia. *Mol Pain* 3:17.
- Ponath G, Park C, Pitt D (2018) The role of astrocytes in multiple sclerosis. *Front Immunol*.
- Price DD, Verne GN, Schwartz JM (2006a) Plasticity in brain processing and modulation of pain. *Prog Brain Res* 157:333–352.
- Price TJ, Cervero F, de Koninck Y (2005) Role of cation-chloride-cotransporters (CCC) in pain and hyperalgesia. *Curr Top Med Chem* 5:547–555.
- Price TJ, Cervero F, Gold MS, Hammond DL, Prescott S a (2009) Chloride regulation in the pain pathway. *Brain Res Rev* 60:149–170.
- Price TJ, Hargreaves KM, Cervero F (2006b) Protein expression and mRNA cellular distribution of the NKCC1 cotransporter in the dorsal root and trigeminal ganglia of the rat. *Brain Res* 1112:146–158.
- Price TJ, Prescott SA (2015) Inhibitory regulation of the pain gate and how its failure causes pathological pain. *Pain* 156:789–792.
- Puthalakath H, O'Reilly LA, Gunn P, Lee L, Kelly PN, Huntington ND, Hughes PD, Michalak EM, McKimm-Breschkin J, Motoyama N, Gotoh T, Akira S, Bouillet P, Strasser A (2007) ER Stress Triggers Apoptosis by Activating BH3-Only Protein Bim. *Cell*.
- Rahn EJ, Iannitti T, Donahue RR, Taylor BK (2014) Sex differences in a mouse model of multiple sclerosis: neuropathic pain behavior in females but not males and protection from neurological deficits during proestrus. *Biol Sex Differ* 5:4.
- Rang HP, Bevan S, Dray A (1991) Chemical activation of nociceptive peripheral neurones. *Br Med Bull* 47:534–548.
- Ransohoff RM (2016) A polarizing question: Do M1 and M2 microglia exist. *Nat Neurosci*.
- Ratté S, Prescott SA (2016) Afferent hyperexcitability in neuropathic pain and the inconvenient truth about its degeneracy. *Curr Opin Neurobiol* 36:31–37.
- Rees H, Sluka KA, Westlund KN, Willis WD (1994) Do dorsal root reflexes augment peripheral inflammation? *Neuroreport* 5:821–824.
- Rexed B (1954) A cytoarchitectonic atlas of the spinal cord in the cat. *J Comp Neurol* 100:297–379.
- Robinson AP, Harp CT, Noronha A, Miller SD (2014) The experimental autoimmune encephalomyelitis (EAE) model of MS: utility for understanding disease pathophysiology and treatment. *Handb Clin Neurol* 122:173–189.
- Rodrigues DH, Leles BP, Costa VV, Miranda AS, Cisalpino D, Gomes DA, de Souza DG, Teixeira AL (2016) IL-1?? Is Involved with the Generation of Pain in Experimental

- Autoimmune Encephalomyelitis. *Mol Neurobiol* 53:6540–6547.
- Rojas-Rivera D, Delvaeye T, Roelandt R, Nerinckx W, Augustyns K, Vandenabeele P, Bertrand MJM (2017) When PERK inhibitors turn out to be new potent RIPK1 inhibitors: Critical issues on the specificity and use of GSK2606414 and GSK2656157. *Cell Death Differ*.
- Rosenberg H, Davis M, James D, Pollock N, Stowell K (2007) Malignant hyperthermia. *Orphanet J Rare Dis* 2:21.
- Rossi D, Simeoni I, Micheli M, Bootman M, Lipp P, Allen PD, Sorrentino V (2002) RyR1 and RyR3 isoforms provide distinct intracellular Ca²⁺ signals in HEK 293 cells. *J Cell Sci* 115:2497–2504.
- Ruscheweyh R, Forsthuber L, Schoffnegger D, Sandkühler J (2007) Modification of classical neurochemical markers in identified primary afferent neurons with Aβ-, Adelta-, and C-fibers after chronic constriction injury in mice. *J Comp Neurol* 502:325–336.
- Sandkuhler J (2009) Models and mechanisms of hyperalgesia and allodynia. *Physiol Rev* 89:707–758.
- Sano R, Reed JC (2013) ER stress-induced cell death mechanisms. *Biochim Biophys Acta* 1833:3460–3470.
- Sarzi-Puttini P, Salaffi F, Di Franco M, Bazzichi L, Cassisi G, Casale R, Cazzola M, Stisi S, Battellino M, Atzeni F (2014) Pain in rheumatoid arthritis: a critical review. *Reumatismo* 66:18–27.
- Schattling B, Fazeli W, Engeland B, Liu Y, Lerche H, Isbrandt D, Friese MA (2016) Activity of NaV1.2 promotes neurodegeneration in an animal model of multiple sclerosis. *JCI Insight*.
- Schenk GJ, Dijkstra S, van het Hof AJ, van der Pol SMA, Drexhage JAR, van der Valk P, Reijerkerk A, van Horssen J, de Vries HE (2013) Roles for HB-EGF and CD9 in multiple sclerosis. *Glia* 61:1890–1905.
- Schreiner B, Heppner FL, Becher B (2009) Modeling multiple sclerosis in laboratory animals. *Semin Immunopathol* 31:479–495.
- Shamu CE, Walter P (1996) Oligomerization and phosphorylation of the Ire1p kinase during intracellular signaling from the endoplasmic reticulum to the nucleus. *EMBO J* 15:3028–3039.
- Shen J, Chen X, Hendershot L, Prywes R (2002) ER stress regulation of ATF6 localization by dissociation of BiP/GRP78 binding and unmasking of Golgi localization signals. *Dev Cell* 3:99–111.
- Shi C, Qiu S, Riester SM, Das V, Zhu B, Wallace AA, van Wijnen AJ, Mwale F, Iatridis JC, Sakai D, Votta-Velis G, Yuan W, Im H-J (2018) Animal models for studying the etiology and treatment of low back pain. *J Orthop Res* 36:1305–1312.
- Shutov LP, Warwick CA, Shi X, Gnanasekaran A, Shepherd AJ, Mohapatra DP, Woodruff TM, Clark JD, Usachev YM (2016) The Complement System Component C5a Produces Thermal Hyperalgesia via Macrophage-to-Nociceptor Signaling That Requires NGF and

- TRPV1. *J Neurosci* 36:5055–5070.
- Siedler DG, Chuah MI, Kirkcaldie MTK, Vickers JC, King AE (2014) Diffuse axonal injury in brain trauma: insights from alterations in neurofilaments. *Front Cell Neurosci* 8.
- Sivilotti LG, Thompson SW, Woolf CJ (1993) Rate of rise of the cumulative depolarization evoked by repetitive stimulation of small-caliber afferents is a predictor of action potential windup in rat spinal neurons in vitro. *J Neurophysiol* 69:1621–1631.
- Slugg RM, Meyer RA, Campbell JN (2000) Response of cutaneous A- and C-fiber nociceptors in the monkey to controlled-force stimuli. *J Neurophysiol* 83:2179–2191.
- Smith AL et al. (2015) Discovery of 1H-pyrazol-3(2H)-ones as potent and selective inhibitors of protein kinase R-like endoplasmic reticulum kinase (PERK). *J Med Chem* 58:1426–1441.
- Solaro C, Cella M, Signori A, Martinelli V, Radaelli M, Centonze D, Sica F, Grasso MG, Clemenzi A, Bonavita S, Esposito S, Patti F, D'Amico E, Cruccu G, Truini A, Neuropathic Pain Special Interest Group of the Italian Neurological Society (2018) Identifying neuropathic pain in patients with multiple sclerosis: a cross-sectional multicenter study using highly specific criteria. *J Neurol* 265:828–835.
- Spandidos A, Wang X, Wang H, Dragnev S, Thurber T, Seed B (2008) A comprehensive collection of experimentally validated primers for Polymerase Chain Reaction quantitation of murine transcript abundance. *BMC Genomics* 9:633.
- Spandidos A, Wang X, Wang H, Seed B (2010) PrimerBank: a resource of human and mouse PCR primer pairs for gene expression detection and quantification. *Nucleic Acids Res* 38:D792-9.
- Stemkowski PL, Noh M-C, Chen Y, Smith PA (2015) Increased excitability of medium-sized dorsal root ganglion neurons by prolonged interleukin-1 β exposure is K(+) channel dependent and reversible. *J Physiol* 593:3739–3755.
- Stemkowski PL, Smith PA (2012) Long-term IL-1 β exposure causes subpopulation-dependent alterations in rat dorsal root ganglion neuron excitability. *J Neurophysiol* 107:1586–1597.
- Stevenson J, Huang EY, Olzmann JA (2016) Endoplasmic Reticulum-Associated Degradation and Lipid Homeostasis. *Annu Rev Nutr* 36:511–542.
- Stone S, Lin W (2015) The unfolded protein response in multiple sclerosis. *Front Neurosci* 9:264.
- Stone S, Wu S, Jamison S, Durose W, Pallais JP, Lin W (2018) Activating transcription factor 6 α deficiency exacerbates oligodendrocyte death and myelin damage in immune-mediated demyelinating diseases. *Glia* 66:1331–1345.
- Stys PK, Zamponi GW, Van Minnen J, Geurts JGG (2012) Will the real multiple sclerosis please stand up? *Nat Rev Neurosci*.
- Sun D, Whitaker JN, Huang Z, Liu D, Coleclough C, Wekerle H, Raine CS (2001) Myelin antigen-specific CD8⁺ T cells are encephalitogenic and produce severe disease in C57BL/6 mice. *J Immunol* 166:7579–7587.

- Sun W, Yang F, Wang Y, Fu H, Yang Y, Li C-L, Wang X-L, Lin Q, Chen J (2017a) Contribution of large-sized primary sensory neuronal sensitization to mechanical allodynia by upregulation of hyperpolarization-activated cyclic nucleotide gated channels via cyclooxygenase 1 cascade. *Neuropharmacology* 113:217–230.
- Sun WT, Wang XC, Mak SK, He GW, Liu XC, Underwood MJ, Yang Q (2017b) Activation of PERK branch of ER stress mediates homocysteine-induced BKCa channel dysfunction in coronary artery via FoxO3-dependent regulation of atrogin-1. *Oncotarget*.
- Sung KW, Kirby M, McDonald MP, Lovinger DM, Delpire E (2000) Abnormal GABA_A receptor-mediated currents in dorsal root ganglion neurons isolated from Na-K-2Cl cotransporter null mice. *J Neurosci* 20:7531–7538.
- Suzuki CK, Bonifacino JS, Lin AY, Davis MM, Klausner RD (1991) Regulating the retention of T-cell receptor alpha chain variants within the endoplasmic reticulum: Ca²⁺-dependent association with BiP. *J Cell Biol* 114:189–205.
- Tahmasebi S, Khoutorsky A, Mathews MB, Sonenberg N (2018) Translation deregulation in human disease. *Nat Rev Mol Cell Biol* 19:791–807.
- Taniguchi W, Nakatsuka T, Miyazaki N, Yamada H, Takeda D, Fujita T, Kumamoto E, Yoshida M (2011) In vivo patch-clamp analysis of dopaminergic antinociceptive actions on substantia gelatinosa neurons in the spinal cord. *Pain*.
- Taylor CW, Tovey SC (2010) IP(3) receptors: toward understanding their activation. *Cold Spring Harb Perspect Biol* 2:a004010.
- Teng CJ, Abbott F V (1998) The formalin test: a dose-response analysis at three developmental stages. *Pain* 76:337–347.
- Terasaki M, Slater NT, Fein A, Schmidek A, Reese TS (1994) Continuous network of endoplasmic reticulum in cerebellar Purkinje neurons. *Proc Natl Acad Sci U S A* 91:7510–7514.
- Thibault K, Calvino B, Pezet S (2011) Characterisation of sensory abnormalities observed in an animal model of multiple sclerosis: A behavioural and pharmacological study. *Eur J Pain*.
- Thompson AJ, Baranzini SE, Geurts J, Hemmer B, Ciccarelli O (2018) Multiple sclerosis. *Lancet* 391:1622–1636.
- Thorburn KC, Paylor JW, Webber CA, Winship IR, Kerr BJ (2016) Facial hypersensitivity and trigeminal pathology in mice with experimental autoimmune encephalomyelitis. *Pain* 157:627–642.
- Thuerauf DJ, Marcinko M, Belmont PJ, Glembotski CC (2007) Effects of the isoform-specific characteristics of ATF6 alpha and ATF6 beta on endoplasmic reticulum stress response gene expression and cell viability. *J Biol Chem* 282:22865–22878.
- Tingley WG, Ehlers MD, Kameyama K, Doherty C, Ptak JB, Riley CT, Huganir RL (1997) Characterization of protein kinase A and protein kinase C phosphorylation of the N-methyl-D-aspartate receptor NR1 subunit using phosphorylation site-specific antibodies. *J Biol Chem*.

- Tjølsen A, Berge OG, Hunskaar S, Rosland JH, Hole K (1992) The formalin test: an evaluation of the method. *Pain* 51:5–17.
- Trang T, Beggs S, Salter MW (2012) ATP receptors gate microglia signaling in neuropathic pain. *Exp Neurol* 234:354–361.
- Trang T, Beggs S, Wan X, Salter MW (2009) P2X₄-receptor-mediated synthesis and release of brain-derived neurotrophic factor in microglia is dependent on calcium and p38-mitogen-activated protein kinase activation. *J Neurosci* 29:3518–3528.
- Truini A, Barbanti P, Pozzilli C, Cruccu G (2013) A mechanism-based classification of pain in multiple sclerosis. *J Neurol* 260:351–367.
- Tsuda M, Shigemoto-Mogami Y, Koizumi S, Mizokoshi A, Kohsaka S, Salter MW, Inoue K (2003) P2X₄ receptors induced in spinal microglia gate tactile allodynia after nerve injury. *Nature* 424:778–783.
- Tsujino H, Kondo E, Fukuoka T, Dai Y, Tokunaga A, Miki K, Yonenobu K, Ochi T, Noguchi K (2000) Activating transcription factor 3 (ATF3) induction by axotomy in sensory and motoneurons: A novel neuronal marker of nerve injury. *Mol Cell Neurosci* 15:170–182.
- Tully K, Treistman SN (2004) Distinct intracellular calcium profiles following influx through N- versus L-type calcium channels: role of Ca²⁺-induced Ca²⁺ release. *J Neurophysiol* 92:135–143.
- Turk DC, Fillingim RB, Ohrbach R, Patel K V (2016) Assessment of Psychosocial and Functional Impact of Chronic Pain. *J Pain* 17:T21-49.
- Turvey SE, Broide DH (2010) Innate immunity. *J Allergy Clin Immunol* 125:S24-32.
- Urits I, Adamian L, Fiocchi J, Hoyt D, Ernst C, Kaye AD, Viswanath O (2019) Advances in the Understanding and Management of Chronic Pain in Multiple Sclerosis: a Comprehensive Review. *Curr Pain Headache Rep* 23:59.
- Usoskin D, Furlan A, Islam S, Abdo H, Lönnerberg P, Lou D, Hjerling-Leffler J, Haeggström J, Kharchenko O, Kharchenko P V, Linnarsson S, Ernfors P (2015) Unbiased classification of sensory neuron types by large-scale single-cell RNA sequencing. *Nat Neurosci* 18:145–153.
- Valencia-de Ita S, Lawand NB, Lin Q, Castañeda-Hernandez G, Willis WD (2006) Role of the Na⁺-K⁺-2Cl⁻ cotransporter in the development of capsaicin-induced neurogenic inflammation. *J Neurophysiol* 95:3553–3561.
- van den Berg R, Laman JD, van Meurs M, Hintzen RQ, Hoogenraad CC (2016) Rotarod motor performance and advanced spinal cord lesion image analysis refine assessment of neurodegeneration in experimental autoimmune encephalomyelitis. *J Neurosci Methods* 262:66–76.
- Van Hecke O, Austin SK, Khan R a., Smith BH, Torrance N (2014) Neuropathic pain in the general population: A systematic review of epidemiological studies. *Pain* 155:654–662.
- Van Kaer L, Postoak JL, Wang C, Yang G, Wu L (2019) Innate, innate-like and adaptive lymphocytes in the pathogenesis of MS and EAE. *Cell Mol Immunol*.

- Van Petegem F (2015) Ryanodine receptors: allosteric ion channel giants. *J Mol Biol* 427:31–53.
- Vanderheyden V, Devogelaere B, Missiaen L, De Smedt H, Bultynck G, Parys JB (2009) Regulation of inositol 1,4,5-trisphosphate-induced Ca²⁺ release by reversible phosphorylation and dephosphorylation. *Biochim Biophys Acta* 1793:959–970.
- Vázquez-Villoldo N, Domercq M, Martín A, Llop J, Gómez-Vallejo V, Matute C (2014) P2X₄ receptors control the fate and survival of activated microglia. *Glia* 62:171–184.
- Vekich JA, Belmont PJ, Thuerauf DJ, Glembotski CC (2012) Protein disulfide isomerase-associated 6 is an ATF6-inducible ER stress response protein that protects cardiac myocytes from ischemia/reperfusion-mediated cell death. *J Mol Cell Cardiol* 53:259–267.
- Verkhatsky A (2005) Physiology and pathophysiology of the calcium store in the endoplasmic reticulum of neurons. *Physiol Rev* 85:201–279.
- Vidal RL, Hetz C (2013) Unspliced XBP1 controls autophagy through FoxO1. *Cell Res* 23:463–464.
- Vierck CJ, Whitsel BL, Favorov O V, Brown AW, Tommerdahl M (2013) Role of primary somatosensory cortex in the coding of pain. *Pain* 154:334–344.
- Villière V, McLachlan EM (1996) Electrophysiological properties of neurons in intact rat dorsal root ganglia classified by conduction velocity and action potential duration. *J Neurophysiol* 76:1924–1941.
- Voskuhl RR, Peterson RS, Song B, Ao Y, Morales LBJ, Tiwari-Woodruff S, Sofroniew M V. (2009) Reactive astrocytes form scar-like perivascular barriers to leukocytes during adaptive immune inflammation of the CNS. *J Neurosci*.
- Wang B, Bugay V, Ling L, Chuang H-H, Jaffe DB, Brenner R (2016) Knockout of the BK β 4-subunit promotes a functional coupling of BK channels and ryanodine receptors that mediate a fAHP-induced increase in excitability. *J Neurophysiol* 116:456–465.
- Wang I-C, Chung C-Y, Liao F, Chen C-C, Lee C-H (2017a) Peripheral sensory neuron injury contributes to neuropathic pain in experimental autoimmune encephalomyelitis. *Sci Rep* 7:42304.
- Wang J, Lee J, Liem D, Ping P (2017b) HSPA5 Gene encoding Hsp70 chaperone BiP in the endoplasmic reticulum. *Gene* 618:14–23.
- Wang X-T, Pei D-S, Xu J, Guan Q-H, Sun Y-F, Liu X-M, Zhang G-Y (2007) Opposing effects of Bad phosphorylation at two distinct sites by Akt1 and JNK1/2 on ischemic brain injury. *Cell Signal* 19:1844–1856.
- Wang X, Seed B (2003) A PCR primer bank for quantitative gene expression analysis. *Nucleic Acids Res* 31:e154.
- Wang Y, Feng C, He H, He J, Wang J, Li X, Wang S, Li W, Hou J, Liu T, Fang D, Xie S-Q (2018) Sensitization of TRPV1 receptors by TNF- α orchestrates the development of vincristine-induced pain. *Oncol Lett* 15:5013–5019.
- Warwick RA, Hanani M (2013) The contribution of satellite glial cells to chemotherapy-induced

- neuropathic pain. *Eur J Pain* (United Kingdom).
- Warwick RA, Ledgerwood CJ, Brenner T, Hanani M (2014) Satellite glial cells in dorsal root ganglia are activated in experimental autoimmune encephalomyelitis. *Neurosci Lett* 569:59–62.
- Watanabe M, Fukuda A (2015) Development and regulation of chloride homeostasis in the central nervous system. *Front Cell Neurosci* 9:371.
- Waxman SG (2006) Axonal conduction and injury in multiple sclerosis: The role of sodium channels. *Nat Rev Neurosci*.
- Waxman SG, Zamponi GW (2014) Regulating excitability of peripheral afferents: emerging ion channel targets. *Nat Neurosci* 17:153–163.
- Weber MS, Prod'homme T, Youssef S, Dunn SE, Rundle CD, Lee L, Patarroyo JC, Stüve O, Sobel RA, Steinman L, Zamvil SS (2007) Type II monocytes modulate T cell-mediated central nervous system autoimmune disease. *Nat Med* 13:935–943.
- Wilson P, Meyers DE, Snow PJ (1986) The detailed somatotopic organization of the dorsal horn in the lumbosacral enlargement of the cat spinal cord. *J Neurophysiol* 55:604–617.
- Win S, Than TA, Fernandez-Checa JC, Kaplowitz N (2014) JNK interaction with Sab mediates ER stress induced inhibition of mitochondrial respiration and cell death. *Cell Death Dis* 5:e989.
- Woller SA, Eddinger KA, Corr M, Yaksh TL (2017) An overview of pathways encoding nociception. *Clin Exp Rheumatol* 35 Suppl 1:40–46.
- Woolf CJ, Salter MW (2000) Neuronal plasticity: Increasing the gain in pain. *Science* (80-).
- Wu D-F, Chandra D, McMahon T, Wang D, Dadgar J, Kharazia VN, Liang Y-J, Waxman SG, Dib-Hajj SD, Messing RO (2012) PKC ϵ phosphorylation of the sodium channel NaV1.8 increases channel function and produces mechanical hyperalgesia in mice. *J Clin Invest* 122:1306–1315.
- Xie W, Tan Z-Y, Barbosa C, Strong JA, Cummins TR, Zhang J-M (2016) Upregulation of the sodium channel NaV β 4 subunit and its contributions to mechanical hypersensitivity and neuronal hyperexcitability in a rat model of radicular pain induced by local dorsal root ganglion inflammation. *Pain* 157:879–891.
- Xu Q, Garraway SM, Weyerbacher AR, Shin SJ, Inturrisi CE (2008) Activation of the neuronal extracellular signal-regulated kinase 2 in the spinal cord dorsal horn is required for complete Freund's adjuvant-induced pain hypersensitivity. *J Neurosci* 28:14087–14096.
- Xu Z-Z, Kim YH, Bang S, Zhang Y, Berta T, Wang F, Oh SB, Ji R-R (2015) Inhibition of mechanical allodynia in neuropathic pain by TLR5-mediated A-fiber blockade. *Nat Med* 21:1326–1331.
- Yamaguchi Y, Oh-Hashi K, Matsuoka Y, Takemura H, Yamakita S, Matsuda M, Sawa T, Amaya F (2018) Endoplasmic Reticulum Stress in the Dorsal Root Ganglion Contributes to the Development of Pain Hypersensitivity after Nerve Injury. *Neuroscience* 394:288–299.

- Yamamoto K, Ichijo H, Korsmeyer SJ (1999) BCL-2 is phosphorylated and inactivated by an ASK1/Jun N-terminal protein kinase pathway normally activated at G(2)/M. *Mol Cell Biol* 19:8469–8478.
- Yang ES, Bae JY, Kim TH, Kim YS, Suk K, Bae YC (2014) Involvement of endoplasmic reticulum stress response in orofacial inflammatory pain. *Exp Neurobiol* 23:372–380.
- Yoneda T, Imaizumi K, Oono K, Yui D, Gomi F, Katayama T, Tohyama M (2001) Activation of caspase-12, an endoplasmic reticulum (ER) resident caspase, through tumor necrosis factor receptor-associated factor 2-dependent mechanism in response to the ER stress. *J Biol Chem* 276:13935–13940.
- Yousuf M, Ali L (1997) A study of 22 cases of tropical splenomegaly and chloroquine therapy. *J Coll Physicians Surg Pakistan* 7.
- Yousuf MS, Noh M, Friedman TN, Zubkow K, Johnson JC, Tenorio G, Kurata HT, Smith PA, Kerr BJ (2019) Sensory Neurons of the Dorsal Root Ganglia Become Hyperexcitable in a T-Cell-Mediated MOG-EAE Model of Multiple Sclerosis. *eneuro*.
- Yousuf MS, Zubkow K, Tenorio G, Kerr B (2017) The chloride co-transporters, NKCC1 and KCC2, in experimental autoimmune encephalomyelitis (EAE). *Neuroscience* 344:178–186.
- Yue Y, Stanojlovic M, Lin Y, Karsenty G, Lin W (2019) Oligodendrocyte-specific ATF4 inactivation does not influence the development of EAE. *J Neuroinflammation* 16:23.
- Zalk R, Clarke OB, des Georges A, Grassucci RA, Reiken S, Mancina F, Hendrickson WA, Frank J, Marks AR (2015) Structure of a mammalian ryanodine receptor. *Nature* 517:44–49.
- Zeilhofer HU, Wildner H, Yévenes GE (2012) Fast synaptic inhibition in spinal sensory processing and pain control. *Physiol Rev* 92:193–235.
- Zhang E, Yi M-H, Shin N, Baek H, Kim S, Kim E, Kwon K, Lee S, Kim H-W, Chul Bae Y, Kim Y, Kwon O-Y, Lee WH, Kim DW (2015) Endoplasmic reticulum stress impairment in the spinal dorsal horn of a neuropathic pain model. *Sci Rep* 5:11555.
- Zhang J, Liang Y, Lin Y, Liu Y, YouYou, Yin W (2016) IRE1 α -TRAF2-ASK1 pathway is involved in CSTMP-induced apoptosis and ER stress in human non-small cell lung cancer A549 cells. *Biomed Pharmacother* 82:281–289.
- Zhang JM, Donnelly DF, Song XJ, Lamotte RH (1997) Axotomy increases the excitability of dorsal root ganglion cells with unmyelinated axons. *J Neurophysiol* 78:2790–2794.
- Zhang W, Liu L-Y, Xu T-L (2008) Reduced potassium-chloride co-transporter expression in spinal cord dorsal horn neurons contributes to inflammatory pain hypersensitivity in rats. *Neuroscience* 152:502–510.
- Zhang X-L, Mok L-P, Lee KY, Charbonnet M, Gold MS (2012) Inflammation-induced changes in BK(Ca) currents in cutaneous dorsal root ganglion neurons from the adult rat. *Mol Pain* 8:37.
- Zhang XL, Mok LP, Katz EJ, Gold MS (2010) BKCa currents are enriched in a subpopulation of adult rat cutaneous nociceptive dorsal root ganglion neurons. *Eur J Neurosci*.

Zhu W, Acosta C, MacNeil B, Cortes C, Intrater H, Gong Y, Namaka M (2013) Elevated expression of fractalkine (CX3CL1) and fractalkine receptor (CX3CR1) in the dorsal root ganglia and spinal cord in experimental autoimmune encephalomyelitis: implications in multiple sclerosis-induced neuropathic pain. *Biomed Res Int* 2013:480702.

Zhu W, Frost EE, Begum F, Vora P, Au K, Gong Y, MacNeil B, Pillai P, Namaka M (2012) The role of dorsal root ganglia activation and brain-derived neurotrophic factor in multiple sclerosis. *J Cell Mol Med* 16:1856–1865.